Synthesis of Nanometer-sized Yttrium Oxide Particles in Diisooctyl Sodium Sulphosuccinate (AOT)/Isooctane Reverse Micelle Solution

Cheng, Xu

A Thesis Submitted to the Faculty of
the Virginia Polytechnic Institute and State University
in Partial Fulfillment of the Requirements for the Degree of

Master of Science

in

Chemistry

Brian M. Tissue, Chair

Paul A. Deck

Brian E. Hanson

March 12, 1999

Blacksburg, Virginia

Keywords: Synthesis, Nanoparticle, Reverse Micelle, Y_2O_3, Yttrium Nitrate, Yttrium Isopropoxide, AOT/Isooctane, Annealing

Synthesis of Nanometer-sized Yttrium Oxide Particles in Diisooctyl Sodium Sulphosuccinate (AOT)/Isooctane Reverse Micelle Solution

Cheng, Xu

Abstract

This thesis describes the synthesis of yttrium oxide nanoparticles in an AOT/isooctane reverse micelle solution. Two synthetic methods are compared. First is the precipitation reaction between yttrium nitrate and ammonia, second is the hydrolysis of yttrium isopropoxide. The effects of annealing of the resulting the yttrium oxide nanoparticles are also described.

The nitrate method produced network-like aggregates of yttrium oxide nanoparticles ranging from 10 nm to 40 nm in diameter. Reaction conditions, including the water/AOT ratio (1 to 15), the nitrate concentration (0.02 M to 1.0 M), the ammonia concentration (2 M to 14.8 M), the AOT concentration (0.1 M and 0.5 M), the aging time (1 h to 5 d), and the washing method, were varied to investigate their influence on nanoparticle formation. The optimized synthetic conditions were: a water/AOT ratio of 7.5, $[NO_3^-]$ = 0.5 M, $[NH_3]$ = 2 M, and [AOT] = 0.1 M.

The as-prepared yttrium oxide nanoparticles had highly distorted structures related to the cubic Y_2O_3 phase. Annealing improved the crystallinity of the as-prepared nanoparticle products and led to larger particles. As annealing temperatures increased, the yttrium oxide nanoparticles gradually evolved into the cubic Y_2O_3 phase. However, an unknown intermediate phase was also observed during the annealing process, which disappeared when the annealing temperature was sufficiently high and the annealing time was long enough (>1000 °C and 4 h).

As-prepared products from the isopropoxide hydrolysis also contained network-like nanoparticle aggregates. Particle sizes ranged from 10 nm to 20 nm. Some experimental conditions were varied; they were the water/AOT ratio (10 to 40), the isopropoxide concentration (0.0001 M to 0.003 M), the aqueous phase pH (7.0 and 12.0), the aging temperature (room temperature, approximately 25 °C, and refluxing temperature, approximately, 100 °C), and the aging time (1 h to 5 d). Transmission Electronic Micrographs showed that products of desirable morphology could be produced in a much wider range of experimental conditions by this method compared to those produced by nitrate hydrolysis.

Acknowledgements

I want to thank Professor Brian Tissue for his support and guidance during my graduate research for the Master's Degree at Virginia Tech. It has been a great opportunity for me to work in his group and gain extensive research experience in the field of nanomaterials science.

I also want to thank my committee members, Professors Paul Deck and Brian Hanson, for their helpful discussions and experimental supports during the course of my research.

I am grateful to Professor William Reynolds in the Materials Science Department for his helps in the S.A.D.P. experiments and result discussions.

I am indebted to Dr. Gang Chen and Messrs. Frank Cromer, Steven McCartney, and Todd Solberg for their help with the TEM, SEM, TEM, and XRD instrument, respectively.

During the last two and a half years, I also received a great deal of help from my group members, Steven Hunsucker, Jen Milora, Craig Watson, Diane Williams, and Huabiao Yuan. I am especially grateful for their friendship, which encouraged me to overcome many difficulties in my research. I wish to take this opportunity to thank them.

Finally, without the support and endless love of my parents, I would not have been the person I am. They were, are, and will be forever the most important source of encouragement to me. This thesis is dedicated to them.

Table of Content

Chapter One: Introduction 1

1.1 Properties and Applications of Nanomaterials 1

1.1.1 Some Properties of Nanomaterials 1

1.1.2 Applications of Nanomaterials 3

1.1.3 Applications of Nanocrystalline Y_2O_3 4

1.2 Review of Methods to Synthesize Nanocrystalline Y_2O_3 6

1.2.1 Homogeneous Precipitation 7

1.2.2 The Sol-gel Process 8

1.2.3 The Combustion Synthesis 9

1.2.4 The Electrodispersion Technique 10

1.2.5 The Spray-Pyrolysis Techniques 11

1.2.6 The Evaporation-Condensation Processes 13

1.3 The Reverse Micelle Approach 14

1.3.1 Reverse Micelles as Microreactors 14

1.3.2 Examples of Reverse Micelle Syntheses 17

1.4 General Experimental Approach in the Research 20

1.5 Characterization 23

Chapter Two: Nitrate-Hydrolysis Method 28

2.1 Effects of Varying the Water/AOT Ratio 29

2.2 Effects of Varying the Nitrate Concentration 33

2.3 Effects of Varying the Ammonia Concentration 34

2.4 Effects of Varying the AOT Concentration 34

2.5 Effects of Varying the Aging Time 35

2.6 Effects of Varying the Washing Method 36

2.7 Conclusion 39

Chapter Three: Isopropoxide-Hydrolysis Method 50

3.1 Effects of Varying the Water/AOT Ratio 51

3.2 Effects of Varying the Yttrium Isopropoxide Concentration 53

3.3 Effects of Varying the pH Value 53

3.4 Effects of Varying the Aging Time and Temperature 54
3.5 Conclusion 55
Chapter Four: Annealing Effects 61
4.1 Effects of Varying the Annealing Temperature 61
4.1.1 Color Change and Weight Loss 61
4.1.2 TEM Results 62
4.1.3 SAD Results 63
4.1.4 XRD Results 64
4.2 Effects of Varying the Annealing Time 66
4.3 Effects of Surfactant 67
4.4 Effects of Europium Doping 68
4.5 Conclusion 69
Chapter Five: Conclusion and Outlook 85
Vita 88

Table of Figures

Figure 1.1 Formation of Reverse Micelles in Non-polar Solvent 25
Figure 1.2 Structure of a Reverse Micelle formed by AOT molecules 26
Figure 1.3 Structure of an AOT Molecule 27
Figure 2.1 Influence of Water/AOT Ratio on Product Morphology 41
Figure 2.2 Comparison of XRD Patterns of Products Prepared from Reverse Micelle Solution and Aqueous Solution 42
Figure 2.3 Influence of Yttrium Nitrate Concentration on Product Morphology 43
Figure 2.4 Influence of Ammonia Concentration on Product Morphology 44
Figure 2.5 Influence of AOT Concentration on Product Morphology 45
Figure 2.6 Comparison of Products of Different Aging Time 46
Figure 2.7 Comparison of Ethanol-washed Product and Water-washed Product 47
Figure 2.8 Comparison of Refluxed Product and Non-refluxed Product 48
Figure 3.1 Influence of Water/AOT Ratio on Product Morphology 56
Figure 3.2 Influence of $Y(O^iPr)_3$ Concentration on Product Morphology 57
Figure 3.3 Influence of Aqueous Phase pH Value on Product Morphology 58
Figure 3.4 Influence of Aging Time on Product Morphology 59
Figure 3.5 Influence of Aging Temperature on Product Morphology 60
Figure 4.1 Effects of Annealing Temperature (TEM) 71
Figure 4.2 Annealing Effects of the Product of the Isopropoxide Method 73
Figure 4.3 An Aggregate of Several Crystallites in a Sample Annealed at 1000 °C for 4 hrs 74
Figure 4.4 [100] Pattern of a Single Crystallite from Microprobe 75
Figure 4.5 Calculated [100] Pattern of Cubic Y_2O_3 76
Figure 4.6 XRD Pattern of a Sample Annealed at 1000 °C for 4 hrs 77
Figure 4.7 Effects of Annealing Temperature (XRD) 78
Figure 4.8 Effects of Annealing Time (TEM) 79
Figure 4.9 Effects of Annealing Time (XRD) 80
Figure 4.10 Effects of AOT (XRD) 81
Figure 4.11 Effects of Eu-Doping (TEM) 82
Figure 4.12 Effects of Eu-Doping (XRD) 83

Table of Tables

Table 2.1 Washing Effects of Different Solvents 49
Table 2.2 Effects of Different Washing Methods 49
Table 4.1 Weight Loss of Samples Annealed for 16 hrs 84
Table 4.2 Sizes of Crystalline Regions in Samples Annealed at Different Temperatures 84
Table 4.3 Sizes of Crystalline Regions in Samples Annealed for Different Periods of Time ... 84

Chapter One:
Introduction

1.1 Properties and Applications of Nanomaterials

1.1.1 Some Properties of Nanomaterials

Nanomaterials are materials with particle sizes less than one micrometer, usually less than 100 nm. These small particle sizes impart different physical and chemical properties compared to the bulk forms. Different phases are also found in some nanocrystalline materials. For example, bulk Er_2O_3 exists in two hexagonal phases, but its nanocrystalline Er_2O_3 exhibits two phases (fcc cubic and monoclinic) that are not found in the bulk.[1]

A well-known property of nanomaterials is that their surface areas are tremendously increased. Their surface-to-volume ratios are very high, so that most of the molecules/atoms are on the surface or at the grain boundaries. Since surface molecules/atoms don't have any force above the particle surface to balance the attractive force from inside the particle, they are in high-energy states.[2] In addition, molecules/atoms at the grain boundaries are in highly distorted lattice structures, and forces exerted on a molecule/atom from surrounding species are not balanced, so molecules/atoms at the grain boundaries are also in high energy states. Therefore, the surface energy of a nanomaterial is very high.[2] The large surface area and number of grain boundaries of nanomaterials provide a high concentration of low-energy diffusion paths. Therefore, nano-materials have higher self-diffusivity and solute diffusivity than the bulk forms.[3]

Nanoparticles have electrical and optical properties that are not observed in the bulk. These "quantum-size" effects appear when particle sizes are comparable with or smaller than some characteristic lengths, such as a phonon wavelength, an electron de Broglie wavelength, or an effective Bohr radius around impurity centers.

The energy states of doped impurity atoms are strongly modulated in nanocrystallites, whose sizes are smaller than the Bohr radius of the impurity atoms. This phenomenon is called

[1] Li, Z.; Hahn, H.; Siegel, R. W.: *Mater. Lett.* **6**, 342 (1988).
[2] Adamsom, A. W.; Gast, A. P.: In *Physical Chemistry of Surfaces 6th ed.*, Wiley Interscience, New York, 257 (1997).

quantum confinement. Quantum confinement effect changes overlaps of the wave functions of the impurity atoms with those of host atoms, leading to more efficient interactions between impurity atoms and the host atoms.

For example, luminescent properties of activators in nanocrystalline phosphors are enhanced.[4] In nanocrystalline Y_2O_3:Tb, the luminescent efficiency increases proportionally with square of decreasing particle size (10 nm to 4 nm), which is predicted accurately by a quantum-confinement model.[5] Decrease in particle sizes causes localization of exciton wave-functions near the impurities (activators), which results in higher overlaps of the exciton wave-functions with those of the impurities, so energy transfer rate from the excitons to the impurities is higher. Therefore, non-radioactive decay rate is relatively reduced, and luminescent efficiency increases.[6] However, if there are many extinguishing defects at the grain boundaries, the luminescent efficiency of a nanocrystalline phosphor decreases.[7] Controlling grain-boundary defects is an important factor to further improve efficiencies of nanocrystalline phosphors. Nanocrystalline monoclinic Y_2O_3:Eu prepared by laser ablation method has a longer $^5D_0 \rightarrow {}^7F_2$ transition lifetime than that of the bulk.[8] In addition, line widths in the excitation spectra increase with decreasing particle sizes. This phenomenon has been attributed to inhomogeneous broadening from lattice distortion. A blue shift in the emission spectra of nanocrystalline Y_2O_3:Eu was also observed.[9]

Phonons of wavelengths greater than the particle sizes cannot propagate in nanocrystalline materials, so phonon distributions (density-of-states) in nanocrystalline materials change greatly from the bulk materials (the phonon-confinement effect).[10] Due to this effect, as particle sizes become smaller, nanocrystalline Si becomes more emissive.[11] It is suggested that the emission centers in porous Si are actually nanocrystallites of Si.[12] Because of their novel properties due to the quantum-size effects, nanocrystallites of semiconductors are often called

---

[3] Gleiter, H.: *Progress in Materials Science* **33**, 223 (1989).
[4] Bhargava, R.: *J. Lumin.* **72-74**, 46 (1997).
[5] Goldburt, E. T.; Kulkarni, B.; Bhargava, R. N.; Taylor, J.; Libera, M.: *J. Lumin.* **72-74**, 190 (1997).
[6] Bhargava, R. N.; Gallagher, D.; Hong, X.; Nurmikko, A.: *Phys. Rev. Lett.* **72**, 416 (1994).
[7] Hase, T.; Kano, T.; Nakazawa, E.; Yamamoto, H.: *Adv. Electronics and Electron Phys.* **79**, 271 (1990).
[8] Williams, D. K.; Bihari, B.; Tissue, B. M.; McHale, J. M.: *J. Phys. Chem. B* **102**, 916 (1998).
[9] Li, Q.; Gao, L.; Yan, D.-S.: *NanoStruct. Mater.* **8**, 825 (1997).
[10] Wolf, D.; Wang, J.; Phillpot, S. R.: Gleiter, H.: *Phys. Rev. Lett.* **74**, 4686 (1995).
[11] Birringer, R.; Herr, U.; Gleiter, H.: *Suppl. Trans. Japan Inst. Metals* **27**, 43 (1986).
[12] Prokes, S. M.: *J. Mater. Res.* **11**, 305 (1996).

quantum dots.[13] The phonon-confinement effect is also observed in Raman spectra of nanocrystalline Y_2O_3[14] and TiO_2.[15] As the particle size decreases from 40 nm to 7nm, the characteristic Raman lines of nanocrystalline Y_2O_3 shift to lower frequencies, accompanied by significant broadening.

The term super-plasticity is used to describe the ability of a material to exhibit high tensile ductility (elongation) without significant necking. If treated at high homologous testing temperatures, conventionally brittle polycrystalline ceramic materials of average grain sizes smaller than 10 μm, such as Y_2O_3-stabilized ZrO_2, exhibit super-plasticity (elongation > 100%).[16] Decreasing particle sizes further into the nanometer range will not only increase the overall ductility of a material prior to failure, but also decrease the super-plasticity-appearance temperature of the material.[17] Room-temperature super-plasticity is observed in nanocrystalline TiO_2 (rutile).[18] The origin of super-plasticity is grain-boundary sliding with some true sliding contribution accommodated by matter transportation, grain-boundary migration, grain rotation, and diffusion or dislocation motion.[19]

Hardness and fracture toughness of a bulk ceramic material increase with increasing sintering temperature. however, same hardness and fracture toughness can be achieved by the nanocrystalline form, such as nanocrystalline TiO_2, sintered at much lower temperatures.[20] This observation indicates that nanocrystalline compacts densify much more rapidly than polycrystalline compacts.

1.1.2 Applications of Nanomaterials

Because of the novel properties of nanomaterials compared to their bulk forms, they are promising candidates for many advanced technical applications. Nanomaterials inherently have a very high surface-to-volume ratio. Therefore, nanometer-sized catalyst supports, or nanometer-sized catalysts have greatly improved efficiencies.[21] Nanocrystallites of optically active materials

[13] Murray, C. B.; Kagan, C. R.; Bawendi, M. G.: *Science* **270**, 1335 (1995).
[14] Bruch, C.; Krüger, J. K.; Unruh, H.-G.; Krauss, W.; Zimmermeier, B.; Beck, C.; Hempelmann, R.: *Ber. Bunsenges. Phys. Chem.* **101**, 1761 (1997).
[15] Bersani, D.; Lottici, P. P.; Ding, X.-Z.: *Appl. Phys. Lett.* **72**, 73 (1998).
[16] Langdon, T. G.: *Metall. Trans.* **13A**, 689 (1982).
[17] Langdon, T. G.: *Key Eng. Mater.* **97-98**, 109 (1994).
[18] Karch, J.; Birringer, R.; Gleiter, H.: *Nature* **330**, 556 (1987).
[19] Wakai, F.; Kondo, N.; Ogawa, H.; Nagano, T.; Tsurekawa, S: *Mater. Character.* **37**, 331 (1996).
[20] Averback, R. S.; Hahn, H; Höfler, H. J.; Logas, J. L.; Shen, T.-C.: *Mater. Res. Soc. Symp.* **153**, 3 (1989).
[21] Masui, T.; Fujiwara, K.; Machida, K.; Adachi, G.; Sakata, T.; Mori, H.: *Chem. Mater.* **9**, 2197 (1997).

(such as Cr:Mg_2SiO_4, Cr:$CaMgSi_2O_6$), whose single crystals are difficult to be grown and are sensitive to their environment, can be embedded in transparent host materials (typically a polymer) to form optical composites.[22] The optical composites have the properties of nanocrystallites and the processability of the polymer hosts. Nanoparticles of magnetic materials exhibit greatly improved magnetic properties and much smaller particle sizes, which find many potential applications in magnetic recording, magnetic refrigeration, and ferrofluids.[23] Nanometer-sized semiconductor clusters are promising materials to prepare devices for efficient conversion of light into electricity (for example, ruthenium polypyridyl sensitizers anchored to porous colloidal TiO_2 films),[24] or electricity into light (for example, nanocrystalline Si).[25] Nanocrystallites of semiconductor materials are considered as quantum dots due to quantum-confinement effects, and doped quantum dots are candidates for advanced displays (High Definition TV, Field Emission Display, Plasma Display, Electroluminescent Display), ultra-fast sensors, and lasers.[26] Super-plasticity of nanometer-sized ceramic materials creates a new processing technology for ceramics, the super-plastic forming technology.[27] Superior hardness and fracture toughness of some nanomaterials make them ideal materials for cutting tools.[28] The mechanical properties of nanocrystalline ceramics lead them to be called "ceramic steel".[29] Commercial realization of ceramic engines also depends on the development of such nanocrystalline ceramics.[30]

1.1.3 Applications of Nanometer-sized Y_2O_3

Y_2O_3 is one of the most important host materials for phosphors, scintillators, lasers, and fiber-optic communications. Eu-doped Y_2O_3 is an important red-emitting phosphor, and Tb-doped Y_2O_3 is a green-emitting phosphor. Because of the quantum-size effects, luminescent properties of nanocrystalline phosphors are different from their bulk forms,[4] which may greatly

[22] Barber, D. B.; Pollock, C. R.; Beecroft, L. L.; Ober, C. K.: *Opt. Lett.* **22**, 1247 (1997).
[23] Dagani, R.: *Chem. & Eng. News* **70**, 18 (1992).
[24] Argazzi, R.; Bignozzi, C. A.: *J. Am. Chem. Soc.* **117**, 11815 (1995).
[25] Chin, R. P.; Shen, Y. R.; Petrova-Koch, V.: *Science* **270**, 776 (1995).
[26] Bhargava, R. N.: *J. Lumin.* **70**, 85 (1996).
[27] Wittenauer, J.: In *Plastic Deformation of Ceramics*, R. C. Bradt, C. A. Brookes, and J. L. Routbort (eds.), Plenum, New York, 321 (1995).
[28] Skandan, G.; Kear, B. H.: *Mater. Sci. Forum* **243-245**, 217 (1997).
[29] Jack, K. H.: *High Technology Ceramics, Past, Present, and Future; Ceramics and Civilization* **3**, W. D. Kingery (ed.), 259 (1986).
[30] Cahn, R. W.: *Nature* **332**, 761 (1988).

improve their performance and extend their applications. Due to a maximum field gradient before charge leaking, the maximum voltage (approximately 1 kV)[26] that can be applied on flat panel display devices (FED, EL, and PD) is much smaller than that on normal display devices (approximately 5 kV). As nanocrystalline phosphors generally have higher efficiencies, lower voltages are adequate to achieve a same efficiency. Therefore, nanocrystalline phosphors are ideal candidates for flat panel displays.[31] HDTV requires phosphors of very small particle size, narrow size distribution, uniform shape, and high intensity without light saturation. Nanocrystalline phosphors have very fast luminescent recombination rate, so the saturation can be eliminated, while their nanometer-scale sizes fulfill the other requirements of HDTV.[26]

SiO_2 is the gate oxide/dielectric material in metal oxide semiconductors (MOS) in very-large-scale-integrated (VLSI) circuits. By decreasing the thickness of the SiO_2 layer, increases in charge-storage capacity and trans-conductance are achieved. However, the smallest practical thickness of the SiO_2-gated dielectric layer is being approached in modern silicon devices. Further improvement needs materials of higher dielectric constants as the gate material. Y_2O_3 thin films are excellent substitute gate materials. They can be made very thin (25 nm), and the dielectric constant is approximately four times higher than that of SiO_2.[32] In addition, they have lower leakage current for a given gate voltage, and higher breakdown strength.

Y_2O_3 is an important additive in many structural and functional ceramics. ZrO_2 is valued for strength and toughness in industrial ceramic applications. Y_2O_3-stabilized ZrO_2 avoids the destructive phase transformations (volume change during phase transformation causes material cracking) from monoclinic to tetragonal and further to cubic at elevated temperatures. Y_2O_3-stabilized ZrO_2 is used in high-temperature refractory, heating cells in oxidation atmospheres, ceramic engines.[33] Y_2O_3-stabilized ZrO_2 also has high oxygen-ion conductivity at elevated temperatures,[34] which makes it suitable for use in oxygen sensors and oxygen pumps at elevated temperatures.[35] Similarly, Y_2O_3 is also used to stabilize HfO_2, which is a promising ultra-refractory ceramic material for nuclear applications (control rods and neutron shielding).[36] Y_2O_3-

[31] Goldburt, E. T.; Kulkarni, B.; Bhargava, R. N.; Taylor, J.; Libera, M.: *Mater. Res. Symp. Proc.* **424**, 441 (1997).
[32] Agarwal, M.; DeGuire, M. R.; Heuer, A. H.: *Appl. Phys. Lett.* **71**, 891 (1997).
[33] Glaussen, N.; Ruhle, M.; Heuer, A. H.: In *Science and Technology of Zirconia II*, The ACS Inc., Columbus, 1984.
[34] Badwal, S. P. S.: *J. Mater. Sci.* **19**, 1767 (1984).
[35] Jagannathan, K. P.; Tiku, S. K.; Ray, H. S.; Ghosh, A.; Subbarao, E. C.: In *Solid Electrolytes and their Applications*, E. C. Subbarao (ed.), Plenum, New York, 201 (1980).
[36] Tilloca, G.: *J. Mater. Sci.* **30**, 1884 (1995).

doped ThO_2 is also used in oxygen sensors.[37] Addition of Y_2O_3 nanoparticles influences density and elastic moduli of Si_3N_4 ceramics, and improves their sinterability.[38] Nanocrystalline Y_2O_3 additives also help to prepare AlN ceramics of higher density and thermal conductivity.[39]

Nanocrystalline Y_2O_3 is also used in high-density magnetic recording. To achieve high-density magnetic recording, the recording medium must have high coercivity (>3000 Oe) with thin or no overcoat. Particle sizes of the medium must be very small (< 10 nm), but magnetically isolated to minimize the transition noise. Y_2O_3-doping effectively reduces particle sizes in thin films of nanocrystalline $Ba_{1.25}Fe_{12}O_{19}$ magnetic material from several hundreds of nanometer to approximately 50 nm, while keeping the high coercivity of the material.[40]

Y_2O_3, Al_2O_3, MgO, and ZrO_2 are novel transparent ceramic materials that can be used in severe environments instead of traditional glasses. Y_2O_3 has a higher melting point and better chemical stability, which makes it suitable for heat-resistant transparent windows and walls for high-pressure sodium electric discharge light bulbs. There are two methods to prepare transparent Y_2O_3 material. One is the traditional sintering method, and the other is the hot-pressing of Y_2O_3 nanoparticles in vacuum. Due to the improved sinterability of nanocrystalline Y_2O_3, the hot-pressing method has the advantage of much lower operation temperature (1300 °C) and much lower operation pressure (44 MPa) than those of the sintering method (2300 °C and 980 MPa, respectively).[41]

1.2 Review of Methods to Synthesize Nanometer-sized Y_2O_3

Many methods have been investigated to synthesize Y_2O_3 nanoparticles and related materials. All of the methods can be separated into two categories. The first category is to combine molecules into nanoparticles (homogeneous precipitation, sol-gel, and combustion), and the other is to convert bulk materials into nanoparticles (electrodispersion, spray-pyrolysis, and evaporation-condensation). Every method has its advantages and disadvantages. Some methods need special equipment, high vacuum, and/or great amount of energy, such as electrodispersion, spray-pyrolysis, and evaporation-condensation. Some are very difficult to scale up, such as

[37] Cosentino, I. C.; Muccillo, R.: *Mater. Lett.* **32**, 295 (1997).
[38] Takata, H.; Martin, C.; Ishizaki, K.: *J. Ceram. Soc. Jpn.* **96**, 894 (1988).
[39] Watari, K.; Ishizaki, K.; Fuyuki, T.: *J. Mater. Sci. Lett.* **8**, 641 (1989).
[40] Chen, Y.-J.; Kryder, M. H.: *J. Appl. Phys.* **79**, 4878 (1996).
[41] Majima, K.; Niimi, N.; Watanabe, M.; Katsuyama, S.; Nagai, H.: *Mater. Trans. J. I. M.* **35**, 645 (1994).

evaporation-condensation and spray-pyrolysis. Some have hard-to-control operation conditions, such as sol-gel.

1.2.1 Homogeneous Precipitation

In normal precipitation processes, aqueous solutions of reactants are mixed to produce precipitates of insoluble substance by exceeding the solubility limits. Since the mixing processes are not controlled, large concentration gradients during mixing produce a broad distribution of particle sizes. Many methods can reduce the concentration gradient during precipitation, so that precipitates can be uniformly produced. Homogeneous precipitation is a method to introduce the precipitant gradually and uniformly throughout the entire solution, so that the precipitation processes happen simultaneously everywhere in the solution. Precipitates thus generated have small particle sizes and very narrow size distributions.

Sordelet and Akinc used the homogeneous precipitation method to make nanocrystalline Y_2O_3.[42] An Y^{3+} solution was mixed with a urea solution at room temperature. The mixture, with magnetic stirring, was then heated to boiling. Due to the uniform production of CO_2 and NH_3 molecules during thermal hydrolysis of urea, there was essentially no concentration gradient in the solution, so the precipitation process was very uniform. A bluish tint appeared in the solution, indicating precipitate formation. After a period of aging under mild boiling, the then-opaque mixture was filtered. The resulting precipitate was washed with water and acetone. The composition of as-prepared samples was $YOHCO_3$, which could be converted into cubic Y_2O_3 by annealing above 610 °C. The as-prepared products contained nanoparticles of uniform spherical shape with narrow size distributions. The average particle sizes ranged from less than 100 nm to several hundreds of nanometers. Highly concentrated Y^{3+} (> 0.05 M) resulted in serious particle agglomeration and deviation from the spherical shape, while excess urea had little effect. Longer aging time led to larger particles. To understand the roles of CO_2 and NH_3 in the precipitation process, the authors replaced urea (NH_2CONH_2) with CCl_3COOH, which generates only CO_2 precipitant on decomposition, and $HCONH_2$, which generates only NH_3 precipitant on decomposition. They found that CO_2 played a critical role in the precipitation process. In the experiment using CCl_3COOH, a similar product was obtained, but no precipitate was found in the experiment using $HCONH_2$. The authors argued that concentration of NH_3 produced during

[42] Sordelet, D.; Akinc, M.: *J. Colloid and Interface Sci.* **122**, 47 (1988).

decomposition was not high enough to precipitate Y^{3+}. Different supporting anions, such as NO_3^-, Cl^-, and $C_2O_4^{2-}$, were also investigated in the study. NO_3^- and Cl^- gave very similar results, for they are non-coordinating anions to Y^{3+} and very weak bases. However, $C_2O_4^{2-}$ changed the precipitate morphology. Oxalate might affect the precipitation process in two ways: by buffering the solution pH, or by complexing Y^{3+}. Kobayashi studied effects of the chelating EDTA ligand on the urea precipitation process.[43] Nanoparticles (60~70 nm) were produced, which were aggregates of much smaller particles. Li et al. used the homogeneous precipitation method to prepare a nanocrystalline Y_2O_3:Eu phosphor.[9] They obtained nanoparticles in the range of 40 to 70 nm. They found blue shift of the emission spectra of the prepared nanoparticle phosphor samples. XRD results indicated a smaller unit cell than that of bulk Y_2O_3.

1.2.2 The Sol-gel Process

The sol-gel process is also a controlled precipitation process. The particles formed have such small sizes that they don't precipitate but rather disperse in the solution as stable colloids (sol). The colloid particles can agglomerate with each other to form precipitate of particle networks (gel). Solubility variations with temperature can be used to prepare sol. First, the substance is dissolved in a solvent at high temperature. Then, the temperature is lowered so that the solubility limit is exceeded, and sol is uniformly created in the solution. Another way to prepare a sol is to add into a solution a reagent slowly, which is either a poor solvent or a precipitant of the solute, so that a sol forms once the solubility limit is exceeded. In sol-gel processes, precipitation conditions, such as solution pH, temperature, reagent concentration, stirring rate, addition rate, and aging time, must be controlled precisely to achieve uniform nucleation throughout the solution.

Several authors used the sol-gel method to prepare nanoparticles of Y_2O_3, Y_2O_3:Eu, and Y_2O_3:Tb. Hours and coworkers prepared submicron Y_2O_3 precipitate by adding NH_3 aqueous solution slowly into YCl_3 solution.[44] The samples they obtained were of various morphologies, and the particle sizes were very large (450 nm from light scattering). Goldburt et al. prepared Y_2O_3:Tb nanoparticles via sol-gel process.[5] They found that luminescent efficiency of the prepared phosphor samples increased with decreasing particle size from 10 nm to 4 nm. They did

[43] Kobayashi, M.: *J. Mater. Sci. Lett.* **11**, 767 (1992).
[44] Hours, T.; Bergez, P.; Charpin, J.; Larbot, A.; Guizard, C.; Cot, L.: *Ceram. Bull.* **71**, 200 (1992).

not describe the sol-gel process in detail, but it is believed that they first prepared a solution of $Y(OBu)_3$ and $Tb(OBu)_3$ in butanol.[45] Then, water was added slowly to hydrolyze the butoxide mixture to obtain Y_2O_3:Tb sol. Rao[46] tried several different precursors, such as alkoxides, nitrates, oxalates, and chlorides in the sol-gel method to prepare Y_2O_3:Eu and Y_2O_3:Tb nanoparticles. He first prepared sols of Y, Eu, and Tb hydroxides and used an ion-exchange column to eliminate cross-contamination from anions other than hydroxide. Then, Y sol and Eu (or Tb) sol were mixed. The mixtures were aged for several days. The aged sol mixtures were forced to gelatinize by slow evaporation at approximately 40 °C in a rotary evaporator. The gel was dried at room temperature to form a xerogel, which was ground into powder. The gel powder samples were further dried and annealed at elevated temperatures to calcine hydroxides into oxides. The particle sizes of the phosphors after annealing were in the range of 1 to 2 μm.

1.2.3 The Combustion Synthesis

Combustion synthesis has been used to prepare many simple and complex oxide ceramics, such as aluminates,[47] ferrites,[48] and chromites.[49] In combustion synthesis, an aqueous solution of an oxidizer, typically a mixture of metal nitrate of the metal elements in the target product, and an organic fuel, such as urea (CH_4N_2O), carbohydrazide (CH_6N_4O), or glycine ($C_2H_5NO_2$), is dehydrated and ignited in a muffle furnace or on a hot plate at temperatures less than 500 °C. The dehydrated mixture undergoes a vigorous, exothermic oxidation-reduction reaction. The heat created causes a flame for several minutes, resulting in voluminous and foamy powder product occupying the entire reaction container. The exothermic combustion reaction releases a large amount of heat, which can quickly heat up the system to reach a temperature higher than 1600 °C.[50] The combustion method results in uniform and pure powders of high surface-to-volume ratio.

The mechanism of nanoparticle formation in the combustion synthesis is complicated. Many parameters need to be considered, including the type of fuel, the fuel-to-oxidizer ratio, the

[45] Soo, Y.-L.; Huang, S.-W.; Ming, Z.-H.; Kao, Y.-H.; Smith, G. C.; Goldburt, E.; Hodel, R.; Kulkarni, B.; Veliadis, J. V. D.; Bhargava, R. N.: *J. Appl. Phys.* **83**, 5404 (1998).
[46] Rao, R. P.: *J. Electrochem. Soc.* **143**, 189 (1996).
[47] Ravindranathan, P.; Komarneni, S.; Roy, R.: *J. Mater. Sci. Lett.* **12**, 369 (1993).
[48] Zhang, Y.; Stangle, G. C.: *J. Mater. Res.* **9**, 1997 (1994).
[49] Kingsley, J. J.; Pederson, L. R.: *Mater. Lett.* **18**, 89 (1993).
[50] Kingsley, J. J.; Pederson, L. R.: *Mater. Res. Soc. Symp. Proc.* **296**, 361 (1993).

use of an assistant oxidizer, the ignition temperature, and the water content. In the combustion method used by Shea et al. to prepare Y_2O_3:Eu,[51] an aqueous solution mixture of nitrates and an fuel was heated in a muffle furnace at different temperatures. The resulting porous powder after combustion was crushed and annealed at different temperatures. The high adiabatic reaction temperature (achieved by increasing the fuel-to-oxidizer ratio), as well as post-combustion annealing, increased the crystallinity and luminous intensity of the as-prepared phosphor. The highest brightness was achieved with carbohydrazide as the fuel, which created the highest adiabatic reaction temperature (1825 °C) with an optimized furnace temperature of approximately 500 °C. The average particle size determined from XRD line-widths was around 40 to 50 nm. Ye et al. used essentially the same combustion method to prepare Y_2O_3:Eu nanocrystalline phosphor.[52] They found that lower fuel-to-oxidizer ratio (oxidizer rich) led to smaller particles. The smallest average particle size (8 nm) was found in a sample prepared from a reaction with the ratio equal to 1.0, compared with the average particle size of approximately 40 nm found in a sample from another reaction with the ratio equal to 1.3. They also found many size-dependent effects of the prepared Y_2O_3:Eu nanoparticles. For example, as particle sizes decreased, red shifts were found in the excitation spectra, as well as narrower peak widths.

1.2.4 The Electrodispersion Technique

In this technique, a pulsed DC electric field breaks a conducting aqueous solution into unstable micrometer-sized droplets in a non-conducting organic phase. The dispersed aqueous solution contains desired metal ion(s). The metal ion(s) can react with precipitants dissolved in the organic phase, such as NH_3, which can diffuse into the aqueous droplets. Since the precipitation process takes place simultaneously in billions of separated aqueous droplets, it is highly uniform. Therefore, the precipitate produced contains particles of small sizes and narrow size distribution. Another similar method is also investigated, in which a precipitant aqueous solution, such as NH_3, is dispersed in an organic phase which contains dissolved metal alkoxides. The pulsed electric field also causes coalescence of the droplets, which is minimized by using a flowing organic phase to sweep the formed aqueous droplets quickly away from the electric field. Harris et al. used this method in preparing Y_2O_3 particles, and other metal hydrous oxide

[51] Shea, L. E.; McKittrick, J.; Lopez, O. A.; Sluzky, E.: *J. Am. Ceram. Soc.* **79**, 3257 (1996).
[52] Ye, T.; Zhao, G.-W.; Zhang, W.-P.; Xia, S.-D.: *Mater. Rec. Bull.* **32**, 501 (1997).

particles, such as 1:2:3 Y, Ba, Cu complex oxide particles.[53] They successfully obtained spherical hydrous oxide particles. However, the particles were large, and the size distribution ranged from 0.1 μm to approximately 10 μm.

1.2.5 The Spray-Pyrolysis Techniques

In the spray-pyrolysis technique, a precursor solution is atomized into tiny droplets. As the solvent evaporates, tiny precursor particles of uniform sizes and shapes are produced. The precursor particles may be further pyrolyzed at elevated temperatures to obtain a desired compound. Since the particles are generated from individual aerosol droplets separated from one another in space, particle agglomeration is minimized.

Xu and coworkers[54] used a modified spray-pyrolysis technique to prepare Y_2O_3:Eu and Y_2O_3:Tb nanocrystalline phosphors. They mixed a mixed-nitrate solution of Y^{3+} and Eu^{3+} (Tb^{3+}) with supercritical CO_2 at high pressure (1500 psi) to form a microemulsion. Once the microemulsion was decompressed by release from a nozzle in an atomizer, the rapid expansion of CO_2 transformed the microemulsion into an aerosol. The aerosol was then introduced into a tube furnace, dried, and pyrolyzed (1010 °C) to form phosphor nanoparticles. Spherical particles of sizes ranging from 0.1 μm to 1.0 μm were found in the products.

Rulison and Flagan[55] used an electro-spray-pyrolysis technique to prepare nanocrystalline Y_2O_3. This technique is another modified spray-pyrolysis technique, in which electric field assistance was applied. Hydrated yttrium nitrate in normal propanol was introduced into a steel capillary (an electrode) of a specially designed atomizer, which was placed above a flat steel plate (the counter-electrode), pointing towards a hole in the plate. A voltage was applied on the two electrodes, so that the solution sprayed out of the end of the capillary was broken into charged aerosol droplets. The electrostatic-assisted spray produced a much smaller capillary jet than a common spray, so that smaller aerosol droplets were expected. The aerosol droplets were neutralized with a corona needle beneath the plate, and then carried away from under the plate into a tube furnace by purified airflow. Passing through the furnace in the flowing air, the aerosol droplets were pyrolyzed to form Y_2O_3 solid particles at 550 °C. The particles were spherical, and

[53] Harris, M. T.; Scott, T. C.; Byers, C. H.: *Mater. Sci. Eng.* **A168**, 125 (1993).
[54] Xu, C.-Y.; Watkins, B. A.; Sievers, R. E.; Jing, X.-P.; Trowga, P.; Gibbons, C. S.; Vecht, A.: *Appl. Phys. Lett.* **71**, 1643 (1997).
[55] Rulison, A. J.; Flagan, R. C.: *J. Am. Ceram. Soc.* **77**, 3244 (1994).

their sizes were several hundred nanometers. Hollow particles were found in the samples prepared from highly hydrated precursor nitrate, namely $Y(NO_3)_3 \bullet 6H_2O$. The high level of hydration caused an impermeable particle surface to the alcohol vapor inside the particles, so that the trapped vapor inflated the particle during pyrolysis, resulting in a hollow structure.

Suzuki et al. used spray-ICP (Inductively Coupled Plasma) technique in preparing nanocrystallites of several refractory metal oxides, including Y_2O_3.[56] The high temperature and high dispersing ability of this technique makes it an excellent way to prepare well-crystallized nanoparticles of refractory oxides. In this method, an aqueous salt solution (typically nitrate) containing metal ions of the target oxide was ultrasonically atomized into tiny droplets then introduced with argon carrier gas into a coil of a specially designed ICP. In the coil, the conducting droplets oscillated under oscillating electric field created by the coil and collided with each other vigorously, creating a large amount of heat. A plasma torch was formed, whose temperature can reach several thousand degrees Celsius. The droplets were dried and decomposed completely into atoms in the plasma. Then, through condensation and solidification processes, highly crystallized oxide nanoparticles were deposited on the inner surface of a quartz tube enclosing the plasma torch. The sizes of most nanocrystallites obtained were only several nanometers or several ten nanometers (< 50 nm). The nanocrystallites were of various shapes, but Y_2O_3 nanocrystallites were sphere-shaped and in monoclinic phase. The sphere-shaped morphology suggested that condensed liquid droplets coalesced into larger droplets, which then solidified into spherical particles. If the liquid droplets solidified into crystallites before coalescence, further growth of the crystallites would be through gas-solid reaction on the crystallites surfaces instead of particle coalescence, so that the shapes of the formed nanocrystallites would depend on the crystal structures of the oxides. Vogt[57] dispersed powder Y_2O_3 in Ar/O_2 carrier gas and introduced it into ICP, instead of a precursor solution. He also used hydrogen gas to quench the hot flame. The produced spherical particles were in monoclinic phase, with particle sizes ranged from 10 nm to 100 nm. Milewski[58] used microwave plasma to prepare nanocrystalline Y_2O_3:Eu, cubic phase was obtained, instead of the monoclinic phase found in spray-ICP.

[56] Suzuki, M.; Kagawa, M.; Syono, Y.; Hirai, T.: *J. Mater. Sci.* **27**, 679 (1992).
[57] Vogt, G. J.: *Proc. Electrchem. Soc.* **88-5**, 572 (1988).
[58] Milewski, P. D.: *Dissert. Abs. Inter.* **58B**, 4399 (1998).

1.2.6 The Evaporation-Condensation Processes

In the evaporation-condensation processes, metal oxide or pure metal vapors are condensed on cold surfaces where nanocrystalline metal oxides or metals are formed.

In the method designed by Skandan and coworkers to prepare nanocrystalline Y_2O_3, yttrium metal was evaporated from a resistively-heated tungsten crucible under helium.[59] Yttrium nanocrystallites were then condensed on a liquid-N_2 cold finger. Helium was then slowly replaced with pure O_2 to oxidize the metal nanoparticles. The oxidized nanoparticles were transferred into a furnace and heated under pure O_2 at 200 °C to achieve complete oxidization. Micrographs showed an average particle size of approximately 7 nm. The average particle size as well as particle agglomeration were reduced compared to a fast post-oxidation process, in which the gas replacement was much faster. XRD showed that the prepared Y_2O_3 nanocrystallites were in the monoclinic phase,[60] which is stable at high temperature and high pressure. The appearance of the monoclinic phase at low pressure (650 Pa in the chamber) was due to the Gibbs-Thomson effect: There was an additional hydrostatic pressure exerted on the nanoparticles because of their great curvatures.[61] The monoclinic phase was transformed into the cubic phase after the samples were annealed above 600 °C.

Since Y_2O_3 has very high melting point (~ 2400 °C) and boiling point (~ 4300 °C), it is difficult to evaporate Y_2O_3 directly. The energy density of a laser beam is sufficient to heat a substance in a small area up to several thousand degrees, which makes the laser a suitable energy source to evaporate refractory substances. Eilers and Tissue[62] used CO_2 laser as the heating source to evaporate bulk metal oxides to prepare nanocrystalline ZnO, Y_2O_3:Eu, and ZrO_2. In their method, the CO_2 laser beam was directed onto a pellet of bulk ceramic placed on a rotating platform in a chamber filled with N_2 gas. A cold finger was placed approximately 2 cm above the pellet, so that vaporized species could condense on the cold surface to form nanocrystallites. They obtained network-like aggregates of distinct Y_2O_3:Eu nanocrystallites. The average particle sizes varied with the background N_2 pressure. As the pressure increased from 1 Torr to 400 Torr,

[59] Skandan, G.; Hahn, H.; Parker, J. C.: *Scripta Metallurgica et Materialia* **25**, 2389 (1991).
[60] Skandan, G.; Foster, C. M.; Frase, H.; Ali, M. N.; Parker, J. C.; Hahn, H.: *NanoStruct. Mater.* **1**, 313 (1992).
[61] Porter, D. A.; Easterling, K. E.: In *Phase Transformations in Metals and Alloys 2nd ed.,* Chapman & Hall, New York, 46 (1992).
[62] Eilers, H.; Tissue, B. M.: *Mater. Lett.* **24**, 261 (1995).

the average particle sizes increased from 4 nm to 18 nm for Y_2O_3. Large nanocrystallites (> 7 nm) were in the high-pressure monoclinic phase, but smaller particles were in the cubic phase.[62]

Günther and Kumpmann[63] used a different energy source, an electron beam, to evaporate bulk Y_2O_3. Bulk Y_2O_3 material was placed on a water-cooled stage in a chimney-like chamber filled with 1 mb helium and bombarded by a 45 kV electron beam from an electron gun. Y_2O_3 nanocrystallites were deposited on the cooling chamber walls. Y_2O_3 nanocrystallites (4-6 nm) in network aggregates were found in the prepared samples, which were in cubic phase, consistent with the observation of Eilers and Tissue.[62] They also found that particle sizes were relatively insensitive to the gas pressure in the range of 1 mb to 5 mb, which was also consistent with Eilers and Tissue's results, as 5 mb is only 3.8 Torr. This observation indicated that the coalescence stage of particle growth was stopped shortly after the nucleation stage, which leaded to network aggregates rather than larger particles.

1.3 The Reverse Micelle Approach

In the reverse micelle method, precipitation process is forced to occur simultaneously in billions of tiny reverse micelles dispersed spontaneously in an organic solvent. Therefore, the precipitation is very uniform. Comparing with other methods used to Y_2O_3 nanomaterials synthesis, the reverse micelle method has some advantages. The equipment needed is very simple, just some flasks and stirrers. Reverse micelle synthesis is usually carried out at room temperature and ambient pressure. High vacuum, high temperature, or high pressure are not needed. Therefore, this method is easily scaled up for commercial production. However, like the products prepared from homogeneous precipitation and sol-gel process, nanoparticles of Y_2O_3 prepared from reverse micelles are poorly crystallized, which is detrimental to most applications. High-temperature annealing is necessary to improve the crystallinity. Annealing usually leads to larger particle aggregates, which are also unwanted. If these problems can be overcome, the reverse micelle method will be an excellent method to prepare Y_2O_3 and related nanomaterials.

1.3.1 Reverse Micelles as Microreactors

Surfactant molecules are composed of both hydrophilic groups and hydrophobic groups. Usually, the hydrophobic groups are long aliphatic chains. When surfactant molecules are

dissolved in a non-polar solvent, such as cyclohexane, the hydrophobic groups remain in the solution due to favorable interactions with the non-polar solvent, while the hydrophilic groups tend to escape from the organic phase due to unfavorable interactions. As a compromise, many surfactant molecules gather at the surface of the organic phase so that the hydrophilic groups emerge from the organic phase surface into the air. When the concentration of the surfactant is higher than its Critical Micelle Concentration (CMC), the entire organic phase surface is covered with a layer of surfactant molecules. Most extra surfactant molecules in the organic phase gather to form a great number of molecular aggregates, with their hydrophilic groups inward (Figure 1.1). In this way, the hydrophilic groups do not contact the non-polar solvent, so that the system energy is minimized. The aggregates are called reverse micelles. The structure of a reverse micelle formed by AOT molecules (diisooctyl sodium sulphosuccinate) is shown in Figure 1.2.[64] If surfactant of high concentration (> CMC) is put in a polar solvent, such as water, some surfactant molecules form micelles in the polar solvent, with their hydrophobic groups inward.

Because of the nature of reverse micelles addressed above, a polar phase, such as an aqueous solution, can be put in the reverse micelles. Therefore, with the protection of the surfactant molecule shells, a polar phase can be dispersed spontaneously in a non-polar phase as billions of tiny droplets. The dimensions of reverse micelles are typically only several nanometers. Their shape is spherical when the surfactant concentration is not too high.[65] Assuming a spherical shape, the average radius of the reverse micelles, R_{rm}, containing only water molecules is given as:

1.1

$$R_{rm} = \frac{3V_{aq}[H_2O]}{\sigma[S]}$$

where V_{aq} is the volume of a water molecule, σ is the area of the polar head of a surfactant molecule.[66] V_{aq} and σ are constants for a specific reverse micelle system. Therefore, the average size of reverse micelles is proportional to the water/surfactant molar ratio. Reverse micelles also have very narrow size distributions, which follow the Poisson distribution:

1.2

$$P_j = \frac{n^j e^{-n}}{j!}$$

[63] Günther, B.; Kumpmann, A.: *NanoStruct. Mater.* **1**, 27 (1992).
[64] Bru, R.; Sánchez-Ferrer, A.; García-Carmona, F.: *Biochem. J.* **310**, 721 (1995).
[65] Lindman, B.; Wennerström, H.: *Topics in Current Chemistry* **87**, Springer-Verlag, New York, 1 (1980).

where P_j is the probability of a reverse micelle containing j molecules and n is the average number of molecules per reverse micelle.[67]

Due to their nanoscopic sizes, reverse micelles are subject to Brownian motion, which causes frequent collisions among reverse micelles. When micellar content is liquid, their structures are not rigid, and the surfactant shells are mobile. Therefore, rapid exchange occurs among reverse micelles during Brownian collisions.[64] In the reverse micelle system of AOT/isooctane, the rate is on the order of $10^6 \sim 10^8$ $M^{-1}s^{-1}$ at room temperature.

There are three content exchange mechanisms[64]. In the first mechanism, two reverse micelles may combine together during a collision, and the surfactant shells between them may be removed. Therefore, the two reverse micelles coalesce as a larger one and their contents are mixed. However, the coalescence is only temporary. The Poisson-type thermodynamic size distribution of reverse micelles indicates that reverse micelles of sizes much greater than the mean size tend to separate into small ones of sizes close to the mean size. If the coalescence does not happen, content exchange can still occur through the second mechanism, in which species on reverse micelle shells can diffuse from one to the other during the combination of two reverse micelles. In the third content exchange mechanism, there is no reverse micelle combination. Content exchange is achieved through diffusion of solute in the aqueous droplets or in the organic phase into or out of the reverse micelles, though it may not be soluble in the other phase.

All these features (very small sizes, uniform shape, narrow size distribution, mobile structure, and fast content exchange) make reverse micelles ideal nanoscopic reactors. A reaction can be carried out simultaneously in billions of such reactors. If a precipitation reaction occurs simultaneously in billions of similar nanometer-sized reactors, billions of product particles are created simultaneously. Reverse micelles have nanometer-scale sizes and the size distribution is very narrow, so the number of reactant molecules per reverse micelle is about the same. Therefore, precipitate particles also have nanometer-scale sizes and uniform size distribution.

There are three ways to carry out a precipitation reaction in reverse micelles.[68] First, if both reactants are only soluble in water, one reactant is dissolved in aqueous droplets in one reverse micelle solution, and the other reactant in aqueous droplets in another reverse micelle solution. The two reverse micelle solutions are then mixed, so that precipitation reaction occurs

---

[66] Pileni, M. P.: *J. Phys. Chem.* **97**, 6961 (1993).
[67] Atik, S. S.; Thomas, J. K.: *J. Am. Chem. Soc.* **103**, 3543 (1981).
[68] Osseo-Asare, K.; Arriagada, F. J.: *Ceram. Trans.* **12**, 3 (1990).

when the two kinds of reactant molecules encounter one another through content exchange. Second, if one reactant is soluble in the organic phase, the other reactant can be dissolved in aqueous droplets in a reverse micelle solution, and the soluble reactant is dissolved in the continuous organic phase. Precipitation occurs when the soluble reactant molecules diffuse into the reverse micelles. Third, if a precipitation reaction is initialized by incident energies (heat, light, and so on), the reactant(s) can be simply dissolved in the aqueous droplets in a reverse micelle solution. The reaction occurs upon heating or irradiation.

1.3.2 Examples of Reverse Micelle Syntheses

Because of its aqueous-phase-in-organic-phase nature, the reverse micelle method is often used to prepare nanoparticles of inorganic materials. Many inorganic materials,[68] including metals (Pt, Pd, Rh, Ir, Au, Co,[69] Cu,[70] Ag[71]), metal borides (Ni_2B, Co_2B, Fe_2B), metal sulfides, selenides, tellurides, and related composites (CdS, PbS, CuS, CdSe, In_2S_3, Ag_2S,[72] CdTe,[73] $Cd_yZn_{1-y}S$[74]), metal salts (AgCl, $CaCO_3$, $BaCO_3$, $SrCO_3$, $CuSO_4 \cdot 5H_2O$, $Zn_3(PO_4)_2$[75]), zeolites,[76] as well as oxides, hydroxides, and complex oxides (TiO_2, SiO_2, CeO_2, ZrO_2, Fe_3O_4, $Al(OH)_3$, $Zn(OH)_2$,[77] titanates and zirconates[78]) have been prepared by the reverse micelle method. Key examples of preparing nanometer-sized oxide materials in reverse micelles are illustrated below.

Fang and coworkers prepared ZrO_2 nanoparticles in reverse micelle solution.[79] They used mixed non-ionic surfactant of poly(oxyethylene)$_5$nonyl phenol ether (NP-5) and poly-(oxyethylene)$_9$nonyl phenol ether (NP-9). The non-polar phase was cyclohexane, and the polar phase was an aqueous solution of $ZrO(NO_3)_2$ or oxalic acid. Two methods were studied. The single microemulsion method was to add oxalic acid aqueous solution drop by drop into a reverse micelle solution containing $ZrO(NO_3)_2$ aqueous solution. The double microemulsion

[69] Chen, J.-P.; Sorensen, C. M.; Klabunde, K. J.; Hadjipanayis, G. C.: *J. Appl. Phys.* **76**, 6316 (1994).
[70] Lisiecki, I.; Pileni, M.-P.: *J. Phys. Chem.* **99**, 5077 (1995).
[71] Petit, C.; Lixon, P.; Pileni, M.-P.: *J. Phys. Chem.* **97**, 12974 (1993).
[72] Motte, L.; Billoudet, F.; Pileni, M.-P.: *J. Mater. Sci.* **31**, 38 (1996).
[73] Murray, C. B.; Norris, D. J.; Bawendi, M. G.: *J. Am. Chem. Soc.* **115**, 8706 (1993).
[74] a) Hirai, T.; Shiojiri, S.; Komasawa, I.: *J. Chem. Eng. Jpn.* **27**, 590 (1994); b) Cizeron, J.; Pileni, M.-P.: *J. Phys. Chem.* **99**, 17410 (1995); c) Qi, L.-M.; Ma, J.-M.; Cheng, H.-M.; Zhao, Z.-G.: *Colloids and Surfaces A.* **111**, 195 (1996).
[75] Dutta, P. K.; Jakupca, M.; Satya, K.; Reddy, N.; Salvati, L.: *Nature* **374**, 44 (1995).
[76] Dutta, P. K.; Robins, D.: *Langmuir* **7**, 1048 (1991).
[77] Sager, W.; Eicke, H.-F.; Sun, W.-L.: *Colloids and Surfaces A.* **79**, 199 (1993).
[78] Herrig, H.; Hempelmann, R.: *NanoStruct. Mater.* **9**, 241 (1997).
[79] Fang, J.-Y.; Wang, J.; Ng, S.-C.; Chew, C.-H.; Gan, L.-M.: *NanoStruct. Mater.* **8**, 499 (1997).

method was to mix two reverse micelle solutions, one containing $ZrO(NO_3)_2$ and the other containing $H_2C_2O_4$. Prepared oxalate nanoparticles were dried at 90 °C and then annealed at 600°C for 4 h to form ZrO_2 nanoparticles. BET analysis showed that the ZrO_2 nanoparticles from both methods had similar average particle sizes of 20-40 nm. However, a laser scattering technique indicated that particle aggregation was much greater in the samples from the single microemulsion method than those from the double microemulsion method. The ZrO_2 samples from the single microemulsion method contained both tetrahedral phase and monoclinic phase, but those from the double microemulsion method were only in the tetrahedral phase. It was believed that smaller aqueous droplets in the double microemulsion method resulted in smaller oxalate particles, which became smaller oxide particles after annealing. Small enough ZrO_2 crystallites are stable in the metastable tetrahedral phase due to the high surface area.[80]

Yang and Chen[81] attempted to prepare Y_2O_3 or CeO_2 stabilized ZrO_2 nanoparticles in AOT/isooctane reverse micelles. $ZrOCl_2$, $Y(NO_3)_3$, and $Ce(NO_3)_3$ were used. NH_3 was the precipitant. Similar to Fang et al.,[79] they also used the two methods. They found that precipitate samples taken out soon after completion of the mixing process were amorphous with flocculent morphology. Very fine nanoparticles (< 3 nm) were found in the precipitate by re-examining the micrographs under an optical photo-stereo microscope. After annealing at 600 °C for 3 h, the products contained aggregates of particles with average particle sizes in the range of 13 nm to 15 nm. Particle agglomeration in the dried samples was attributed to the presence of residual AOT molecules bound with water molecules, which were not easily eliminated at room temperature. They also thought that water molecules facilitated particle agglomeration during annealing.

CeO_2 nanoparticles were prepared in n-hexanol/Polyoxyethylene(10) octylphenyl ether (OP-10)/cyclohexane reverse micelles through the reaction of cerium nitrate and ammonia[21] using the double microemulsion method. When the surfactant concentration was low, a systematic color change of the reverse micelle solution after mixing was observed, from colorless to translucent to orange to purple to pale purple and finally to light yellow. A final freeze-dried product was light brown. However, when the surfactant concentration was high, though the final product was also light brown, there was no color change in the system upon aging. The concentrated surfactant molecules covered surfaces of the translucent single

[80] Garvie, R. C.: *J. Phys. Chem.* **69**, 1238 (1965).
[81] Yang, C.-F.; Chen, J.-Y.: *J. Mater. Sci. Lett.* **16**, 936 (1997).

nanoparticles and inhibited the formation of nanoparticle aggregates of orange appearance. The prepared CeO_2 nanoparticles were in cubic phase. The particle size distributions of samples prepared with different conditions all fell in the range of 1.5 nm to 6.0 nm. The average particle size increased from 2.6 nm to 4.1 nm, when the water/surfactant ratio increased from 0.5 to 15, but it was almost a constant when the ratio was greater than 9. When the ratio was set at 15 and the cerium nitrate concentration increased from 0.093 M to 0.93 M, the average particle size increased from 3.4 nm to 4.1 nm. Higher water/surfactant ratio and higher cerium nitrate concentration produced a greater number of reactant species per reverse micelle, which produced larger particles. The authors credited the invariance of average particle sizes in the samples prepared with the ratio greater than 9 to multi-particle formation in one reverse micelle.[21]

Hirai et al. prepared TiO_2 nanoparticles in an AOT/isooctane reverse micelle solution and studied the particle formation mechanism.[82] They dissolved titanium tetrabutoxide (TTB) in a reverse micelle solution containing a certain amount of water. Hydrolysis of the TTB molecules diffused into the reverse micelles resulted in TiO_2 nanoparticle formation. They found that higher water content (water/AOT ratio) or higher TTB concentration favored TiO_2 nanoparticle formation. This observation was consistent with Masui and coworkers' results on CeO_2,[21] as higher water content and higher TTB concentration led to more TTB molecules per reverse micelle, so that nucleation in the reverse micelle was easier. From in situ UV absorption study, they derived a kinetic model for TiO_2 precipitate formation:

$$-\frac{dN_h}{dt} = n\frac{dN_p}{dt} + k_G\frac{N_h N_p}{N_m} + \frac{dN_{TTB}}{dt} \qquad 1.3$$

where N_h is the number of hydrolyzed TTB molecules, N_P is the number of formed nuclei, N_m is the number of reverse micelles, N_{TTB} is the number of TTB molecules, n is the minimum number of hydrolyzed TTB molecules required to for a nucleus, and k_G is the rate constant taking into account the probability of the particle growth. The model fit the experimental data well.

Osseo-Asare and Arriagada prepared nanoparticles of SiO_2 in a non-ionic surfactant/ cyclohexane reverse micelle solution.[83] The non-ionic surfactant used was Igepal CO-520, which is a polydispersed preparation of polyoxyethylene nonylphenyl ether with an average of 5 oxyethylene groups per molecule [4-$(C_9H_{19})C_6H_4O(CH_2CH_2O)_4CH_2CH_2OH$]. Tetraethoxysilane

[82] Hirai, T.; Sato, H.; Komasawa, I.: *Ind. Eng. Chem. Res.* **32**, 3014 (1993).
[83] Osseo-Asare, K.; Arriagada, F. J.: *Colloids and Surfaces* **50**, 321 (1990).

(TEOS) was dissolved in a reverse micelle solution containing aqueous ammonia. TEOS molecules that diffused into the reverse micelles underwent hydrolysis. Bluish white opalescence appeared after a few hours of addition of TEOS. The dispersion was stable even after several months of preparation. The nanoparticles prepared were essentially monodispersed and sphere-shaped, forming an ordered, two-dimension particle assembly on a TEM grid after evaporation of solvent. The nanoparticles were in the range of 50 nm to 70 nm, with a standard deviation less than 8.5%. The average particle size decreased (71.6 nm to 48.5 nm) with increasing water/surfactant ratio (0.7 to 2.3). This observation was exactly the opposite of the observations on CeO_2 and TiO_2 nanoparticles. They attributed this contradiction to the different behavior of TEOS compared to the other precursors in a similar reverse micelle system. Particle growth has two mechanisms, one is by addition of monomers to existing particles, and the other is by inter-micelle contact causing aggregation of nuclei. Since hydrolysis of TEOS is very quick, the particle growth (condensation reaction) is diffusion-controlled. Due to high concentration of reverse micelles, particle growth by inter-micelle coalescence was favored when the water/surfactant ratio was low, so large particles formed.

1.4 General Experimental Approach in the Research

AOT is the commercial name for diisooctyl sodium sulphosuccinate (Figure 1.3). AOT/isooctane is a commonly used reverse micelle system in inorganic nanomaterials synthesis. The truncated cone shape of AOT molecules makes it suitable for the packing geometry of surfactant molecules to form reverse micelles.[66] Therefore, AOT/isooctane was chosen as the reverse micelle system in this research. Two methods to prepare yttrium oxide nanoparticles in reverse micelles were studied in this research: hydrolysis of $Y(NO_3)_3$ in ammonia solution and hydrolysis of $Y(O^iPr)_3$. There are some advantages in the nitrate-hydrolysis method. The precursors are cheap, which makes the cost low. The reactants are stable and easy to handle, which makes the operations very simple. Therefore, if this research demonstrates that yttrium oxide nanoparticles of high quality can be produced from this method, it will be excellent for future commercialization.

In the isopropoxide-hydrolysis method, yttrium isopropoxide, which is expensive and moisture-sensitive, was used as the precursor. Special equipment (glovebox) is needed to handle this chemical to avoid any unwanted hydrolysis before its final expected hydrolysis in reverse

micelles. Therefore, the isopropoxide-hydrolysis method is more expensive and more operationally difficult than the nitrate-hydrolysis method. A comparison of yttrium oxide nanoparticle formation using this method to that using the nitrate-hydrolysis method is important, because it might provide useful information about yttrium oxide nanoparticle formation mechanism in reverse micelles.

Chemicals used in this research were: 99.9% $Y(NO_3)_3 \cdot 6H_2O$, 99.9% $Eu(NO_3)_3 \cdot 5H_2O$, 99+% isooctane, and solid AOT from Aldrich, 20~25wt.% $Y(O^iPr)_3$ in toluene from Alfa, 14.8 M aqueous ammonia from Fisher, and 95% ethanol from AAPER Alcohol and Chemical Co. Toluene from Aldrich was dried by passage through activated alumina. All chemicals except toluene were used without further purification. Deionized water was prepared by passing distilled water through a Sybron-Barstead Nanopure II water purification system.

In the nitrate-hydrolysis method, $Y(NO_3)_3$ solutions of different concentrations were prepared in deionized water. NH_3 solutions of different concentrations were prepared by diluting 14.8 M NH_3 with deionized water. AOT/isooctane reverse micelle solutions were prepared by dissolving solid AOT in isooctane. Every prepared solution was filtered through a 0.2-μm Teflon filter (Spartan-T) from Aldrich attached to a glass syringe to remove any insoluble impurities in the solutions.

The general experimental procedure for the nitrate-hydrolysis method follows. Some $Y(NO_3)_3$ aqueous solution was measured with a syringe and injected into 50 mL of AOT/isooctane reverse micelle solution in a sealable glass bottle. Magnetic stirring at room temperature was applied to the solution until it turned clear. In cases when the water/AOT ratios were high, it took more than one day for the solution to become clear. An NH_3 solution of the same volume as the $Y(NO_3)_3$ solution was dissolved in another AOT/isooctane reverse micelle solution (same volume and concentration as that containing $Y(NO_3)_3$). The dissolving process was very quick with magnetic stirring for the NH_3 solution, even at high water/AOT ratios. Some bubbles appeared during dissolving when the ratio was high. The two reverse micelle solutions were mixed in a glass bottle under mild magnetic stirring by using a pipette to add the reverse micelle solution containing NH_3 into the reverse micelle solution containing $Y(NO_3)_3$. The mixture usually turned turbid during mixing. The turbidity was white. The mixture was aged in the capped glass bottle with continuous magnetic stirring for a period of time ranging from one hour to five days after mixing. No obvious change of color was observed during aging.

Precipitate would slowly settle on the bottom of the bottle if magnetic stirring was stopped, leaving the upper solution clear. Except for those specially mentioned, the experiments were carried out at room temperature.

After aging, the suspension containing the precipitate was centrifuged in plastic tubes at approximately 5000 rpm in a Fisher 225 centrifuge for approximately 5 min. The clear AOT/isooctane supernatant was decanted with a pipette and discarded. The precipitate was a semi-transparent gel-like white material. It was then washed and refluxed with various solvents. Solvents were then separated out by centrifuging. A typical procedure was that the precipitate was roughly washed in 20 mL ethanol twice in a tube by pipette bubbling and stirring. The precipitate was then transferred to a round-bottomed flask and refluxed with 20 mL deionized water for an hour. After centrifuging to separate out the water solvent, the reflux process was repeated two more times. The washed precipitate was dried at approximately 80 °C overnight. White product (or light yellow, brown) was obtained as blocks. The product was roughly ground into powder in an Al_2O_3 mortar for several minutes. Annealing experiments of the dried samples were carried out in a muffle furnace (Thermolyne 47900) to study the effects of annealing temperature and time on the as-prepared yttrium oxide nanoparticle samples.

In the isopropoxide-hydrolysis method, the commercial 20~25wt.% yttrium isopropoxide in toluene was 1:4 diluted with anhydrous toluene in a glovebox. AOT/isooctane reverse micelle solutions were prepared by dissolving solid AOT in isooctane.

The general experimental procedure for the isopropoxide-hydrolysis method follows. Deionized water (or aqueous ammonia) was measured with a syringe and injected into 50 mL of 0.1 M AOT/isooctane reverse micelle solution in a sealable glass bottle. Magnetic stirring at room temperature was applied to the solution, which turned clear quickly. 1:4 diluted yttrium isopropoxide/toluene solution was measured with a syringe and added quickly into the reverse micelle solution containing deionized water (or aqueous ammonia) in a glass bottle under mild magnetic stirring. The mixture turned turbid quickly during the addition. The turbidity was white. The mixture was aged in the sealed glass bottle with continuous magnetic stirring for a period of time ranging from one hour to five days after the addition. No obvious change of color was observed during aging. Precipitate would slowly settle on the bottom of the bottle, if magnetic stirring was stopped, leaving the upper solution clear. Except those for specially mentioned, experiments were carried out at room temperature. After aging, the product of an

experiment was treated the same way as that described in the experimental procedure of the nitrate-hydrolysis method.

1.5 Characterization

The prepared samples were characterized by different analysis techniques, including X-ray Powder Diffraction (XRD), Transmission Electronic Microscopy (TEM), and Scanning Electronic Microscopy (SEM).

XRD samples were prepared by putting some powder sample, either a dried as-prepared sample or an annealed sample, on a quartz plate. The powder was lightly pressed with a steel spatula to form a flat thin layer. As a batch of sample was not enough to cover the whole surface of a quartz plate, a powder sample was placed only on the center part of a quartz plate. Sample rotation was applied to average out any inhomogenueity of the sample layer. The instrument used was Scintag 2000 diffractometer. The 2θ range monitored was from 10º to 70º, which includes all major diffraction peaks of cubic Y_2O_3. Two sets of slits were used: set (3, 4, 2, 1) for broad-peak patterns of the as-prepared samples and samples annealed at low temperatures, and set (2, 4, 1, 0.5) for narrow-peak patterns of the samples annealed at high temperatures. Scanning rate and step size were adjusted to achieve good signal-to-noise ratios. Generally, a low scanning rate (0.5º/min) and large step size (0.1º) were used for broad-peak patterns, while a high scanning rate (2º/min) and small step size (0.05º or 0.03º) were used for narrow-peak patterns. Average particle sizes were calculated from peak broadening of the diffraction peaks by a built-in software based on the Scherrer equation in the operating system of the diffractometer.

TEM experiments were carried out on a Phillips EM420. The operating voltage was set at 100 kV for all experiments. All TEM specimens were deposited on 300-mesh Formvar carbon-coated Cu grids from SPI Supplies. In cases of as-prepared samples, a little mixture from an experiment was taken out with a pipette, put in a centrifuging tube, and then centrifuged. The clear supernatant was decanted and discarded. The precipitate was first roughly washed in several milliliters of ethanol twice in the tube by pipette stirring and bubbling, and then roughly washed twice in several milliliters of deionized water. Ethanol and water were separated from the precipitate by centrifuging after each washing step. A TEM specimen was prepared by dropping one or two drops of suspension of the washed precipitate in water on a Cu grid placed on a clean glass slide. The grid was then covered with a beaker and dried in the air at room

temperature. In cases when precipitates were only ethanol-washed, ethanol was used as the dispersing solvent instead of water. In cases of annealed samples, a little annealed sample was put in some deionized water in a 10-mL beaker and then ultrasonicated for 10 min in a Branson 1510 sonicator. A TEM specimen was prepared by dropping one or two drops of suspension of the annealed sample dispersed in water on a Cu grid on a clean glass slide. The grid was then covered with a beaker and dried naturally in the air at room temperature.

SEM specimens were prepared by putting a little dried sample, either as-prepared or annealed, on an adhesive conducting tape adhered to a silver sample holder. As the purpose of SEM analysis was simply to determine element composition from the Energy Dispersing Spectra (EDS), the specimens were not coated with any conducting film. The instrument used was an ISI SX-40, which was operated at 20 kV. The operating vacuum was $5*10^{-5}$ Torr. The EDS equipment used was Noran 5402.

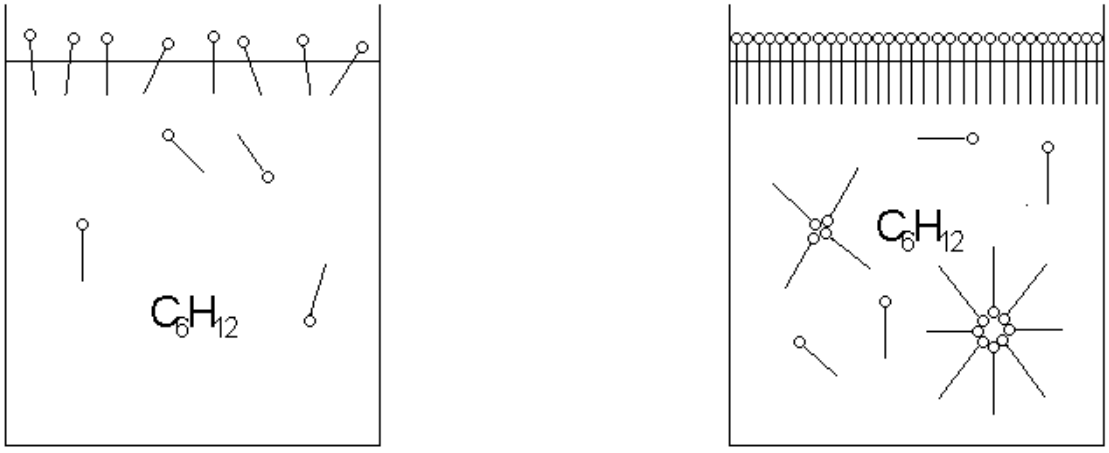

C < CMC **C > CMC**

Figure 1.1

Formation of Reverse Micelles in Non-polar Solvent

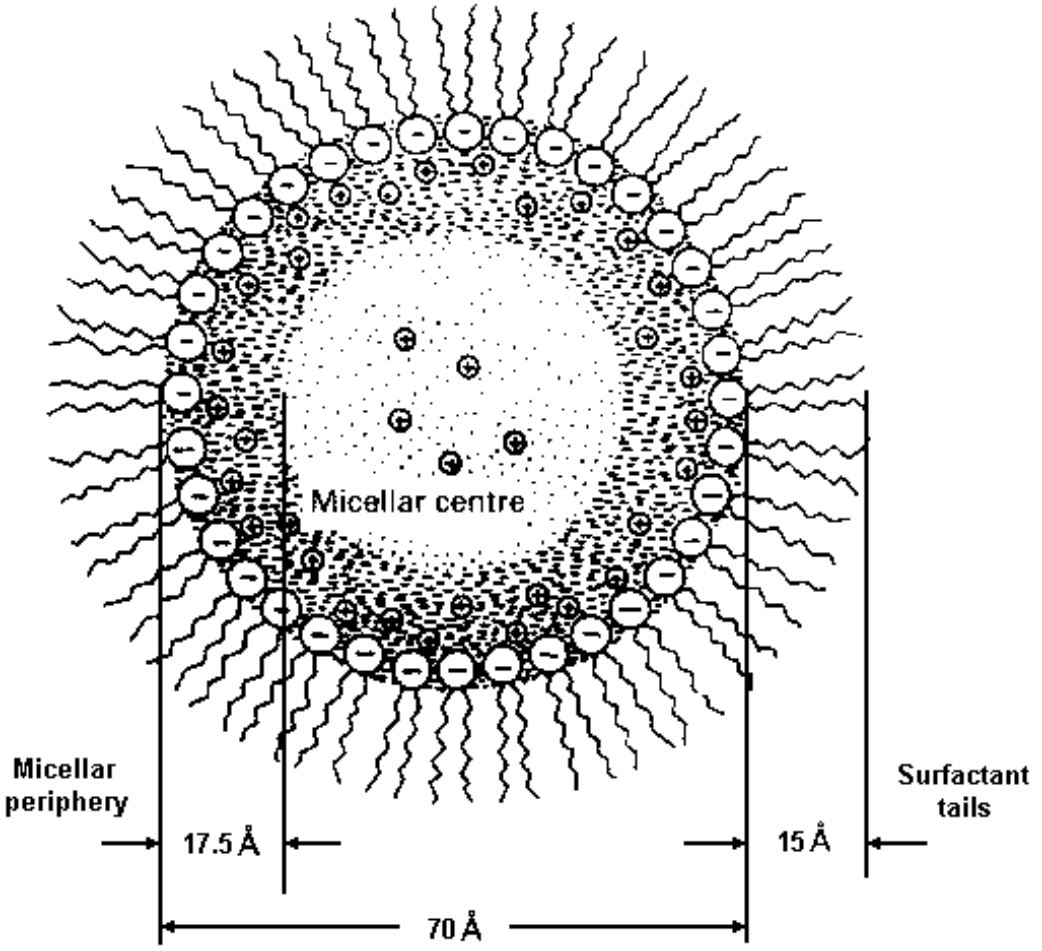

Figure 1.2

Structure of a Reverse Micelle formed by AOT molecules[64]

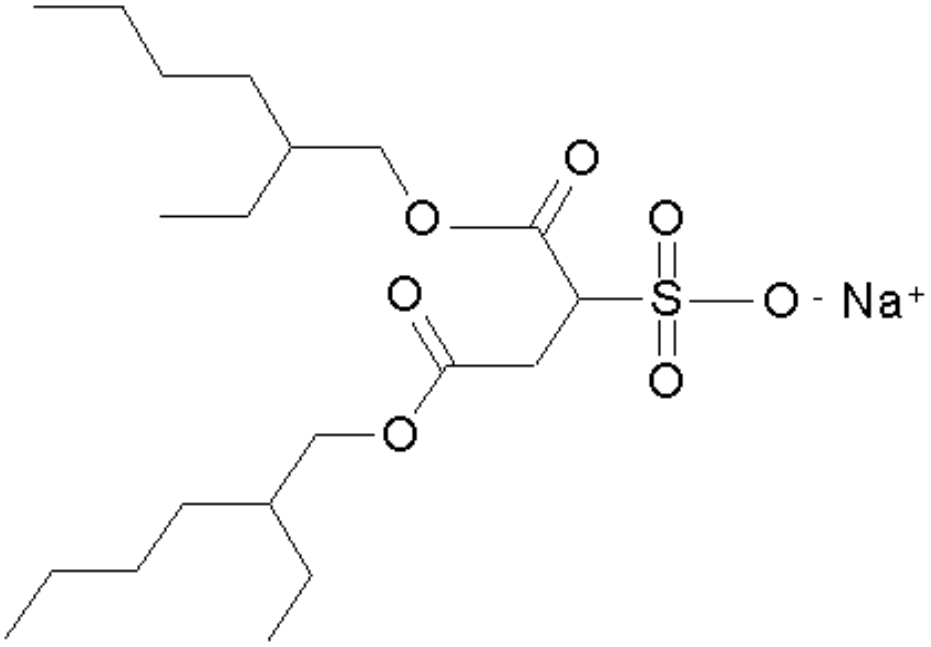

Figure 1.3

Structure of an AOT Molecule

Chapter Two:
Nitrate-Hydrolysis Method

Nitrate hydrolysis is a common reaction used to prepare metal hydroxide and oxide nanomaterials in reverse micelles.[21,84,85] The advantage of the nitrate-hydrolysis method is that the precursors are so cheap and easily handled that experimental operations are affordable and simple. Part of my research investigated the feasibility of preparing yttrium oxide nanoparticles using this method. Content exchange between the aqueous yttrium nitrate solution and the aqueous ammonia solution in the reverse micelles increases the pH value of the aqueous phase, which results in the hydrolysis of Y^{3+}:

$$Y(NO_3)_3 + 3NH_3 + 3H_2O = Y(OH)_3 + 3NH_4NO_3$$

Incomplete hydrolysis of Y^{3+} is also possible:

$$Y(NO_3)_3 + 2NH_3 + 2H_2O = Y(OH)_2^{+} + 2NH_4NO_3$$

$$Y(NO_3)_3 + NH_3 + H_2O = Y(OH)^{2+} + NH_4NO_3$$

If the concentrations of the hydrolyzed species ($Y(OH)_3$, $Y(OH)_2^{+}$, and $Y(OH)^{2+}$) are sufficiently high, a condensation reaction causes Y-O-Y bond formation among the hydrolyzed species:

$$(OH)_xY(OH)^{(2-x)+} + (OH)Y(OH)_y^{(2-y)+} = (OH)_xY\text{-}O\text{-}Y(HO)_y^{(4-x-y)+} + H_2O \quad (x, y = 0, 1, 2)$$

When sufficient Y-O-Y bonds form among hydrolyzed species, clusters of yttrium oxide/hydroxide form. The size of such a cluster is only several angstroms or nanometers. Further growth or aggregation of the clusters results in the nanoparticle product.[86,87]

There are two methods for carrying out metal-nitrate hydrolysis reaction in reverse micelles.[68] One method is to dissolve aqueous solutions of a metal nitrate and a base (usually NH_3) in two separate reverse micelle solutions and then to mix the two solutions. Content exchange during reverse micelle collisions leads to the hydrolysis of the metal nitrate, and subsequently, the condensation of the hydrolyzed species to form nanoparticles. The second method is to dissolve an aqueous solution of a metal nitrate in a reverse micelle solution and to mix it with an aqueous solution of a base (usually NH_3) or to bubble NH_3 gas through the reverse micelle solution. NH_3 molecules enter the reverse micelles containing the metal nitrate by

[84] Ward, A. J. I.; Friberg,S. E.: *MRS Bull.* **14(12)**, 41 (1989).
[85] Smith, R. D.; Matson, D. W.; Fulton, J. L.: *Mater. Lett.* **6**, 31 (1987).
[86] In *Gmelin Handbuch Der Anorganischen Chemie 8th ed.* **39(B7)**, Springer-Verlag, New York, 17 (1979).
[87] In *Gmelin Handbuch Der Anorganischen Chemie 8th ed.* **39(C2)**, Springer-Verlag, New York, 27 (1974).

diffusion and initiate the hydrolysis and condensation reactions to form nanoparticles. For operational convenience, the first method was adopted in this research. The detailed procedure is described in Section 1.4.

As shown in Section 1.3.2, the water/AOT ratio, the metal cation concentration, the NH_3 concentration, the surfactant concentration, and the aging time are important experimental parameters in the synthesis of metal oxide nanoparticles in reverse micelles. For instance, Masui and coworkers found that low surfactant concentration caused systematic color change of cerium oxide colloids in the reverse micelles during aging.[21] This color change process was not observed at high surfactant concentration. When the water/surfactant ratio increased from 0.5 to 15, the average particle sizes increased from 2.6 nm to 4.1 nm. However, when the ratio was greater than 9, average particle sizes were almost a constant. When the ratio was 15, and the cerium nitrate concentration increased from 0.093 M to 0.93 M, the average particle sizes increased from 3.4 nm to 4.1 nm. Hirai and coworkers found that higher water content (water/AOT ratio) or concentration of titanium tetrabutoxide favored TiO_2 nanoparticle formation.[82] Therefore, it is important to investigate the effects of these experimental parameters on yttrium oxide nanoparticles formed in reverse micelles.

2.1 Effects of Varying the Water/AOT Ratio

In this research, the water/AOT ratio in a reverse micelle solution was estimated in the following way. The volume of an aqueous solution added into an AOT/isooctane reverse micelle solution was estimated as the volume of water in the aqueous solution. Since reactions were carried out at room temperature, the number of milliliters of water was estimated as the number of grams of water. Then the number of moles of water molecules in the aqueous solution was calculated from the number of grams of water. This value was then divided by the number of moles of AOT molecules in the reverse micelle solution, and the water/AOT ratio was thus approximately calculated.

Equation 1.1 shows that the water/AOT ratio determines the average reverse micelle size in a reverse micelle solution. In the AOT/isooctane reverse micelle system, the relation between the water/AOT ratio (w) and the average reverse micelle size (R_w) is:[66]

$$R_w\ (\text{Å}) = 1.5\ w \qquad 2.1$$

The water/AOT ratio has an upper-limit in a reverse micelle system. The maximum w in the reverse micelle system of pure water/AOT/isooctane is approximately 60.[88] If too much water is added to a reverse micelle solution causing w to be greater than the maximum value, the reverse micelle solution is no longer stable, and phase separation occurs. The maximum w is affected by the ionic strength of the water content.[89] Preliminary experiments indicated that as the concentration of the $Y(NO_3)_3$ aqueous solution increased, the maximum w value that could be achieved in a uniform AOT/isooctane reverse micelle solution decreased. A water/AOT ratio of approximately 15 was achieved with 0.1 M $Y(NO_3)_3$ aqueous solution in 0.1 M AOT/isooctane reverse micelle solution. However, if the aqueous phase was 0.5 M $Y(NO_3)_3$ in 0.1 M AOT/isooctane, a uniform reverse micelle solution with a water/AOT ratio of only approximately 7.5 was slowly formed after overnight stirring at room temperature. Yang and Chen also found that the maximum w they could achieve in a uniform AOT/isooctane reverse micelle solution decreased with increasing salt concentration.[81]

A frustrating phenomenon was observed in this research. 0.5 M $Y(NO_3)_3$ could not form uniform w = 1 reverse micelle solution with 0.1 M AOT/isooctane. The aqueous phase could not dissolve completely in the reverse micelle solution even after long-term stirring at room temperature. However, if more 0.5 M $Y(NO_3)_3$ aqueous solution was added so that w was equal to or greater than three, a uniform reverse micelle solution formed after short-term stirring.

A series of experiments was conducted with different water/AOT ratios (w = 3, 7.5, and 15), in which other experimental parameters were kept as constants: $[Y^{3+}]$ = 0.1 M, $[NH_3]$ = 5 M, and [AOT] = 0.1 M. The precipitate-appearance time in the experiments using different w values were different. In the w = 15 experiment, the solution turned turbid before the addition of 50% volume of a reverse micelle solution containing NH_3. However, in the w = 7.5 experiment, the solution was only slightly turbid upon completion of the addition, and in the w = 3 experiment, the solution was never turbid after five days of stirring from the time the reverse micelle solution containing NH_3 was added.

Since a higher water/AOT ratio implied that there were more NH_3 and Y^{3+} species in each reverse micelle, and more hydrolyzed species were produced in a single content exchange by a collision between two reverse micelles containing the two different reactants in a reverse

[88] In *Structure and Reactivity in Reverse Micelles*, M. P. Pileni (ed.), Elsevier, Amsterdam, (1989).
[89] Adamsom, A. W.; Gast, A. P.: In *Physical Chemistry of Surfaces 6th ed.*, Wiley Interscience, New York, 500 (1997).

micelle solution. In other words, the content exchange efficiency for larger reverse micelles (higher w values) was greater than that for smaller reverse micelles. During the same period of time, more hydrolyzed species were produced in the experiment of a higher w value than in the experiment of a lower w value. Consequently, precipitation (turbidity) appeared faster in the experiment of higher water/AOT ratio.

The observation of no turbidity in the w = 3 experiment might be rationalized as follows: As the volume and concentration of AOT/isooctane solution were constant, a lower w value led to a smaller amount of Y^{3+} in the reverse micelles that, in turn, limited the production of yttrium oxide precipitate. A small amount of precipitate was unlikely to be found when dispersed in a large volume of solution. On the other hand, a lower w value also indicates a lower number of hydrolyzed species that can be produced per reverse micelle. If the average number of hydrolyzed species per reverse micelle is less than a minimum value required for the formation of a stable cluster,[90] most hydrolyzed species will exist in the reverse micelles as monomers instead of clusters. Therefore, in the w = 3 experiment, it is possible that the average number of hydrolyzed species per reverse micelle was too small to form stable clusters.

TEM specimens were taken from the as-prepared precipitates. In the w = 15 and w = 7.5 experiments, the previously described method (Section 1.5) was followed to prepare the TEM specimens. In the w = 3 experiment, nothing was obtained by centrifuging, although the theoretical yield was 1.9 mg if the product was pure $Y(OH)_3$. Approximately 40 mL ethanol was added to the 50 mL clear solution to destroy the reverse micelle solution. The mixture was separated into two liquid layers. Some white residue found at the interface was collected carefully with a pipette. Then, the same method was used to prepare a TEM specimen for this residue.

The TEM micrographs (Figure 2.1) show that the sample from the w = 3 experiment contained only fuzzy lumps of various shapes: no particle-like objects could be found in the lumps. The morphologies of the products from w = 15 and w = 7.5 experiments were similar, but the morphology of the w = 7.5 product was a little more distinct. They both contained network-like aggregates as well as some lump-like aggregates. Particles could be found easily in the network-like aggregates. Between every two particles, there was a narrow region of amorphous

[90] Adamsom, A. W.; Gast, A. P.: In *Physical Chemistry of Surfaces 6th ed.*, Wiley Interscience, New York, 328 (1997).

material connecting them, which could be called a neck. Apparently, the lump-like aggregates also contained particles that were just ill-dispersed or heavily-covered. The particle boundaries were so unclear that it was extremely difficult to estimate particle sizes and size distribution. Both products contained particles having diameters in the range of 10-35 nm.

Dried as-prepared products showed XRD patterns containing weak and broad peaks (Figure 2.2). Three major peaks were found in the XRD patterns, with 2θ values at approximately 30°, 42°, and 52°. The patterns do not differ significantly from the pattern of an as-prepared product from an uncontrolled aqueous solution precipitation of $Y(NO_3)_3$ and NH_3 (Figure 2.2). Therefore, the reverse micelles did not affect the structure of the as-prepared precipitates. Two factors might contribute to the observed broad XRD peaks: extremely small crystallites, or highly distorted structure. The XRD patterns of the as-prepared products could not be identified with any known Y_2O_3 or $Y(OH)_3$ phases, but the annealing study showed that the peak at around 30° is related to the [222] diffraction of the cubic Y_2O_3 phase (Chapter 4).

If the peak at around 30° is simply assigned to the [222] diffraction, its large full-width-half-maximum (FWHM) gives an average crystallite size (< 3.3 nm) calculated from the Scherrer equation (Section 4.1.4), which is much smaller than the particle size estimated from the TEM micrographs (10-35 nm). A reasonable explanation is that the observed nanoparticles under TEM were aggregates of much smaller clusters. The inconsistency of particle sizes obtained from two different measurements might result from a fast Y^{3+} hydrolysis reaction followed by a relatively slow condensation reaction. Since more hydrolyzed species were created per unit time by the hydrolysis reaction than those consumed by the condensation reaction of cluster growth, the surplus hydrolyzed species might form more clusters themselves, instead of being used in cluster growth through hydrolyzed monomer addition.[68] A higher concentration of clusters in the reverse micelles resulted in a higher possibility of cluster aggregation. Therefore, particle growth was actually achieved through cluster aggregation instead of cluster growth through hydrolyzed monomer addition. This phenomenon is common for many fast-hydrolyzing metal cations, which makes the control of their precipitation reactions difficult.[68] In addition, the observed particle sizes from the TEM micrographs (10-35 nm) are greater than the average size of the reverse micelles, which are typically only several nanometers.[91] A possible explanation is that one

[91] Kawai, T.; Hamada, K.; Shindo, N.; Kon-no, K.: *Bull. Chem. Soc. Jpn.* **65**, 2715 (1992).

nanoparticle observed under TEM was actually an aggregate of clusters from more than one reverse micelle.[83]

2.2 Effects of Varying the Nitrate Concentration

Four experiments were carried out at different yttrium nitrate solution concentrations (0.02 M, 0.1 M, 0.5 M, and 1.0 M). The other reaction conditions were held constant, those are, w = 7.5, $[NH_3]$ = 5 M, and [AOT] = 0.1 M. As mentioned in Section 2.1, the concentration of the yttrium nitrate solution directly affects the water/AOT ratio, with a high concentration decreasing the maximum ratio achievable in a reverse micelle solution. Uniform reverse micelle solutions of w = 7.5 in 0.1 M AOT/isooctane could be easily prepared by short-term stirring with a diluted yttrium nitrate aqueous solution ($[Y^{3+}]$ = 0.02 M or 0.1 M), while the $[Y^{3+}]$ = 0.5 M aqueous solution needed overnight stirring to form a uniform reverse micelle solution of w = 7.5. The $[Y^{3+}]$ = 1.0 M aqueous solution could not form a uniform reverse micelle solution of w = 7.5 with 0.1 M AOT/isooctane. Thousands of tiny droplets were observed in the mixture during stirring. When the stirring was stopped, the droplets gradually settled on the bottle bottom, and coalesced to form a few large droplets. The bulk reverse micelle solution was then clear. The remaining water droplets were not taken out, and the non-uniform reverse micelle solution was used in the $[Y^{3+}]$ = 1.0 M experiment without additional treatment.

No turbidity was observed in the $[Y^{3+}]$ = 0.02 M experiment, but a tiny amount of white precipitate was found after centrifugal separation. A TEM specimen was prepared from the precipitate, which contained fuzzy lumps of different morphologies, such as balls, rods, and cloud (Figure 2.3). The balls' sizes differ, with some measuring 20-40 nm in diameter and some other more than 100 nm. Turbidity appeared slowly in the other three experiments. In the $[Y^{3+}]$ = 1.0 M experiment, the solution was not turbid even though the reverse micelle solution containing $Y(NO_3)_3$ was not uniform. When the reverse micelle solution containing NH_3 was added pipette-wise into the reverse micelle solution containing $Y(NO_3)_3$, the entire solution turned turbid slowly.

TEM specimens of the precipitate products of the three experiments ($[Y^{3+}]$ = 0.1 M, 0.5 M, and 1.0 M) were also prepared. The TEM micrographs show that all the products contained network-like particle aggregates (Figure 2.3). The product morphology of the $[Y^{3+}]$ = 0.5 M experiment was the best, because particles in the aggregates were the most distinct among the

three. A rough estimation showed that the particle sizes of the products of the three experiments were in the range of 12-24 nm diameter. Because insoluble aqueous solution droplets could induce partially non-uniform precipitation in the experiment, the product morphology of the $[Y^{3+}]$ = 1.0 M experiment was not very good.

2.3 Effects of Varying the Ammonia Concentration

Figure 2.4 shows TEM micrographs of a series of yttrium oxide products prepared at different NH_3 concentration (2 M, 5 M, and 14.8 M). Other conditions were held constant: w = 7.5, $[Y^{3+}]$ = 0.5 M, and [AOT] = 0.1 M. Commercial NH_3 solution (approximately 14.8 M) was used directly in the $[NH_3]$ = 14.8 M experiment.

The precipitate-appearance time of the samples was different. Turbidity appeared the fastest (< 20% addition of the reverse micelle solution containing NH_3) in the $[NH_3]$ = 14.8 M experiment, while it appeared the slowest (after the complete addition of the reverse micelle solution containing NH_3) in the $[NH_3]$ = 2 M experiment. Because a high NH_3 concentration led to more NH_3 molecules per reverse micelle, a higher hydrolysis reaction rate was expected, and as a result, turbidity should have appeared faster for the same reason observed in the study of the water/AOT ratio effects (Section 2.1). However, in the study of the $[Y(NO_3)_3]$ effects, turbidity appeared slowly in all the experiments (Section 2.2). Because no accurate measurement of the precipitate-appearance time was carried out, it is unknown whether the precipitate-appearance time varied with the yttrium nitrate concentration. The best product morphology was found in the experiment of the lowest NH_3 concentration ($[NH_3]$ = 2 M). Most distinct nanoparticles were found in the network-like aggregates of the product. Particles sizes were roughly 20-40 nm diameter. This result was consistent with the earlier observation that a higher yttrium nitrate concentration resulted in a better particle morphology (Section 2.2). Because the reverse micelle solution in the $[Y^{3+}]$ = 0.5 M experiment was not uniform, the result of the $[Y^{3+}]$ = 1.0 M experiment should not be considered here. Since $[NH_3]$ was fixed in that series of experiments, higher $[Y^{3+}]$ implied relatively lower $[NH_3]$. Therefore, the Y^{3+}/NH_3 ratio might be a critical factor that controlled product morphology. A higher ratio leaded to more distinct particles.

2.4 Effects of Varying the AOT Concentration

As shown in Figure 2.5, the precipitate from direct aqueous solution precipitation exhibited various morphologies. Therefore, without the assistance of reverse micelles, the precipitation reaction between $Y(NO_3)_3$ and NH_3 in aqueous solution is difficult to control and not uniform. The product prepared from 0.1 M AOT/isooctane reverse micelle solution (w = 7.5, $[Y^{3+}]$ = 0.5 M, $[NH_3]$ = 5 M) contained nanometer-sized particles of uniform size and shape (Figure 2.5). The reverse micelles caused the precipitation reaction to occur simultaneously in billions of nanometer-sized reverse micelles of uniform size, thereby forcing the precipitation reaction to be uniform. The product prepared from 0.5 M reverse micelle solution (w = 7.5, $[Y^{3+}]$ = 0.5 M, $[NH_3]$ = 5 M) showed only large fuzzy lumps (Figure 2.5). It is unknown why the product morphology was poor at a higher AOT/isooctane concentration. The importance of surfactant in nanoparticle formation was also demonstrated in the study of TiO_2 nanoparticle formation in AOT/isooctane reverse micelles.[82] Hirai et al. found that if $3*10^{-5}$ M titanium tetrabutoxide was hydrolyzed in 3 M H_2O/butanol without any surfactant, the nucleation of the hydrolyzed species did not occur. Therefore, no nanoparticle was formed under these conditions. On the contrary, if the hydrolysis of $3*10^{-5}$ M titanium tetrabutoxide was carried out in 0.1 M AOT/isooctane (w = 30), the nucleation of the hydrolyzed species occurred 6 h after the initiation of hydrolysis.

2.5 Effects of Varying the Aging Time

The TEM micrographs in Figure 2.6 show that a longer aging time did not improve product morphology. The morphologies of the three samples taken after 1 h, 1 d, and 5 d of aging were almost the same. However, due to increased aggregation, the five-day aged sample was not as good as the other two. Although particle boundaries were not clear, it seems that a longer aging time resulted in smaller particles. Particle sizes of the one-hour aged sample ranged from roughly 20 nm to 40 nm, those of the one-day aged sample from approximately 17 nm to 34 nm, and those of the five-day aged sample from approximately12 nm to 24 nm.

In one experiment, heat was applied to study the influence of aging temperature on the product morphology. Two reverse micelle solutions containing $Y(NO_3)_3$ and NH_3 were mixed at room temperature. The mixed reverse micelle solution was then refluxed (the boiling point of isooctane is 98-99 °C). Turbidity appeared during room-temperature mixing, but disappeared after refluxing for approximately one day. NH_3 molecules escaped from the solution gradually

during refluxing, thereby reducing the pH value of the solution and causing the dissolution of the precipitate product. Efforts to use non-volatile NaOH as the base instead of NH_3 in the refluxing-aging study failed. NaOH solutions of different concentrations (0.5 M, 1 M, and 5 M) were used, and the other parameters were set at w = 15, $[Y^{3+}]$ = 0.1 M, and [AOT] = 0.1 M. However, no turbidity was observed at either room temperature or refluxing temperature. Ethanol was added at the end of each experiment to destroy the reverse micelle solution. Some white residue did appear at the interface, but its dissolution in water proved that it was not yttrium oxide. This result was puzzling, as a precipitate was obtained immediately after mixing an aqueous solution of 0.1 M $Y(NO_3)_3$ with the same volume of 0.5 M NaOH.

2.6 Effects of Varying the Washing Method

In the early stages of this research, water-washing was not applied in the procedure to prepare a TEM specimen of an as-prepared product (Section 1.5). A precipitate product separated from a reverse micelle solution was only washed with several milliliters of ethanol twice before its suspension in ethanol was deposited on a Cu grid to prepare a TEM specimen. No matter how varied the experimental conditions, the TEM specimens prepared this way contained only large fuzzy lumps with little fine structure (Figure 2.7). The darker regions at the centers of the lumps look like covered particles.

In order to investigate whether the apparent poor morphology was due to the inefficiency of ethanol as a washing solvent, a precipitate product washed with several milliliters of ethanol was further washed two more times with several milliliters of deionized water. The morphology of the specimen of the water-washed product improved greatly (Figure 2.7). The specimen was composed of network-like aggregates of uniform nanometer-sized particles. This result indicated that the fuzzy lumps in a product without the water-washing treatment actually contained nanoparticles that were completely covered by AOT molecules. Water-washing removed AOT molecules so that the regions containing only surfactant aggregates were no longer as dense as the regions containing particle aggregates. An electron beam was able to distinguish between the two kinds of regions. Yang and Chen[81] prepared Y_2O_3-stabilized ZrO_2 nanoparticles in AOT/isooctane reverse micelle solution. They only washed the products with ethanol three times to prepare TEM specimens. The TEM micrographs showed that the precipitate was amorphous

and flocculent, which was very similar to the morphology of the products washed with only ethanol in this research.

Although ethanol-washing was inefficient, it was still used as a step in the procedure to prepare TEM specimens. Ethanol can wet the precipitate produced in an AOT/isooctane reverse micelle solution, but water cannot. Therefore, fresh precipitate separated from reverse micelle solution could be dispersed in ethanol easily, but in water it only formed large clumps. Ethanol, which is polar, but with some non-polar features due to the ethyl group, is miscible not only with non-polar isooctane but also with water. Therefore, it is a good transitional solvent between isooctane and water and makes fresh precipitates from isooctane solution dispersible in water.

Because each AOT molecule contains only one sulfur atom, the molar ratio of yttrium and sulfur in a product can be used as a measure of the relative quantity of residual AOT molecules in the product. Scanning Electron Microscopy (SEM) combined with Energy Dispersion Spectrum (EDS) provides an analytical technique to determine the elemental composition of a solid surface. The penetration depth of SEM-EDS is approximately 5 μm.[92] Because the products in this research contained only nanometer-sized particles, the elemental composition obtained from SEM-EDS represented the mean elemental composition of a product.

Experiments were carried out to find an efficient way to remove residual AOT molecules from a precipitate product. A batch of precipitate was prepared and separated into several portions. Each portion was washed with a different organic solvent of the same volume (approximately 20 mL) three times. Each time, the portion of precipitate was mixed with 20 mL of fresh solvent and stirred in a sealed flask at room temperature for approximately one hour. The solvent was removed by centrifuging, and the same amount of fresh solvent was added for the next cycle. The washed products were dried overnight at approximately 80 °C. The SEM-EDS results of the washed products are shown in Table 2.1. Compared to the Y:S ratio of a product without washing, the Y:S ratios of the products washed with the organic solvents were higher. Therefore, the solvents did remove some residual AOT molecules from the products, but the efficiencies were poor. The highest Y:S ratio, which was achieved by 1-butanol, was only 1.77. However, the data show that a solvent of high polarity, for example, ethanol, acetone, or 1-butanol, had a higher washing efficiency than that of low polarity, for example, isooctane,

[92] Goldstein, J. I.; Newbury, D. E.; Echlin, P.; Joy, D. C.; Fiori, C.; Lifshin, E.: In *Scanning Electron Microscopy and X-Ray Microanalysis*, Plenum, New York, 110 (1984).

benzene, or chloroform. As water is a more polar solvent than any of the organic solvents investigated, better washing efficiency was expected.

Another series of experiments was carried out by dividing a batch of precipitate into several portions, each of which was washed twice with several milliliters of ethanol. Then, each portion was washed in a water-based solvent using different methods (Table 2.2). The washed samples were dried overnight at approximately 80 °C. The Y:S ratios of the washed samples obtained from SEM-EDS (Table 2.2) showed that washing under reflux was more efficient than cool washing and that 1 M $NaNO_3$ solution was better than pure water.

Because of the ionic nature of the yttrium oxide precipitate surface, residual AOT molecules adhere on the surface through strong ionic interaction of their anionic $-SO_3^-$ groups with the inorganic surface. In polar-solvent washing, polar solvent molecules are in direct contact with non-polar alkyl chains of the surfactant molecules. The polarity of the solvent makes the energy of the system unfavorable. To reduce energy some adhered surfactant molecules leave the inorganic precipitate surface and aggregate with each other to form micelles in the polar solvent with their anionic $-SO_3^-$ groups outward. Therefore, the energy of the system decreases and some residual AOT molecules are removed. However, the residual AOT molecules are not completely eliminated. The best Y:S ratio was only 3.2 (Table 2.2). It means that in 1 gram of the dried precipitate, if yttrium existed completely in $Y(OH)_3$, there was 0.5 gram of $Y(OH)_3$, as well as 0.5 gram of residual AOT molecules.

The SEM results indicated a significant amount of residual AOT molecules in as-prepared nanoparticle products. The necks, the narrow regions among nanoparticles in the network-like structure, were only observed in as-prepared products. Aggregates of annealed products did not have the network-like morphology, in which residual AOT molecules were decomposed (Section 4.1.2). In addition, as discussed above, network-like morphology of a water-washed sample was related to the fuzzy morphology of a product before water-washing (Figure 2.7). These observations indicated that the necks were probably composed of AOT/water complex. Yang and Chen also attributed agglomeration of their yttrium oxide or cerium oxide stabilized ZrO_2 nanoparticle samples to a complex of residual AOT and water molecules.[81]

Most parts of the residual AOT molecules were decomposed into water and CO_2 gases during annealing. However, the SEM-EDS data showed a Y:S ratio approximately 0.023 in a sample annealed at 1000 °C for 16 h, since sulfur in AOT molecules might form sulfur-

containing compounds with the yttrium and oxygen during annealing. Therefore, to get rid of sulfur completely by annealing is very difficult. Sulfur residue is a problem in some applications. For example, in the phosphors for FED, such as Y_2O_3:Eu, sulfur poisons the phosphor and decreases its usable lifetime.[93] However, the presence of sulfur is not a problem in other applications. For example, in fluorescent lights, a commonly used phosphor is Y_2O_2S:Eu,[94] which contains sulfur. If sulfur has to be eliminated completely, AOT might be replaced with other non-sulfur-containing surfactants such as polyoxyethylene(10) octylphenyl ether (OP-10), which are composed of only C, H, and O and can probably be eliminated completely by thermal decomposition. In case the complete elimination of adhered surfactant molecules has to achieve without annealing, a non-ionic surfactant, such as poly(oxyethylene)$_5$nonyl phenol ether (NP-5), might be used. As non-ionic surfactants do not have strong ionic interactions with an inorganic precipitate surface, they can be easily removed by washing with a suitable solvent.

There is a reason that complete elimination of residual AOT molecules might not be necessary. With the protection of adhered AOT molecules, the nanoparticles cannot grow by aggregation. Instead, the protected nanoparticles form loose aggregates through weak van der Waals interactions among surfactant alkyl chains.[95] The proposed nature of the observed network-like nanoparticle aggregates in this research is that they were aggregates of nanoparticles separated from each other by AOT layers. However, if most of the protecting surfactant molecules were eliminated, due to the van der Waals interactions among the nanoparticles, the nanoparticles might coalesce to form large particle aggregates.[96] For instance, the two TEM micrographs in Figure 2.8 show a great difference between the morphologies of two specimens prepared from the same sample with and without water refluxing. The specimen with water refluxing contained less distinct particles and serious aggregation, while the one only washed with some water contained well-developed network-like particle aggregates.

2.7 Conclusion

[93] Lehmann, W.: *Electrolumin., Proc. of the Sixth Inter. Workshop*, V. P. Singh; J. C. McClure (Eds.), 65 (1992).
[94] Welker, T.: *J. Lumin.* **48-49**, 49 (1991).
[95] Hiemenz, P. C.; Rajagopalan, R.: In *Principles of Colloid and Surface Chemistry 3rd ed.*, Marcel Dekker, New York, 613 (1997).
[96] Hiemenz, P. C.; Rajagopalan, R.: In *Principles of Colloid and Surface Chemistry 3rd ed.*, Marcel Dekker, New York, 462 (1997).

The results in this chapter indicate that yttrium oxide nanoparticles can be synthesized from an AOT/isooctane reverse micelle solution via the hydrolysis reaction of $Y(NO_3)_3$ with NH_3. Systematic investigation found the following optimized synthesis conditions: 1) water/AOT ratio between 7.5 and 15; 2) yttrium nitrate concentration of 0.5 M; 3) ammonia concentration of 2 M; 4) AOT concentration of 0.1 M. Aging had little effect on product morphology. As-prepared yttrium oxide nanoparticles were in network-like aggregates. Particle boundaries were not clear, making particle size estimation difficult. A rough estimate of particle sizes from TEM micrographs gave the range of 10 to 40 nm in diameter. XRD patterns of the as-prepared products indicated that they had very poor crystallinity. Water-washing was critical to partially remove AOT molecules, so that nanoparticles could be observed under TEM. However, all efforts to remove residual AOT molecules completely failed.

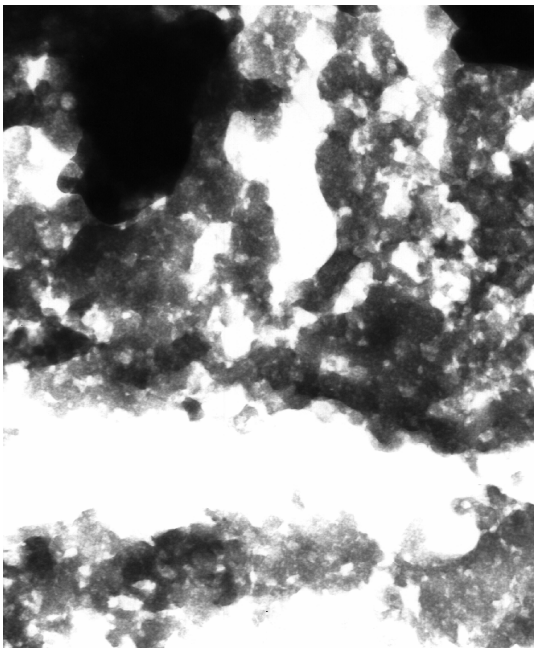

w = 3

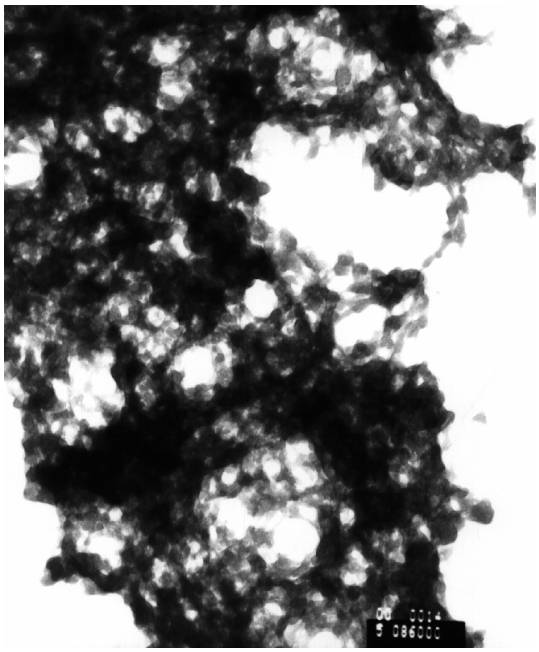

w=7.5

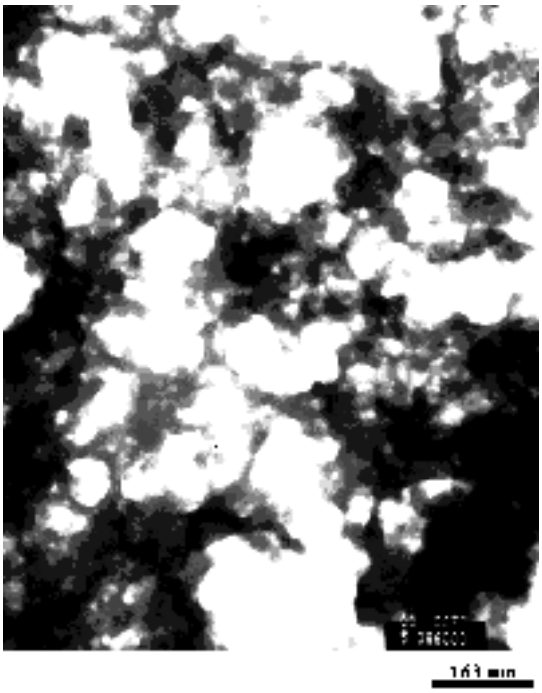

w = 15

Figure 2.1

Influence of Water/AOT Ratio on Product Morphology

Fixed Conditions: $[Y^{3+}]$ = 0.1 M, $[NH_3]$ = 5 M, [AOT] = 0.1 M

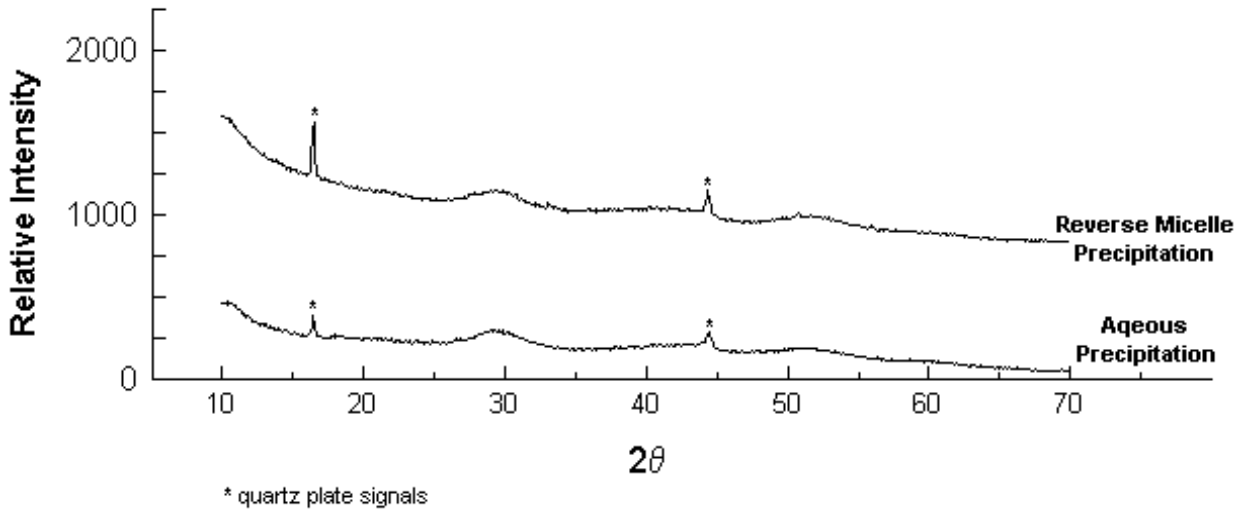

Figure 2.2

Comparison of XRD Patterns of Products Prepared from Reverse Micelle Solution and Aqueous Solution

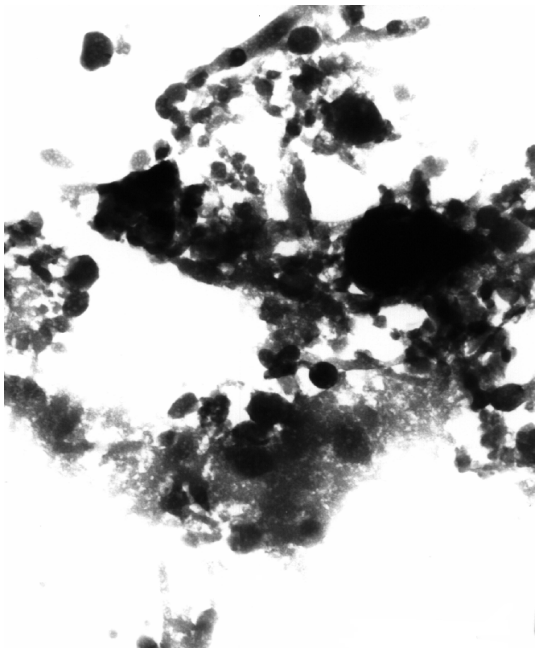

$[Y^{3+}]$ = 0.02 M

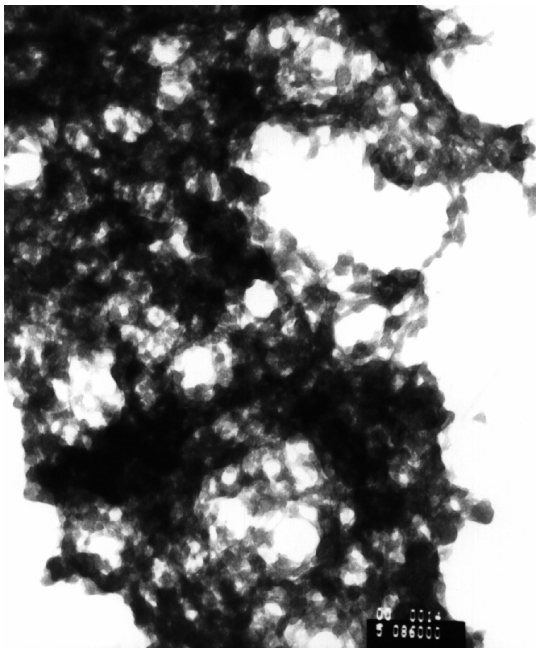

$[Y^{3+}]$ = 0.1 M

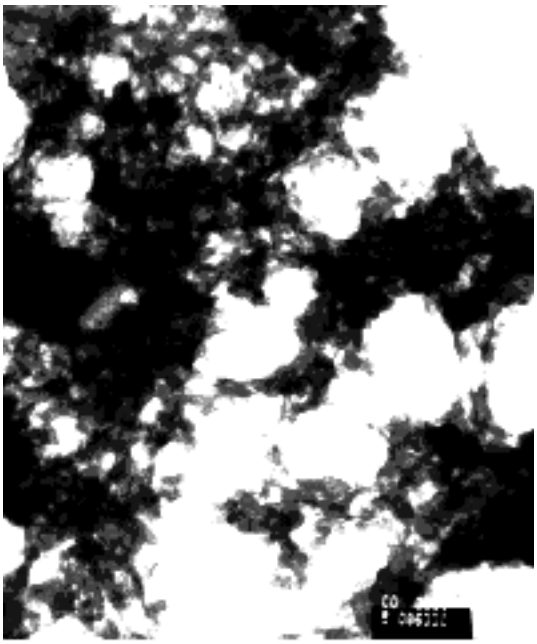

$[Y^{3+}]$ = 0.5 M

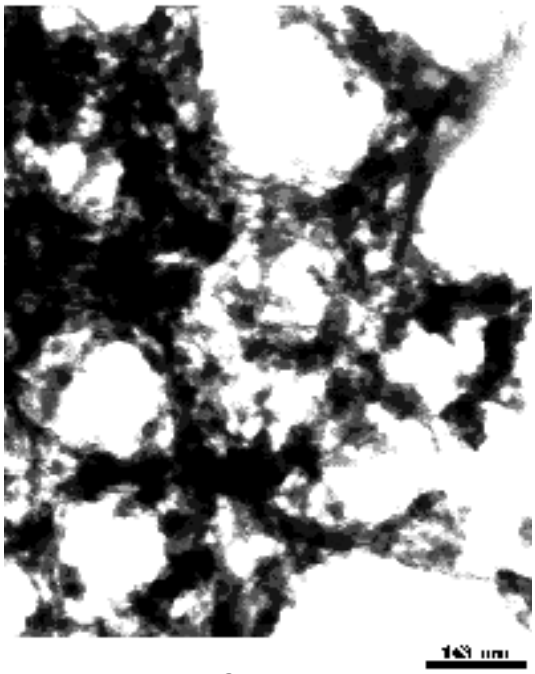

$[Y^{3+}]$ = 1.0 M

Figure 2.3

Influence of Yttrium Nitrate Concentration on Product Morphology

Fixed Conditions: w = 7.5, $[NH_3]$ = 5 M, [AOT] = 0.1 M

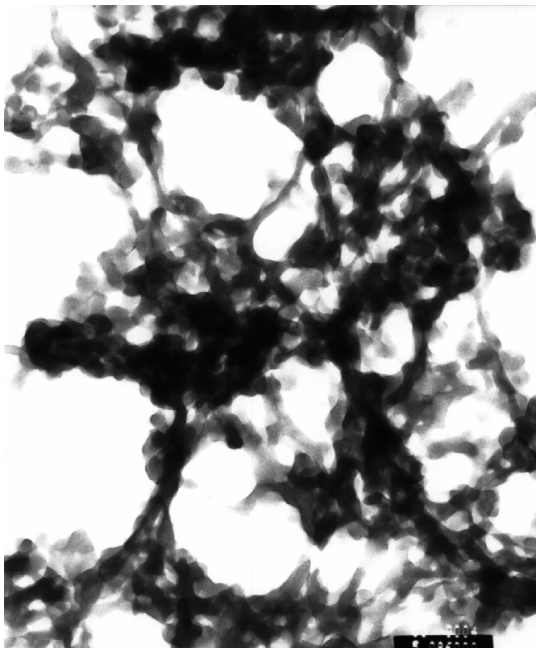

[NH_3] = 2 M

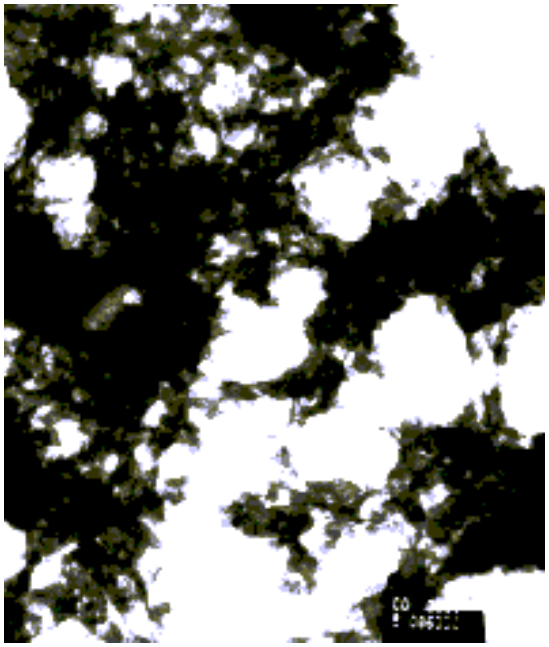

[NH_3] = 5 M

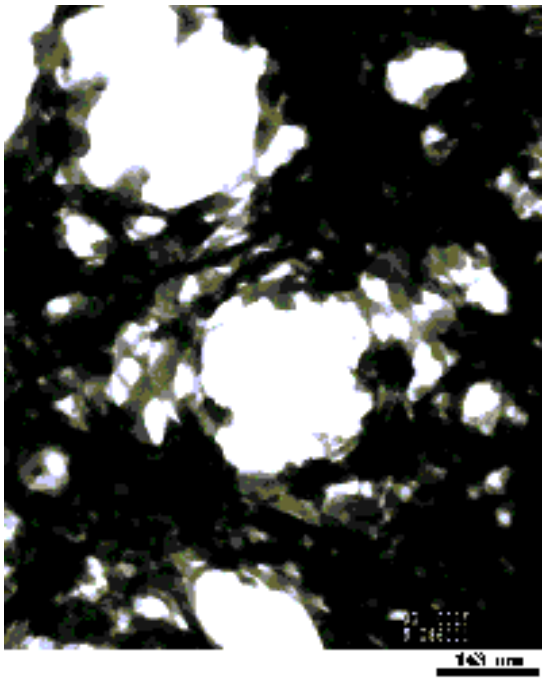

[NH_3] = 14.8 M

Figure 2.4

Influence of Ammonia Concentration on Product Morphology

Fixed Conditions: w = 7.5 M, [Y^{3+}] = 0.5 M, [AOT] = 0.1 M

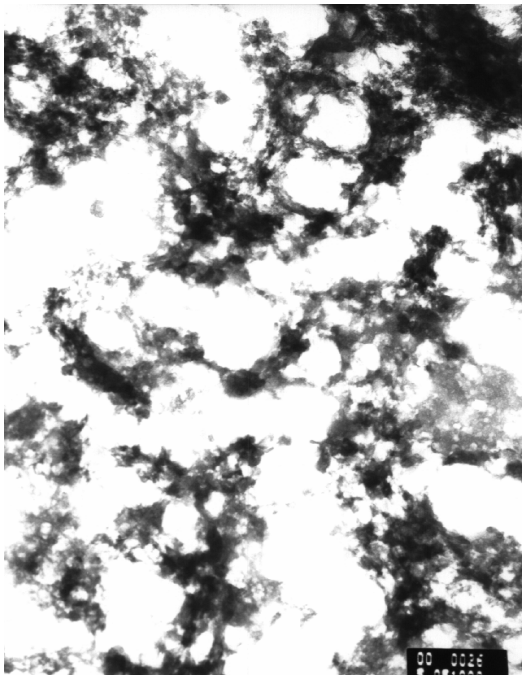

[AOT] = 0 (Aqueous)

[AOT] = 0.1 M

[AOT] = 0.5 M

Figure 2.5

Influence of AOT Concentration on Product Morphology

Fixed Conditions: $[Y^{3+}]$ = 0.5 M, $[NH_3]$ = 5 M

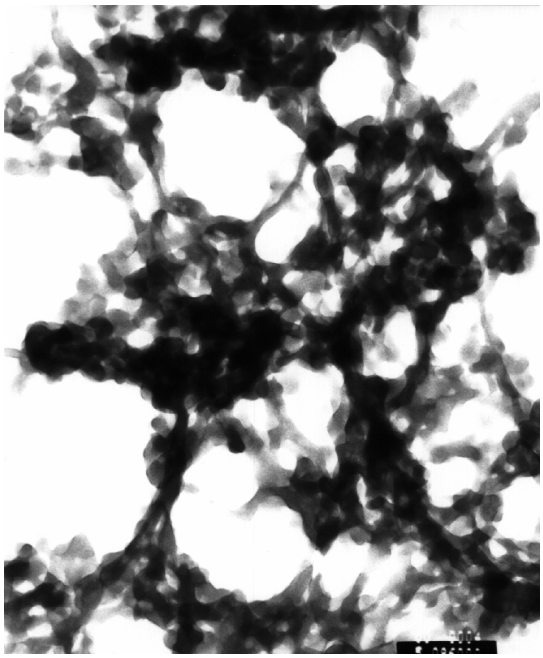

One Hour

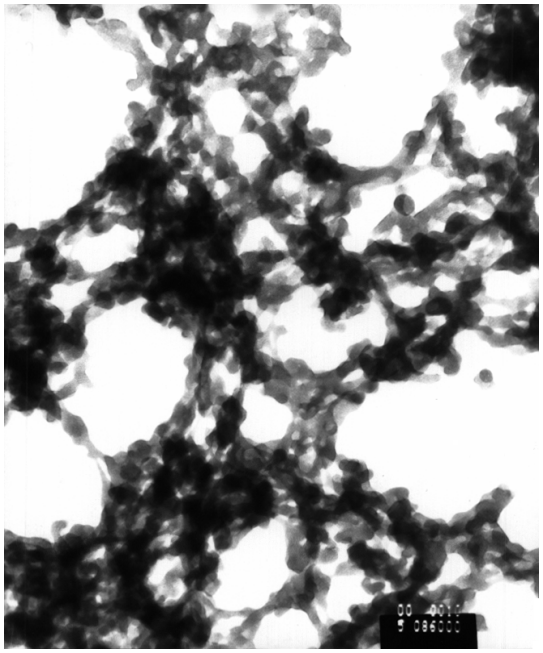

One Day

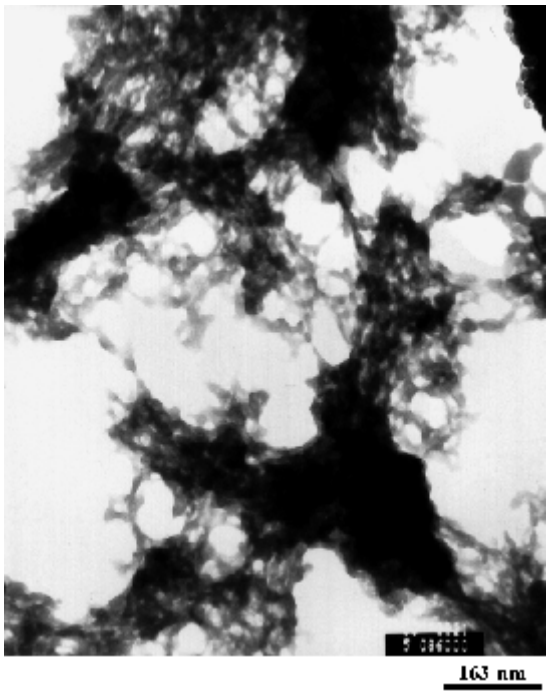

Five Days

Figure 2.6

Comparison of Products of Different Aging Time

Sample I.D.: w = 7.5, $[Y^{3+}]$ = 0.5 M, $[NH_3]$ = 2 M, [AOT] = 0.1 M

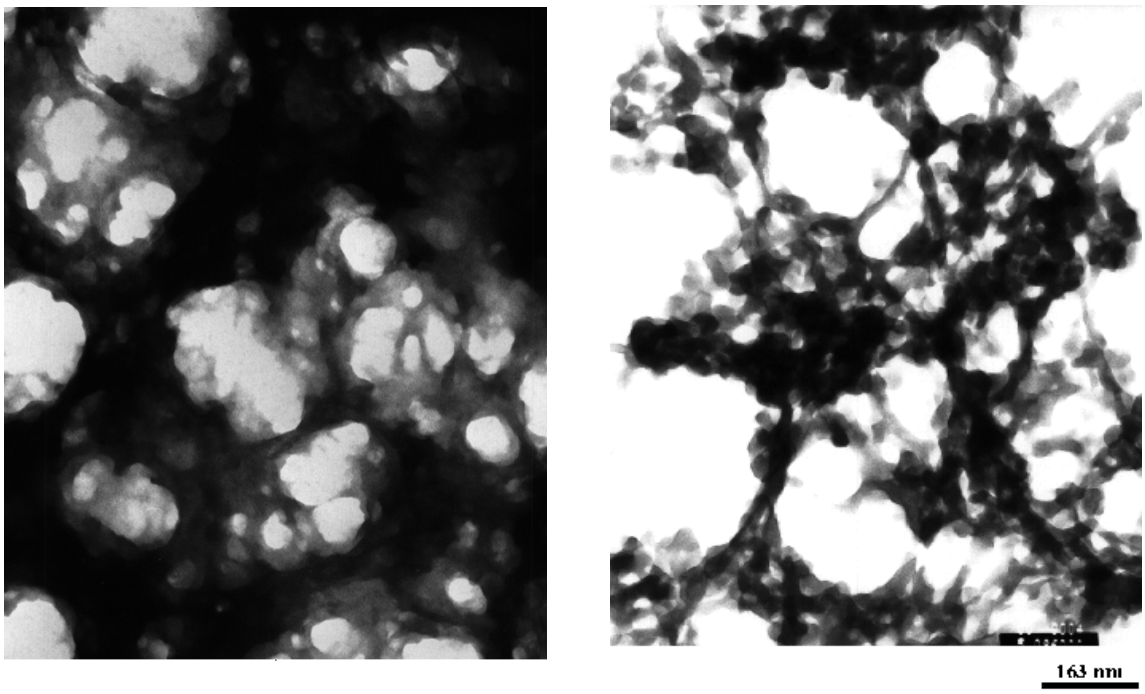

Ethanol-washed **Water-washed**

Figure 2.7

Comparison of Ethanol-washed Product and Water-washed Product

Sample I.D.: w = 7.5, $[Y^{3+}]$ = 0.5 M, $[NH_3]$ = 2 M, [AOT] = 0.1 M

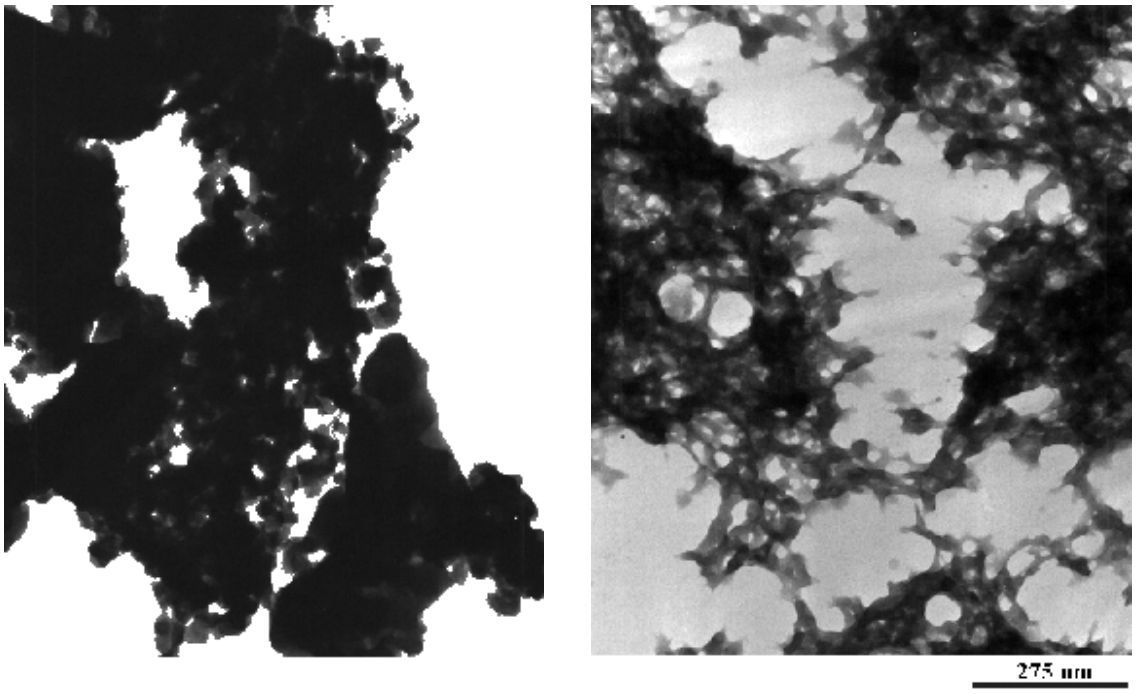

Refluxed **Non-refluxed**

Figure 2.8

Comparison of Refluxed Product and Non-refluxed Product

Sample I.D.: w = 7.5, [Y^{3+}+1%Eu^{3+}] = 0.5 M, [NH_3] = 2 M, [AOT] = 0.1 M

Table 2.1

Washing Effects of Different Solvents

Washing Solvent	ethanol	acetone	1-butanol	isooctane	benzene	chloroform
Y/S Ratio from SEM	1.57±0.01	1.6±0.3	1.8±0.2	1.1±0.2	0.95±0.03	1.09±0.03

Table 2.2

Effects of Different Washing Methods

Washing Method	Washed with a little isooctane	Washed with cool water three times	Refluxed with water three times	Refluxed with 1M $NaNO_3$ three times
Y/S Ratio from SEM	0.7±0.4	1.99±0.03	2.4±0.3	3.2±0.1

Chapter Three:
Isopropoxide-Hydrolysis Method

Metal alkoxides have been used to prepare metal oxide nanoparticles using the reverse micelle method.[78,82,83] Yttrium alkoxides have also been used to prepare yttrium oxide nanoparticles using the sol-gel method.[45,46] These reports indicate that yttrium isopropoxide is a potential precursor for preparing yttrium oxide nanoparticles in AOT/isooctane reverse micelles. Using the yttrium isopropoxide hydrolysis reaction to prepare yttrium oxide nanoparticles in reverse micelles differs from the yttrium nitrate hydrolysis reaction, even though both of them use a reverse micelle solution as the medium. First, the precursors are different: yttrium nitrate is used in the nitrate-hydrolysis method, while yttrium isopropoxide is used in the isopropoxide-hydrolysis method. Second, yttrium nitrate hydrolysis requires a basic solution, but yttrium isopropoxide does not. Third, yttrium nitrate is soluble in water but not in organic solvents, while yttrium isopropoxide behaves in the opposite manner. These differences might affect the yttrium oxide nanoparticles prepared by these two methods, and therefore, it is important to compare the two methods.

Like many other metal alkoxides, yttrium isopropoxide is moisture-sensitive. Water content of < 10 ppm in its organic solution is enough to cause its hydrolytic decomposition.[97] Yttrium isopropoxide is soluble in common organic solvents.[98] It is available as a 20~25 wt.% solution in toluene commercially. In the early stages of this research, many efforts were made to dissolve this chemical in organic solvents outside of a glovebox (either in the air or in a nitrogen-purged glove bag), but all of them failed. In one experiment, 66.5 mg yttrium isopropoxide powder was mixed with 4 mL dehydrated toluene in a sealed bottle in a nitrogen-purged glove bag. If the powder could dissolve completely in the solvent, the concentration of the solution would be approximately 1.9 wt.%, which is much lower than that of the commercial yttrium isopropoxide solution in toluene. However, The powder became a kind of yellowish sticky material in toluene after two days of stirring at room temperature. Opening a bottle of commercial yttrium isopropoxide solution in toluene in air momentarily resulted in the

[97] Brown, L. M.; Mazdiyasni, K. S.: *Inorg. Chem.* **9**, 2783 (1970).
[98] Poncelet, O.; Sartain, W. J.; Hubert-Pfalzgraf, L. G.; Folting, K.; Caulton, K. G.: *Inorg. Chem.* **28**, 263 (1989).

appearance of a precipitate in a few days. Therefore, to avoid any unwanted hydrolysis before the controlled hydrolysis in reverse micelles, the chemical should be handled in a glovebox.

Diluted commercial yttrium isopropoxide solution in toluene was used in this research, following the second method described in Section 1.3.1. The detailed experimental procedures are described in Section 1.4. As discussed at the beginning of Chapter 2, in a reverse micelle synthesis, some experimental parameters, such as the water/AOT ratio, the concentration of precursor chemicals, the pH value of the aqueous content in the reverse micelles, the aging time, and the aging temperature might affect the products. Therefore, to study the effects of variation of these parameters on the yttrium oxide nanoparticle products is very important. Comparison between the yttrium nitrate hydrolysis method described in Chapter 2 and the yttrium isopropoxide hydrolysis method might help to elucidate the mechanism of yttrium oxide nanoparticle formation in the reverse micelles.

3.1 Effects of Varying the Water/AOT Ratio

Since pure water was dissolved in reverse micelles instead of a salt solution, the maximum water/AOT ratio that can be achieved in 0.1 M AOT/isooctane to prepare a reverse micelle solution is very high (approximately 60).[88] For comparison, the maximum ratio for 0.5 M $Y(NO_3)_3$ in 0.1 M AOT/isooctane is less than 15 (Section 2.2). Therefore, effects of variation of the water/AOT ratio on yttrium oxide nanoparticle formation can be analyzed over a larger range. Four experiments were conducted to prepare yttrium oxide nanoparticles at four different water/AOT ratios (w) of: 10, 20, 30, and 40. All other experimental parameters were fixed. The concentration of the AOT/isooctane solution was 0.1 M. The volume of this solution in each experiment was 50 mL. Deionized water was dissolved in the AOT/isooctane solution to prepare a reverse micelle solution of a certain water/AOT ratio. The commercial yttrium isopropoxide/ toluene solution was diluted 1:4. The volume of the diluted yttrium isopropoxide solution added to a reverse micelle solution in each experiment was 1.0 mL. All of the experiments were conducted at room temperature. The detailed experimental procedure is described in Section 1.4. In all of the four experiments, turbidity appeared very quickly during the addition of the 1:4 diluted yttrium isopropoxide/toluene solution to a reverse micelle solution. No obvious time delay was observed.

After approximately one hour of aging at room temperature, TEM specimens of the products from the four experiments were prepared according to the method described in Section 1.5. Figure 3.1 shows the results: The w = 10 and w = 20 products contained a well-developed network structure, which was a little fuzzy due to diffuse-looking edges. Many nanoparticles could be found in the networks. The micrographs of the w = 30 and w = 40 products show that the products also contained a well-developed network structure. The nanoparticles found in the products were more distinct than those found in the w = 10 and w = 20 products. The network-like morphology was essentially the same as that of the best product from the nitrate-hydrolysis method, which was prepared at the optimized conditions (w = 7.5 ~ 15, $[Y^{3+}]$ = 0.5 M, $[NH_3]$ = 2 M, and [AOT] = 0.1 M). The particle sizes of all of the products were in the range of 10 nm to 20 nm in diameter, which were comparable to but a little smaller than the particle sizes of the products from the nitrate-hydrolysis method (10 nm to 40 nm). In the nitrate-hydrolysis method, products of good morphology were obtained at water/AOT ratios between 7.5 and 15, when $[Y^{3+}]$ was 0.5 M in the aqueous phase. This concentration in the aqueous phase indicated approximately 0.0034 M yttrium nitrate in the reverse micelle solution. However, in the isopropoxide-hydrolysis method, products of good morphology were obtained in a much wider water/AOT ratio range (10 to 40), when the volume of 1:4 diluted yttrium isopropoxide solution added was 1.0 mL. This value was equivalent to approximately 0.003 M yttrium isopropoxide in the reverse micelle solution.

It is difficult to compare the two precursor concentrations, because in the nitrate-hydrolysis method, the effective precursor (yttrium nitrate) is mostly in the aqueous solution in the reverse micelles, while in the isopropoxide-hydrolysis method, the effective precursor (yttrium isopropoxide) is dispersed in the bulk isooctane solution. The much wider range of the water/AOT ratio, in which nanoparticles of good morphology were produced indicates that the isopropoxide-hydrolysis method has a more flexible water/AOT ratio range than the nitrate-hydrolysis method. Due to the limitation of the low maximum water/AOT ratio in the nitrate-hydrolysis method, further investigation at higher ratios was impossible. The results of the nitrate-hydrolysis method indicated that high ratios, 7.5 and 15, produced better products than lower ratio, 3 (Section 2.1). Therefore, wider range of w that produced good morphology might result from the much higher maximum water/AOT ratio in the reverse micelle solution.

3.2 Effects of Varying the Yttrium Isopropoxide Concentration

The concentration of commercial yttrium isopropoxide/toluene solution is 20 to 25 weight percent, which is approximately 0.72 M ~ 0.90 M. Due to the fast evaporation of toluene, the commercial solution is difficult to handle. A white solid appeared quickly and clogged the syringe needle during handling of the solution. Therefore, a 1:4 diluted yttrium isopropoxide/ toluene solution (0.14 M ~ 0.16 M) was used in the experiment to investigate the effects of the yttrium isopropoxide concentration.

Three experiments were carried out. The volume of 0.1 M AOT/isooctane solution was 50 mL, and the water/AOT ratio was 10 for all of the experiments. 0.04 mL, 0.2 mL, and 1.0 mL of the 1:4 diluted yttrium isopropoxide/toluene solutions were added separately in the three experiments. These additions made the yttrium isopropoxide concentration in the three experiments approximately 0.0001 M, 0.0006 M, and 0.003 M, respectively. Pure deionized water was used in all the three experiments. Turbidity appeared very quickly during the addition of the yttrium isopropoxide solution to the reverse micelle solution in all three experiments. No obvious delay was observed. TEM specimens were prepared as usual after approximately one hour of aging at room temperature. Micrographs of these specimens (Figure 3.2) indicate that all products were composed of network-like nanoparticles aggregates similar to the product of the nitrate-hydrolysis method at the optimized conditions, although the network structures of the products of both the 0.0006 M experiment and the 0.003 M experiment were a little fuzzier than that of the 0.0001 M experiment. The consistent network-like morphology of the products for these three experiments indicated that the precursor concentration range is more flexible in the isopropoxide-hydrolysis method than in the nitrate-hydrolysis method. Rough estimation indicated that particle sizes of the products were all in the range of 10 nm to 20 nm.

3.3 Effects of Varying the pH Value

Two experiments were carried out to investigate the effects of the pH value in the aqueous phase. In the first experiment, 1.0 mL 1:4 diluted yttrium isopropoxide solution was added to a 50 mL 0.1 M AOT/isooctane solution containing 0.9 mL deionized water (w = 10). In the other experiment, the AOT/isooctane reverse micelle solution contained 0.9 mL of 5 M NH_3 aqueous solution. All other experimental conditions were the same in the two experiments. If it is

assumed that NH_3 molecules stay only in the reverse micelles, the pH value of the aqueous phase in the reverse micelles in the second experiment was approximately 12.0, compared to a pH value close to 7.0 in the first experiment. Turbidity appeared in both experiments quickly during the addition of the yttrium isopropoxide/toluene solution. After approximately one hour of aging at room temperature, TEM specimens were prepared for both experiments using the method described in Section 1.5. The network morphology of the product of the experiment using deionized water is a little fuzzier than that of the experiment using 5 M ammonia, but they were both good (Figure 3.3). Particle sizes in both products were in the same range (10 nm to 20 nm).

3.4 Effects of Varying the Aging Time and Temperature

To study the influence of aging temperature on yttrium oxide nanoparticles, two experiments were carried out using identical conditions (w = 10, 1:4 diluted yttrium isopropoxide 1.0 mL, deionized water). After completion of the yttrium isopropoxide addition, one batch was aged in a sealed bottle at room temperature with magnetic stirring. The other was transferred to a round-bottomed flask and refluxed at the boiling point of isooctane (98~99 °C). TEM specimens were prepared for both experiments 1 h after the addition of the yttrium isopropoxide solution. The mixture from the room-temperature-aging experiment was still turbid after five days of stirring at room temperature. A TEM specimen was prepared for this five-day-aged product. However, in the refluxing experiment, the turbidity disappeared gradually and the solution became clear after approximately one day. Ethanol (50 mL) was added to the clear liquid to destroy the reverse micelles. The mixture separated into two clear liquid layers slowly, with a little amount of flocculent residue at the interface of the two layers. This residue was collected and put through the aqueous washing procedure described in Section 1.4. However, no solid precipitate was found after the first water-washing cycle, so the residue at the interface could not have been yttrium oxide.

The two TEM specimens prepared at different aging times in the room-temperature-aging experiment were of the same morphology (Figure 3.4). The particle sizes were in the same range (10 nm to 20 nm) for both samples, which differed from the observation in the study of the nitrate-hydrolysis method. In the nitrate-hydrolysis method, even though products of different aging time had the same morphology, the apparent particle sizes decreased with increasing aging time (Section 2.5).

The morphologies of the products aged at room temperature and refluxed were not significantly different. Both of the products contained network-like nanoparticle aggregates. The particle sizes of the two products were both in the range of 10 nm to 20 nm (Figure 3.5).

3.5 Conclusion

Yttrium oxide nanoparticles can be prepared from AOT/isooctane reverse micelles using the isopropoxide-hydrolysis method. TEM results showed that the products contained network-like nanoparticle aggregates. Their morphology was essentially the same as that of the products from the nitrate-hydrolysis method. Particle sizes were in the range of 10 nm to 20 nm. Nanoparticle products of good morphology were obtained in a wide range of experimental conditions: the water/AOT ratio (10 ~ 40), the yttrium isopropoxide concentration (0.0001 M ~0.003 M), and the pH value of the aqueous phase in reverse micelles (7.0 and 12.0). Aging time and aging temperature had no significant effects on the product morphology, but long-time refluxing (> 1 d) caused disappearance of the precipitate. The isopropoxide method is more flexible than the nitrate method.

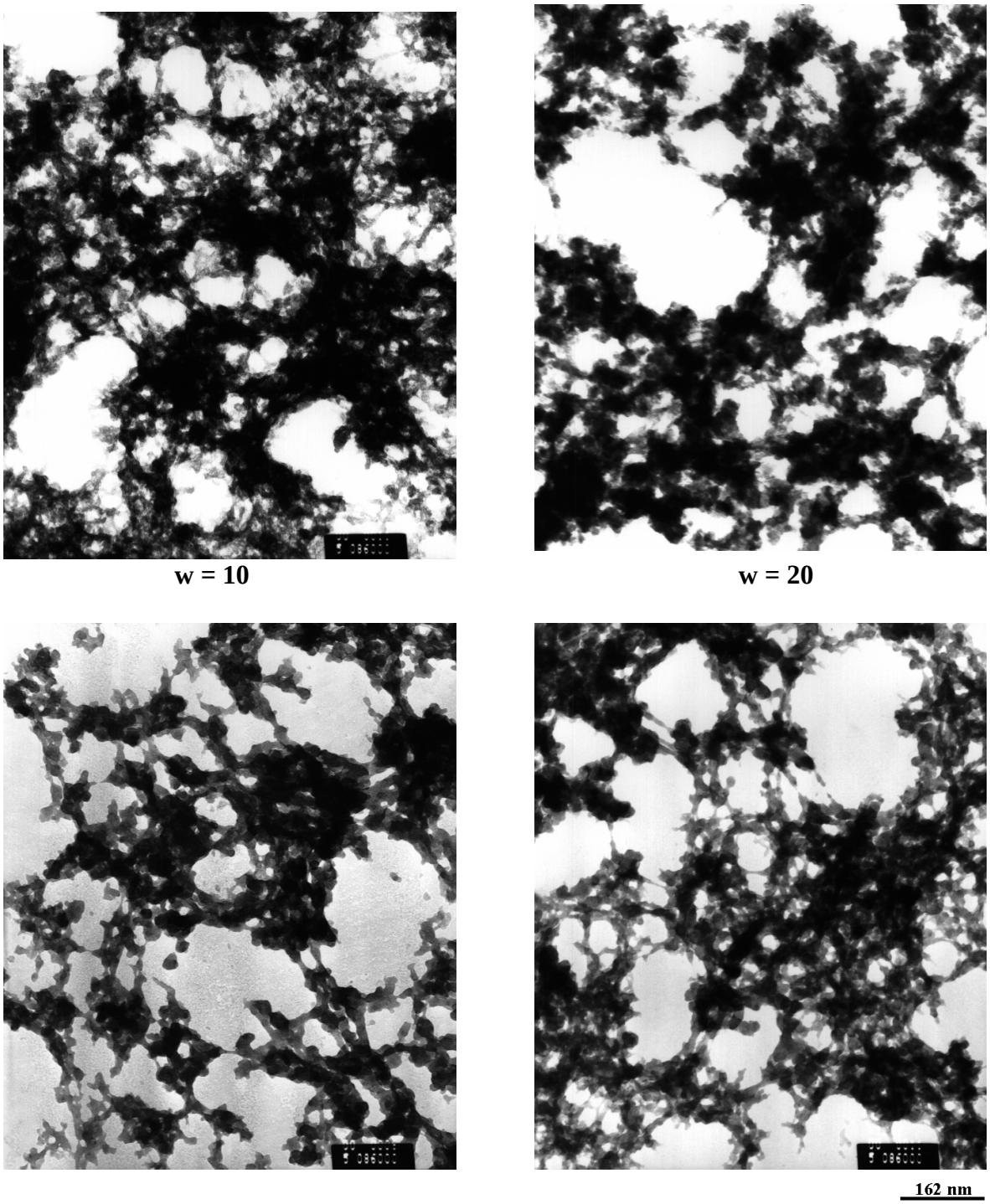

Figure 3.1

Influence of Water/AOT Ratio on Product Morphology

Fixed Conditions: V(Y($O^{i}Pr$)$_3$/toluene) = 1.0 mL, [AOT] = 0.1 M

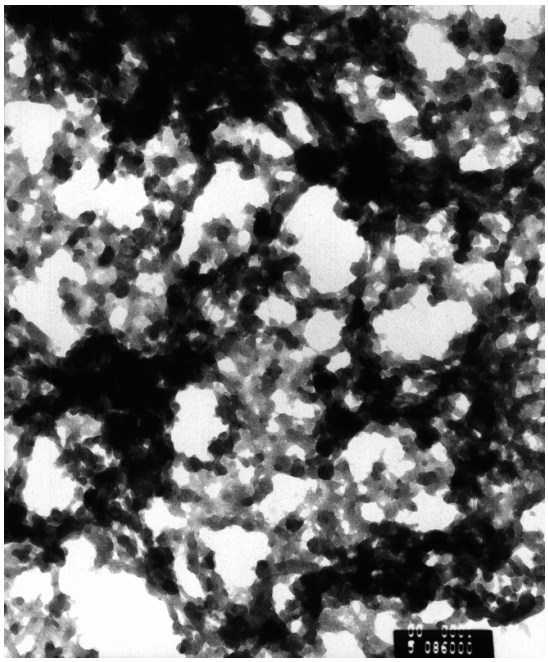

0.0001 M

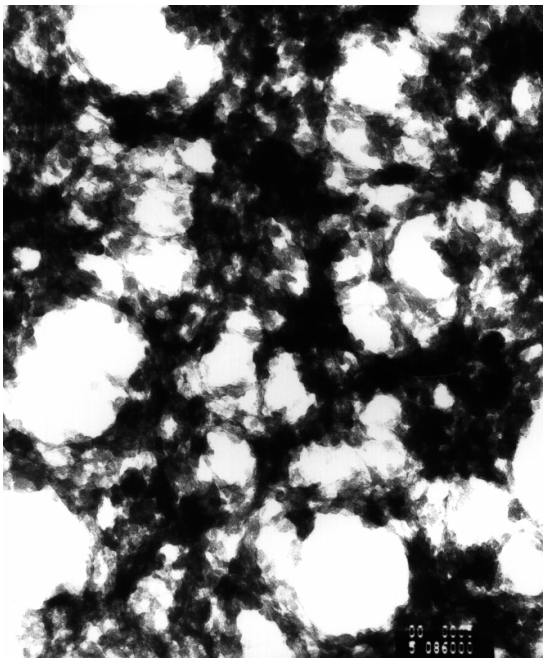

0.0006 M

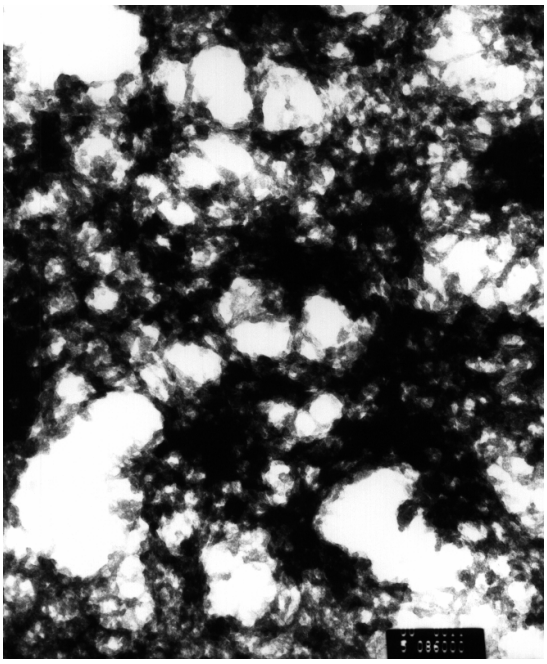

0.003 M

Figure 3.2

Influence of $Y(O^iPr)_3$ Concentration on Product Morphology

Fixed Conditions: w = 10, [AOT] = 0.1 M

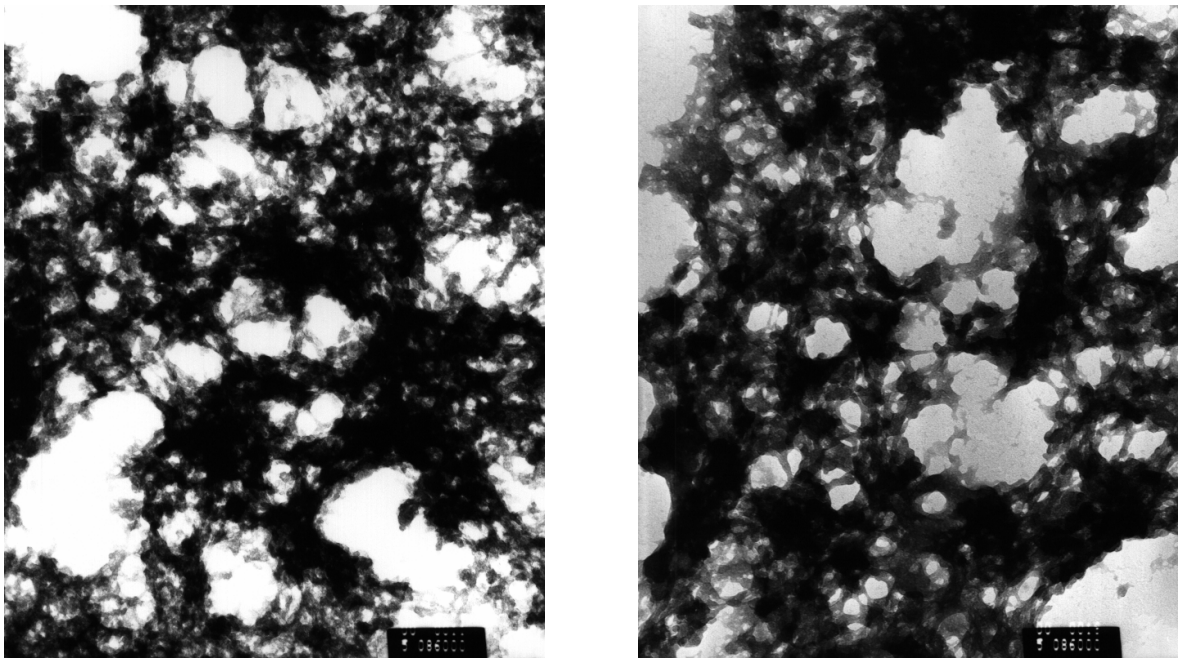

Deionized Water **5 M Ammonia**

Figure 3.3

Influence of Aqueous Phase pH Value on Product Morphology

Fixed Conditions: w = 10, V(Y(O^iPr)$_3$/toluene) = 1.0 mL, [AOT] = 0.1 M

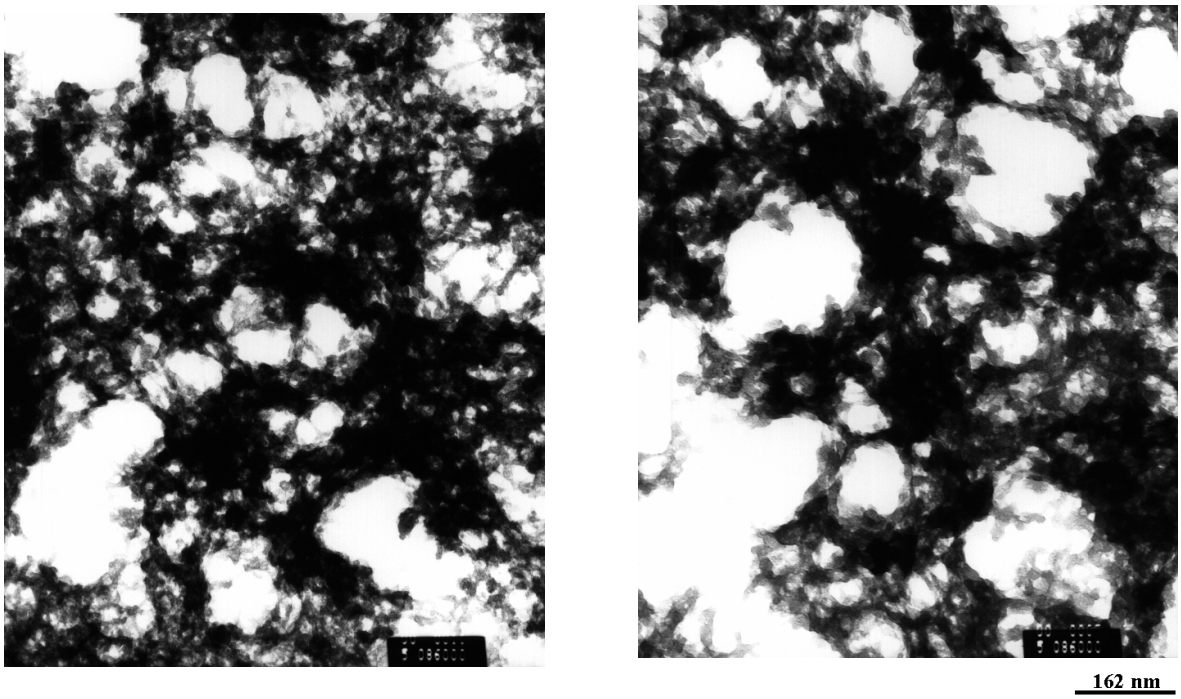

One Hour **Five Days**

Figure 3.4

Influence of Aging Time on Product Morphology

Sample I.D.: w = 10, V(Y($O^{i}Pr$)$_3$/toluene) = 1.0 mL, [AOT] = 0.1 M

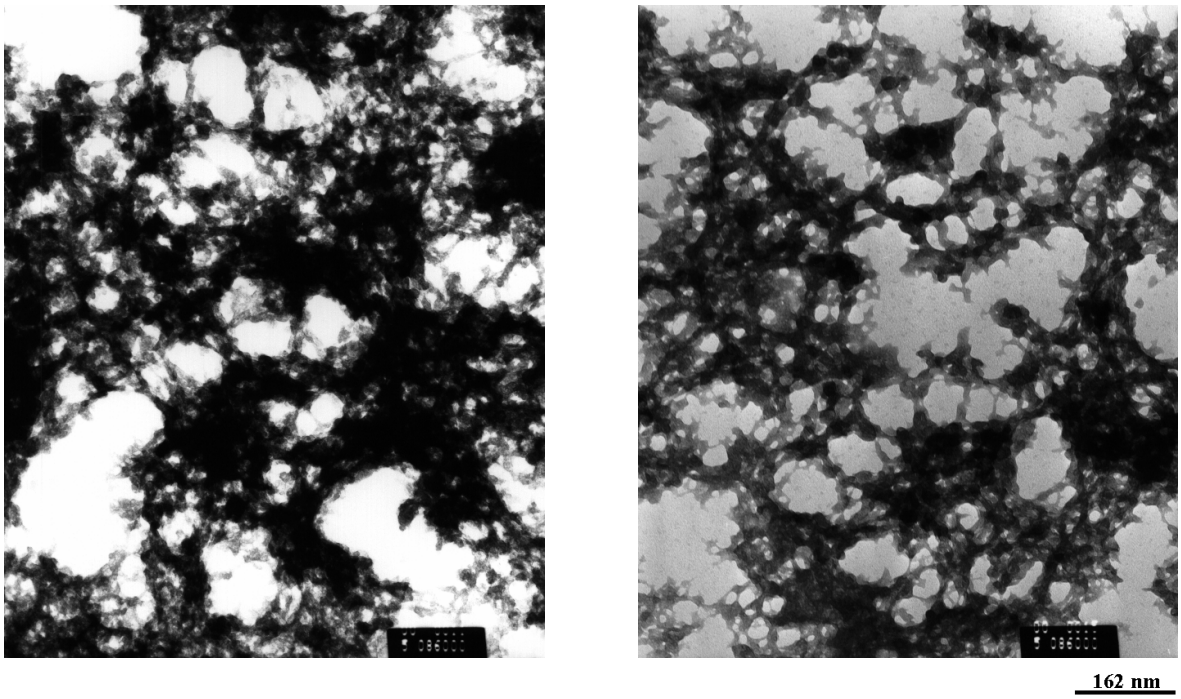

Room Temperature **Refluxing**

Figure 3.5

Influence of Aging Temperature on Product Morphology

Sample I.D.: w = 10, V(Y(O^iPr)$_3$/toluene) = 1.0 mL, [AOT] = 0.1 M

Chapter Four:
Annealing Effects

As shown in Chapter 2, the as-prepared nanoparticles were not well crystallized. Due to residual AOT molecules, the as-prepared nanoparticles did not appear clearly in TEM micrographs but existed in network-like aggregates. Residual AOT molecules were difficult to remove by solvent washing. These features are possible disadvantages in some applications. Because high-temperature annealing can improve crystallinity, and because organic surfactant molecules can decompose into gases at high temperatures, it is necessary to study the annealing effects of the as-prepared nanoparticle products. Results of the annealing experiments are summarized in Tables 4.1 to 4.3.

4.1 Effects of Varying the Annealing Temperature

To study temperature effects on yttrium oxide nanoparticles, a batch of dried as-prepared product from the yttrium nitrate hydrolysis method (preparation conditions: w = 7.5, $[Y^{3+}]$ = 1.0 M, $[NH_3]$ = 5 M, and [AOT] = 0.1 M) was divided into several portions. Because dried as-prepared product was usually in blocks, it was first ground into powder in an Al_2O_3 mortar for several minutes. Each of the portions was put in an Al crucible with a cover and annealed at a different temperature (200 °C, 400 °C, 600 °C, 800 °C, or 1000 °C) for a same period of time (16 h) in a muffle furnace with auto temperature control. After the power was turned off, the annealed sample was cooled at the intrinsic rate of the furnace with the furnace door closed. Overnight cooling reduced the temperature of a sample to room temperature. Each annealed sample was then removed for characterization. The annealed samples were still in powder form, and no obvious sintering was observed. TEM specimens of the annealed samples were prepared according to the procedure described in Section 1.5. XRD experiments were also conducted on the annealed samples.

4.1.1 Color Change and Weight Loss

The sample annealed at 200 °C was white or slightly yellow, but the sample annealed at 400 °C was dark-brown. Samples annealed at 600 °C or higher were white. The dark-brown

color of the sample annealed at 400 °C probably resulted from carbon produced during decomposition of AOT molecules. At 200 °C, only a few AOT molecules began decomposing. The weight loss of the sample annealed at 200 °C (17%) probably resulted from dehydration (Table 4.1).[46] Both the color change and weight loss (42%) of the sample annealed at 400 °C (Table 4.1) indicate significant decomposition of AOT at this temperature. After 16 h of heating, the weight loss of the samples appears to be complete between 600 °C and 800 °C. Therefore, the decomposition of AOT was initialized at approximately 200 °C and was complete at approximately 600 °C (Table 4.1).

4.1.2 TEM Results

TEM micrographs of specimens prepared from the samples annealed at different temperatures are shown in Figure 4.1. Evolution of the particle morphology is apparent with annealing temperatures. Compared to the original unannealed product, the sample annealed at 200 °C showed much larger particles and less network-like aggregation (Figure 4.1). However, the larger particles were not single crystallites, because some internal structures could be found, suggesting aggregation. The morphology change from network-like aggregates in an as-prepared product to larger particle aggregates in the sample annealed at 200 °C was probably caused by surface tension variation during heating. The deep dehydration might cause a surface tension change of the solid sample and, therefore, a morphology change. As mentioned above, both color change and weight loss indicate significant AOT decomposition in the sample annealed at 400°C for 16 h. The TEM micrograph also implies significant AOT decomposition in the sample. In the micrograph (Figure 4.1), particle aggregates were fluffy. The fluffy regions might be the regions of AOT molecules that have decomposed.

The TEM micrograph (Figure 4.1) of the sample annealed at 600 °C showed much more distinct particles with particle boundaries that were much clearer than those in the as-prepared product. This observation is consistent with the observation that the color change and weight loss are nearly complete at approximately 600 °C. The distinct particles in the TEM micrograph of the sample annealed at 600 °C indicates that 600 °C might be a turning point of the annealing process. Below this temperature, the process is mainly a dehydration and AOT-decomposition process. Above this temperature, it is a particle-growth process. Particle sizes obtained from

TEM were in the range of 10 nm to 100 nm, which were larger than the sizes of unannealed nanoparticles (10 nm to 40 nm) (Table 4.2).

After being annealed at 800 °C, the TEM specimen of the annealed sample contained larger particles of sizes in the range of 20 nm to 100 nm (Table 4.2). Some particles in the micrograph (Figure 4.1) were obviously single crystallites that had a light "ring" region in the nanoparticle image, representing the existence of well-oriented crystalline planes. If a crystalline plane of a single crystallite is well-oriented to the incident electron beam, the reflection of the beam by the plane will cause the plane look like with light ring in it. Even larger particles (some were approximately 130 nm) were found in the sample annealed at 1000 °C. Particle aggregation was not too serious in the annealed samples. Many single crystallites could be found in the micrographs (Figure 4.1). The products from the isopropoxide method have similar annealing effects (Figure 4.2).

4.1.3 SAD Results

An electron beam can be focused on a single isolated crystallite or a large single crystallite region in a particle aggregate in a TEM specimen to illuminate only a single selected crystallite. The spot diffraction pattern obtained this way only carries structural information from that single crystallite. A single crystallite found in a specimen can also be tilted by tilting the specimen stage carefully to exhibit spot diffraction patterns from different crystalline planes, which provide more structural information about that single crystallite. This technique is called the microprobe technique, or the Selected Area Diffraction technique (SAD).[99] It was used to investigate lattice structure of a single crystallite from a sample annealed at high temperatures in this research.

A particle approximately 200 nm in size was found in the specimen of a sample annealed at 1000 °C for 4 h (Figure 4.3). It was composed of several single crystallites, as shown in Figure 4.3. The electron beam was focused on the largest single crystallite region in the middle of the particle to investigate its structure. A spot pattern originating from the cubic [001] zone axis, in which the 4-fold symmetric Kikuchi bands[100] were very clear, was observed (Figure 4.4). Three

[99] In *Electron Microscopy and Microanalysis of Crystalline Materials*, J. A. Belk (Ed.), Applied Science, London, (1979).
[100] Cowley, J. M.: In *Electron Diffraction Technique I*, J. M. Cowley (Ed.), Oxford University Press, New York, 53 (1992).

different spot patterns ([001], [012], and [111]) observed on the same single crystallite were also found on other single crystallites in the same sample. These patterns indicated a body-centered cubic structure, which is consistent with that of the cubic Y_2O_3 phase. However, the detailed patterns were not exactly the same as the calculated [001] pattern of the cubic Y_2O_3 phase (Figure 4.5). Some diffraction spots were systematically lost. This observation was very strange because the XRD pattern of the same sample was identical to that of the cubic Y_2O_3 phase (Figure 4.6). The systematic change of diffraction pattern was caused by some systematical change of the lattice, which might result from impurity elements (sulfur, and so on) from decomposed AOT molecules.

4.1.4 XRD Results

XRD patterns of the samples annealed at different temperatures showed clear phase evolution from the highly distorted structure to the cubic Y_2O_3 phase (Figure 4.7). The XRD pattern of a dried as-prepared product had three very weak and broad peaks at approximately 30°, 42°, and 52°. The XRD patterns of the samples annealed at 200 °C and 400 °C resembled that of the as-prepared product, but the peak at around 30° gradually shifted toward a lower angle closer to the strongest peak of the cubic Y_2O_3 phase at 29.15° ([222]). This peak finally became the strongest, and was identical to the strongest peak of the cubic Y_2O_3 phase at approximately 29.15° (Figure 4.7). Therefore, the structure of the as-prepared yttrium oxide nanoparticles was related to the cubic Y_2O_3 phase. The other two peaks became weaker and finally disappeared. The similarity between the XRD patterns of the as-prepared sample and the sample annealed at 200 °C, which implies similar structure, further supports the conclusion that the larger particles observed by TEM in the sample annealed at 200 °C were not single crystallites.

Some relatively narrow and stronger peaks at approximately 30°, 42°, and 55° appeared in the sample annealed at 600 °C for 16 h (Figure 4.7). In fact, these peaks were first found in the sample annealed at 600 °C for 4 h and did not belong to the cubic Y_2O_3 phase. Since they did not match the peaks of any yttrium related phases in the JCPDS database, these peaks are assigned as an unknown phase. This unknown phase further developed at higher annealing temperatures (800 °C for 16 h). The peaks became stronger and sharper, indicating larger and better-crystallized regions of the unknown phase. At this annealing condition, the cubic Y_2O_3 phase was also well-

developed, and the four strongest peaks of the cubic phase, as well as some much weaker peaks, appear clearly in the XRD pattern (Figure 4.7). The XRD pattern of the sample annealed at 1000 °C for 4 h was identical to that of the cubic Y_2O_3 phase (Figure 4.6). The unknown phase disappeared in the sample annealed at 1000 °C for either 4 h or 16 h (Figure 4.7). This unknown phase might be some oxide complex phase formed among yttrium and impurity elements (sulfur, and so on) from the decomposed AOT molecules.

The estimated ranges of particle sizes measured from TEM photographs and the average sizes of the crystalline regions calculated from XRD peak broadening of the annealed samples are listed in Table 4.2. Due to particle aggregation, the accuracy of particle size estimation from TEM photographs is limited. The average sizes of the crystalline regions in the annealed samples were calculated from XRD peak broadening with a function of the instrument software applying the Scherrer equation:[101]

$$D = \frac{K\lambda}{\beta \cos\theta} \qquad 4.1$$

where D is the average size of crystalline regions, which can be considered as the average thickness of a set of crystalline planes of a same index. K is a constant, which is usually between 0.9 and 1.0. It was set at 0.94 in the software. λ is the incident X-ray wavelength, which for Cu K_α radiation is 1.5406 Å. β is the contribution to the full-width-half-maximum (FWHM) of a peak due to the broadening caused by small sizes of crystalline regions. θ is the angle of a diffraction peak, which is one-half of the 2θ position of the peak in the XRD patterns. Original FWHM of a diffraction peak obtained directly from a XRD pattern contains not only components caused by small crystallites and distorted crystalline structure, but also some other broadening components, such as instrumental broadening and K_α doublet broadening.[101] To eliminate the other broadening factors, calibration scans were conducted at the same instrumental conditions on a standard sample, bulk α-Al_2O_3 powder (>1 μm), that has no peak broadening due to small crystallites and distorted crystalline structure. The peak broadening data of the standard sample, were collected by the diffractometer automatically and used in the calculation of the broadening due to small sizes of crystalline regions in the nanocrystalline samples. The FWHMs of the strongest peak of the cubic Y_2O_3 phase at 29.15° was used to calculate average sizes of the

crystalline regions of the cubic Y_2O_3 phase in the annealed samples, while the FWHMs of the peaks at 45.3° and 55.4° of the unknown phase were used to calculate those of the unknown phase in the annealed samples. Computer deconvolution by the instrument software was used to resolve any peak overlaps. Since it is hard to tell whether the peak broadening is caused by small crystallites or distorted crystalline structure, the calculated sizes have only relative meaning. Larger calculated sizes not only indicate really larger crystallites, but also indicate better crystalline. The average sizes of the crystalline regions increased with increasing annealing temperatures for both of the phases. The data were consistent with the estimated ranges of particle sizes from TEM micrographs (Table 4.2). The very small size of the crystalline regions of the cubic Y_2O_3 phase in the sample annealed at 600 °C for 16 h (4.7 nm) indicated that the much larger particles of that sample observed under TEM were probably particles mostly in the unknown phase, whose calculated average size of crystalline regions (29.7 nm and 17.4 nm) is consistent with the TEM estimation (10 ~ 100 nm).

4.2 Effects of Varying the Annealing Time

The effects of annealing time on the annealed samples were similar to those of annealing temperatures. The three TEM micrographs in Figure 4.8 were taken from three samples from the same batch prepared through the nitrate hydrolysis method but annealed at 800 °C for different intervals (1, 4, and 16 h). The micrographs showed that longer annealing time resulted in larger particles. Crystallinity was better in samples annealed for longer periods of time, and more single crystallites appeared. Some flocculent material, possibly the regions containing AOT molecules that have decomposed, was found in the specimen annealed for only 1 h. Since the sample was annealed at 800 °C for only 1 h, some AOT molecules might not decompose completely during such a short interval, even though the annealing temperature was much higher than the AOT "decomposition" temperature (200 °C to 600 °C). Particle aggregation was minimal in the samples, but longer annealing time did facilitate aggregation.

The XRD pattern showed that only the unknown phase clearly appeared in the sample annealed at 800 °C for 1 h (Figure 4.9). The peak at around 30° was still very broad. The peak at 64.5°, which was at the same position of the [721] diffraction of the cubic phase, was weak.

[101] Klug, H.; Alexander, L.: In *X-ray Diffraction Procedures,* John Wiley & Sons, New York, 491 (1954).

When the sample was annealed for 4 h, the cubic phase became well-developed, but its abundance was still less than that of the unknown phase, as indicated by the peak intensities. In the sample annealed for 16 h, the two phases had about the same abundance. The relative intensity of the peak at 64.5° ([721] diffraction) to that of the strongest peak at 29.15° of the cubic phase ([222] diffraction) was much higher than the value from JCPDS (3%). However, it decreased with increasing annealing time (63%, 34%, and 29% in the samples annealed for 1 h, 4 h, and 16 h, respectively). When the annealing time was long enough or the annealing temperature was high enough, the ratio became close to the reported value (6% in the sample annealed at 1000 °C for 16 h).

The annealing temperature effects were greater than the annealing time effects. As shown in Figure 4.9, the sample annealed at 1000 °C for only 1 h contained much more cubic-structured material than the sample annealed at 800 °C for 16 h. Sizes of the crystalline regions in the samples annealed for different periods of time were also calculated from XRD peak broadening by the software. The sizes calculated were consistent with the particle sizes estimated from TEM micrographs (Table 4.3). Longer annealing time resulted in larger crystalline regions.

4.3 Effects of Surfactant

As discussed in Section 2.4, reverse micelles formed by AOT molecules enabled uniform yttrium oxide nanoparticles to be produced. AOT molecules influenced the annealing of the nanoparticle products. An yttrium oxide sample was prepared by mixing the same volume of 0.5 M $Y(NO_3)_3$ with 5 M NH_3. The precipitate was separated by centrifuging and dried. It was then divided into several portions. Each portion was annealed at different temperatures for 16 h. Figure 4.10 shows XRD patterns of the as-prepared product as well as the annealed ones. The XRD pattern of the dried as-prepared product from aqueous solution was the same as that of the as-prepared product prepared from reverse micelle solution using the nitrate hydrolysis method (Figure 2.2). The result can not tell any significant difference in structure between the as-prepared product from reverse micelle solution and the as-prepared product form aqueous solution. When the product prepared from aqueous solution was annealed at elevated temperatures, XRD patterns of the annealed samples showed clearly the evolution of the cubic Y_2O_3 phase (Figure 4.10). The unknown phase was not found in the annealed sample at any

annealing temperature. This observation confirms that the unknown phase found in the annealed samples prepared from reverse micelle solution was due to AOT residue (Section 4.1).

In addition, the growth rate of the cubic phase in the product prepared from the aqueous solution was much greater than that in the product prepared from the reverse micelle solution. In Figure 4.10, the XRD patterns show that the cubic phase did not appear in the product prepared from reverse micelle solution when it was annealed at 600 °C for 16 h. However, the cubic phase was well-developed in the product prepared from aqueous solution precipitation when it was annealed at only 400 °C for 16 h. Because it is known that AOT molecules are difficult to remove from the as-prepared products (Section 2.6), nanoparticles in the products were covered with residual AOT molecules. A possible explanation is that, before complete decomposition of AOT molecules, atom migration between nanoparticles was limited by the surface AOT molecules during annealing. Therefore, the cubic phase formation was delayed. However, the residual elements of decomposed AOT molecules (S, and so on) on nanoparticle surfaces might diffuse into the nanoparticles to form the unknown phase. Only after complete decomposition of AOT molecules at approximately 600 °C, the cubic phase began growing, as observed from the XRD patterns (Figure 4.7). The abnormally high intensity of the [721] diffraction peak observed in the annealed samples prepared from the reverse micelle solution was not observed in the annealed sample prepared from the aqueous solution. The relative intensity of this peak was approximately 5% to 7% of the strongest [222] peak in the annealed samples.

4.4 Effects of Europium Doping

Y_2O_3:Eu is an important red-emitting phosphor.[94] Nanocrystalline Y_2O_3:Eu is believed to have improved performance.[4] Both cubic Eu_2O_3 and cubic Y_2O_3 have the body-centered cubic structure of the Ia3 (No. 206) space group. $(Y_{1-x}Eu_x)_2O_3$ samples (x = 0.1%, 0.5%, 1.0%, 10.0%) were prepared through the nitrate hydrolysis method at the optimized condition (w = 7.5, $[Y^{3+}+Eu^{3+}]$ = 0.5 M, $[NH_3]$ = 2 M, [AOT] = 0.1 M). The Eu-doping was accomplished by replacing 0.5 M yttrium nitrate aqueous solution with a mixed nitrates aqueous solution of the same concentration and volume. Eu-doped products had the same network-liked morphology as the pure yttrium oxide products prepared at the same condition (Figure 4.11). Therefore, europium ions had no effects on the morphology of the as-prepared nanoparticle products. Since the crystallinity of the as-prepared products was very poor, studies were carried out to investigate

annealing effects on the Eu-doped yttrium oxide products. A batch of 1% Eu-doped product was divided into several portions, each portion was annealed at different temperatures for different periods of time. XRD experiments of the annealed samples were also carried out.

The diffraction patterns of the doped sample annealed at below 400 °C showed no significant difference from the patterns of the pure sample annealed at low temperatures (Figure 4.12). The unknown phase appeared clearly in the doped sample annealed at 600 °C for only 1 h. It became stronger when the annealing time was increased to 4 h. However, the unknown phase barely appeared in the pure sample when it was annealed at 600 °C for 4 h (Figure 4.12). The cubic phase was insignificant in the pure sample annealed at 800 °C for 1 h (Figure 4.9), but it had become the dominant phase in the doped sample annealed at 800 °C for 1 h (Figure 4.12). Therefore, Eu-doping increased the evolution rate of the phases. Although cubic Eu_2O_3 and cubic Y_2O_3 have the same crystal structure, the ionic radius of Eu^{3+} (108.7 pm) is a little larger than that of Y^{3+} (104.0 pm). Therefore, the Eu^{3+} impurity in an yttrium oxide sample caused a distortion of the structure that made atom migration faster. This process increased the crystalline growth rate. Like the pure sample, the doped sample annealed at 1000 °C for 4 h was completely cubic phase. No significant difference was found between the XRD pattern of the cubic phase obtained from the doped sample and that from the pure sample. A XRD pattern of 5% Eu-doped cubic Y_2O_3 was found in JCPDS database (#25-1011), which is the same as that of pure cubic Y_2O_3 (#41-1105).

4.5 Conclusion

High temperature annealing improved the crystallinity of the as-prepared yttrium oxide nanoparticle products, and caused growth and aggregation of the nanoparticles. Decomposition of residual AOT molecules in the as-prepared products occurred in temperatures ranging from 200 °C to 600 °C. Before the complete decomposition of AOT molecules, cubic phase growth was prevented by the protection of AOT molecules. An unknown intermediate phase appeared in the samples annealed between 600 °C and 1000 °C, which disappeared after annealing at 1000°C for over 4 h. The unknown phase was related to AOT residue, since it was not found during annealing of yttrium oxide products prepared from aqueous solution precipitation. XRD patterns of the samples annealed at 1000 °C over 4 h were identical to the pattern of cubic Y_2O_3 phase.

However, the TEM microprobe technique indicated systematic structure deviation in single nanocrystallites. Eu-doping, which had no effects on the morphology of as-prepared products, accelerated the annealing process. The annealing effects of a product prepared through the isopropoxide hydrolysis method have no significant difference from those of the nitrate hydrolysis method.

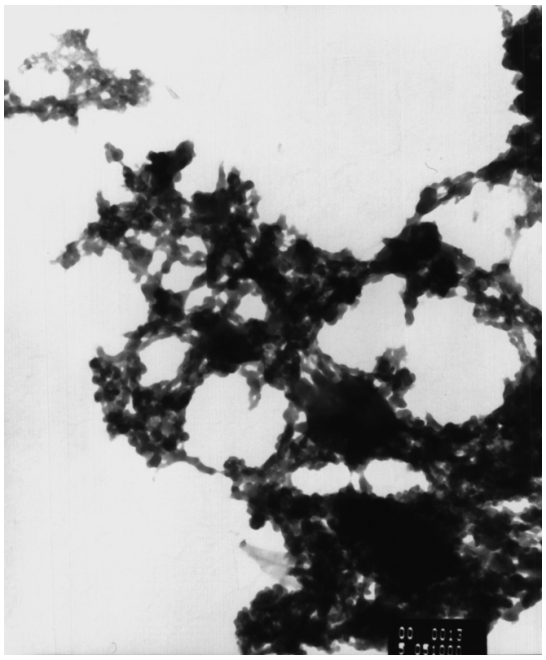

Original

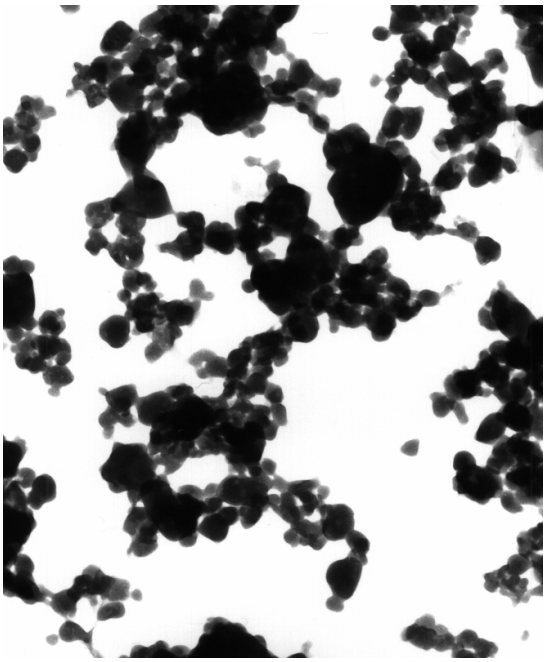

200 °C 16 h

400 °C 16 h

Figure 4.1

Effects of Annealing Temperature (TEM)

Sample I.D.: w = 7.5, $[Y^{3+}]$ = 1.0 M, $[NH_3]$ = 5 M, [AOT] = 0.1 M

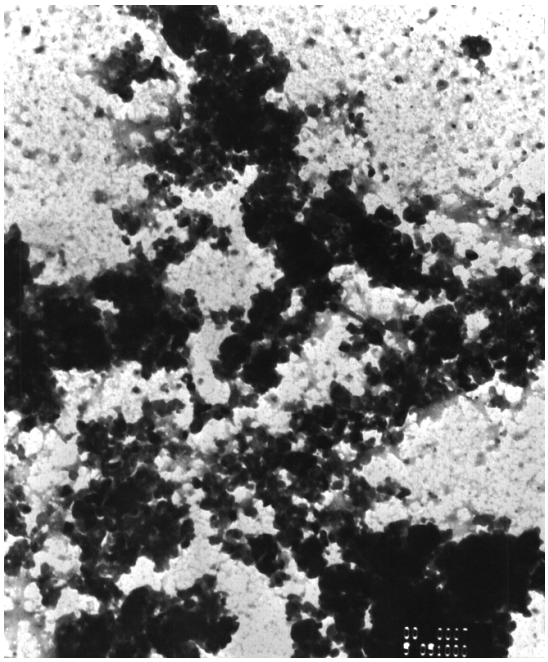

600 °C 16 h

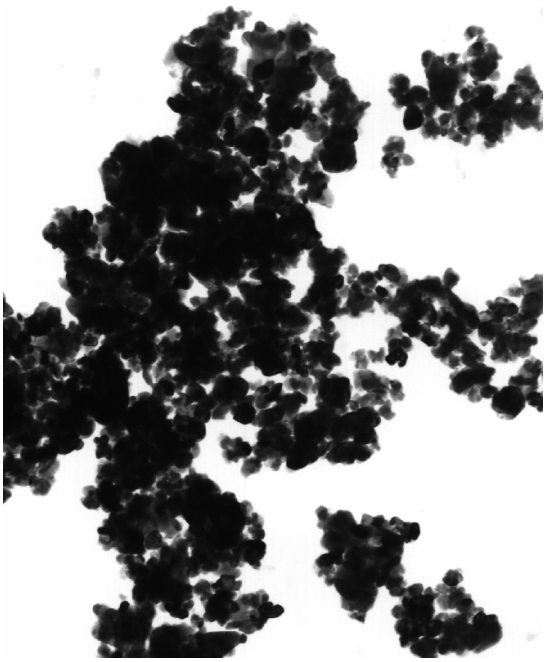

800 °C 16 h

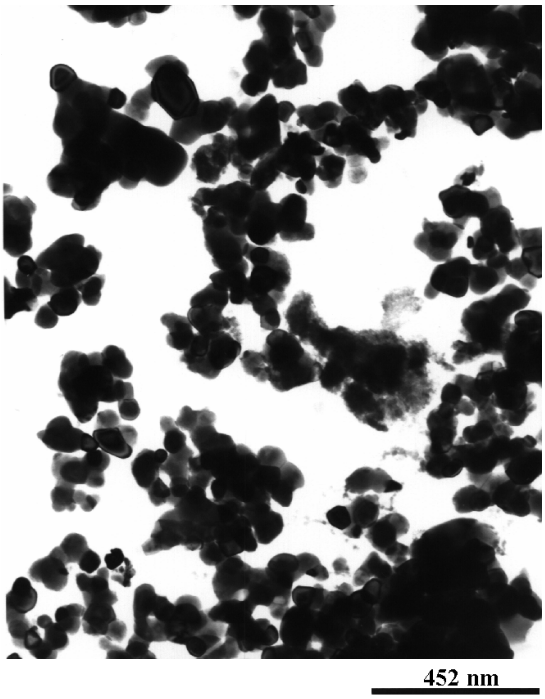

1000 °C 16 h

Figure 4.1 (Continued)
Effects of Annealing Temperature (TEM)

Sample I.D.: w = 7.5, $[Y^{3+}]$ = 1.0 M, $[NH_3]$ = 5 M, [AOT] = 0.1 M

200 °C 4 h

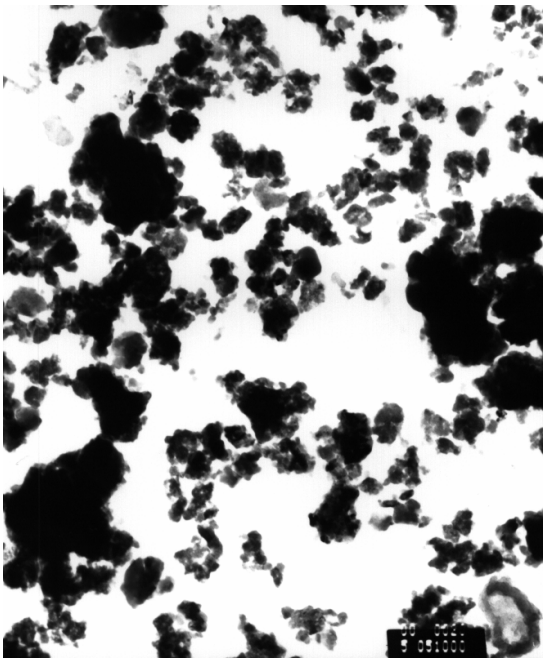

600 °C 4 h

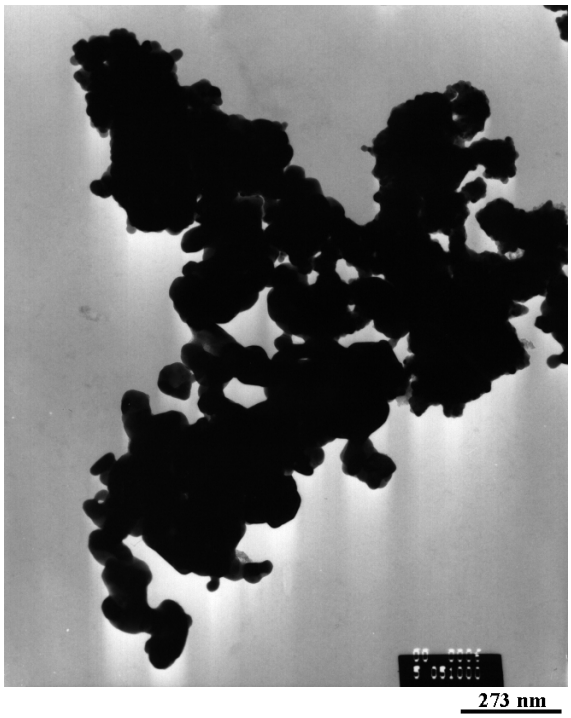

1000 °C 4 h

Figure 4.2

Annealing Effects of the Product of the Isopropoxide Method

Sample I.D.: w = 10, V(Y(O^iPr)$_3$/toluene) = 1.0 mL, [AOT] = 0.1 M

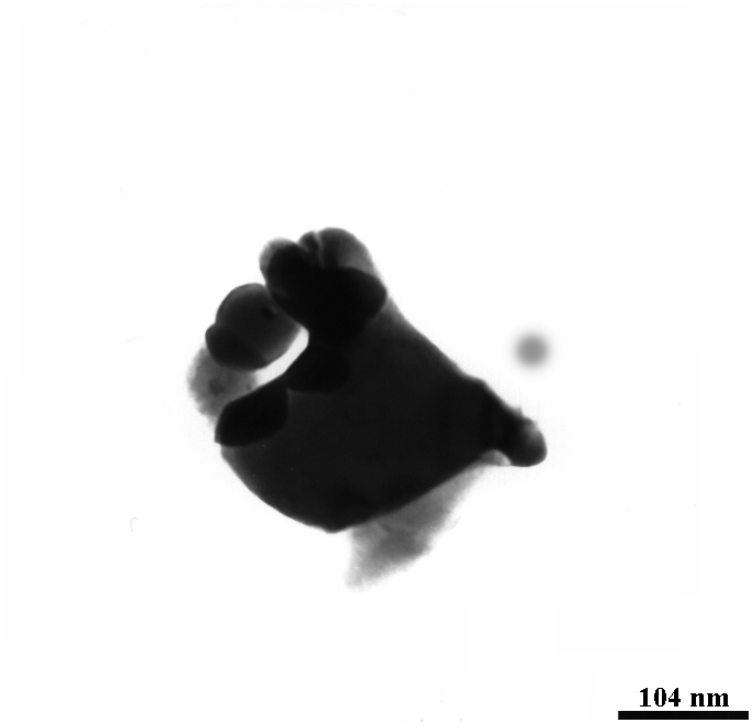

Figure 4.3

An Aggregate of Several Crystallites in a Sample Annealed at 1000 °C for 4 hrs

Sample I.D.: w = 7.5, $[Y^{3+}]$ = 1.0 M, $[NH_3]$ = 5 M, [AOT] = 0.1 M

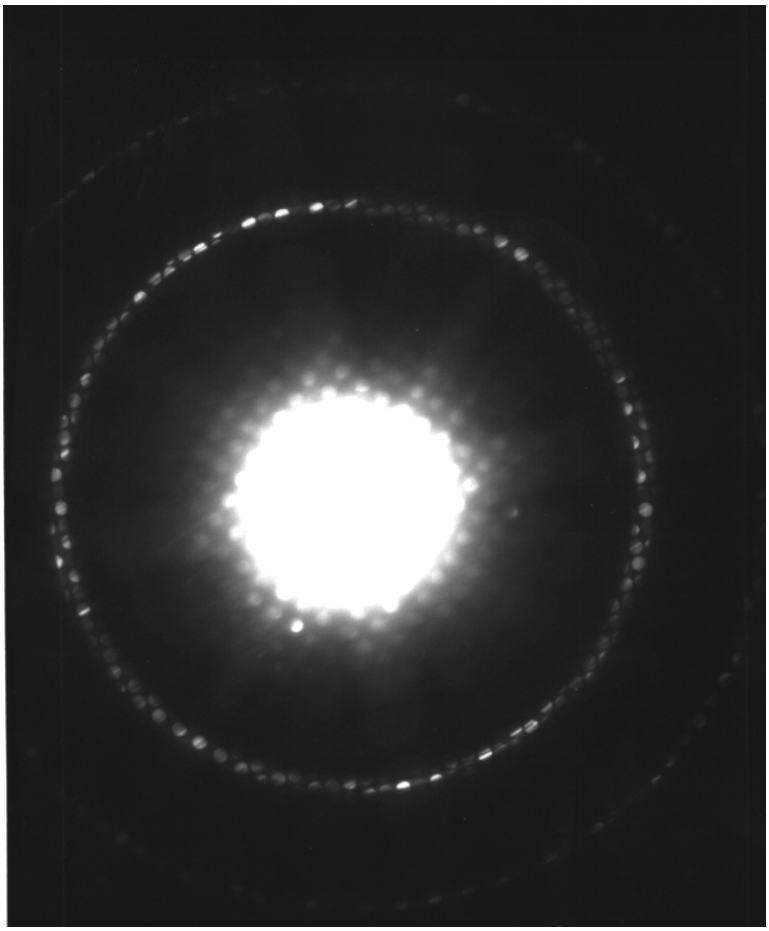

Figure 4.4

[100] Pattern of a Single Crystallite from Microprobe
(Camera Length 350 mm)

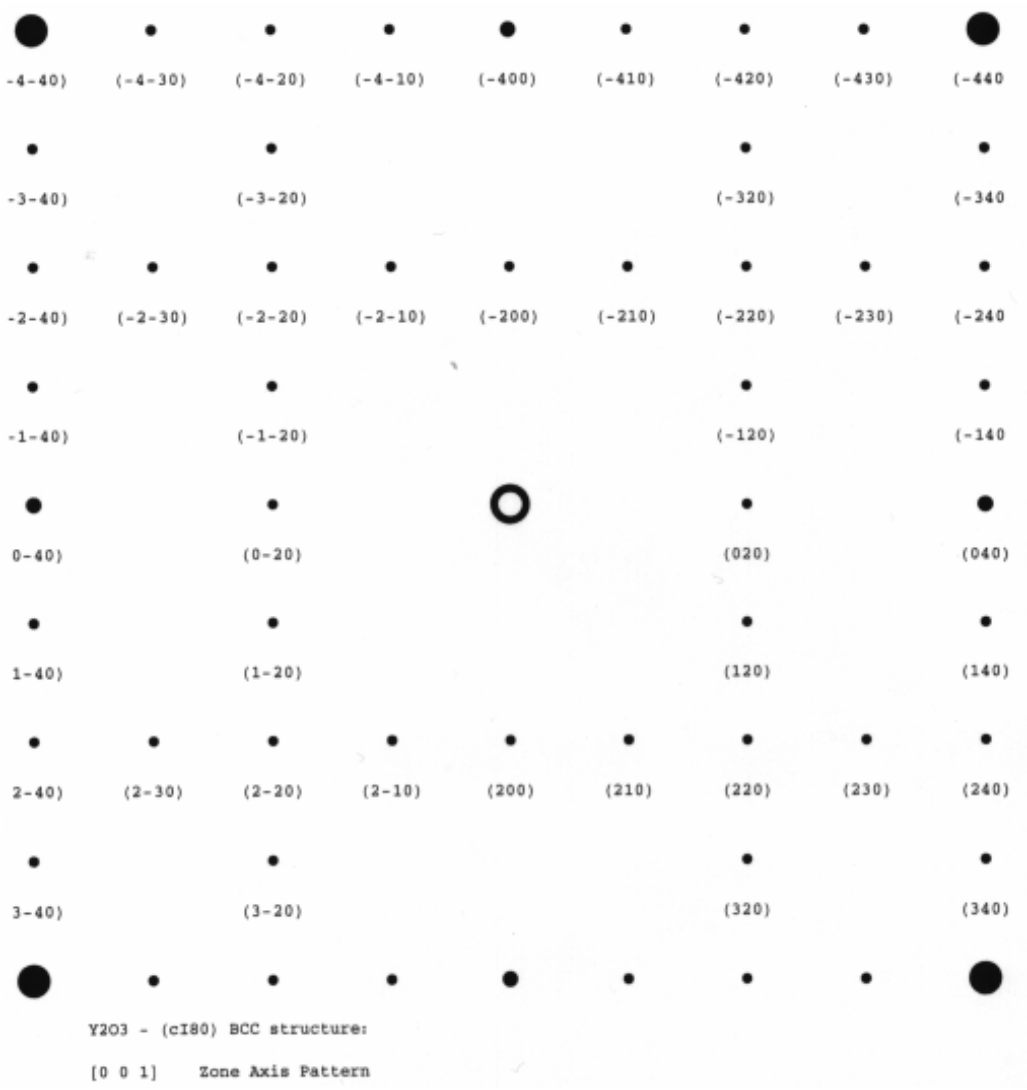

Figure 4.5

Calculated [100] Pattern of Cubic Y_2O_3

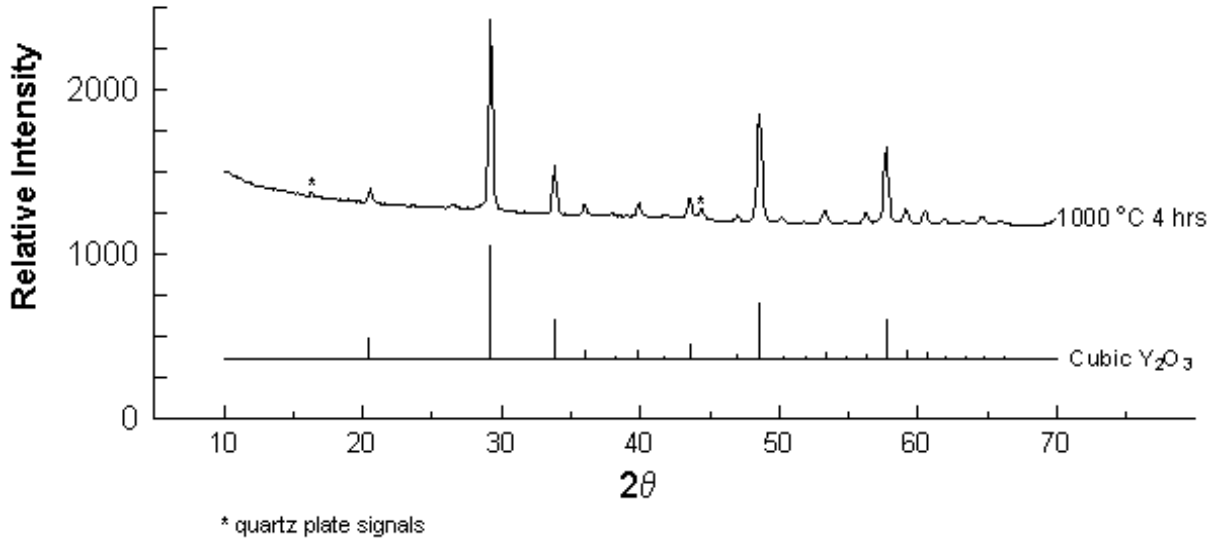

Figure 4.6

XRD Pattern of a Sample Annealed at 1000 °C for 4 hrs

Sample I.D.: w = 7.5, [Y^{3+}] = 1.0 M, [NH_3] = 5 M, [AOT] = 0.1 M

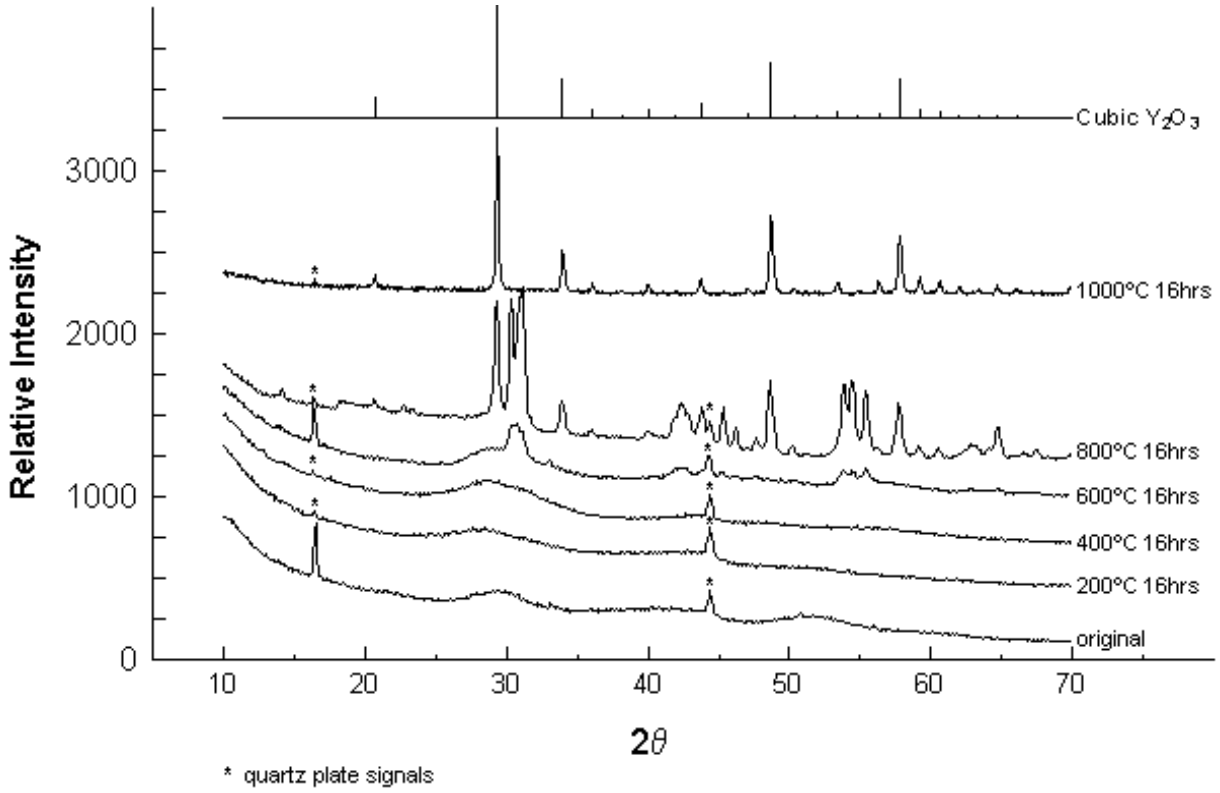

Figure 4.7

Effects of Annealing Temperature (XRD)

Sample I.D.: w = 7.5, $[Y^{3+}]$ = 1.0 M, $[NH_3]$ = 5 M, [AOT] = 0.1 M

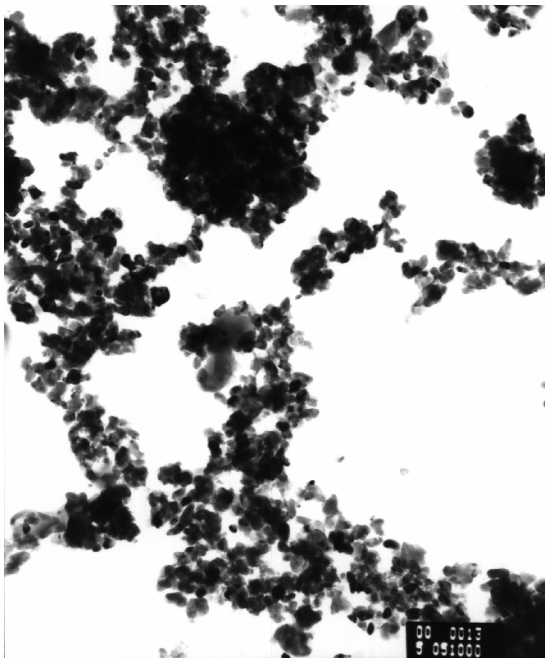

800 °C 1 h

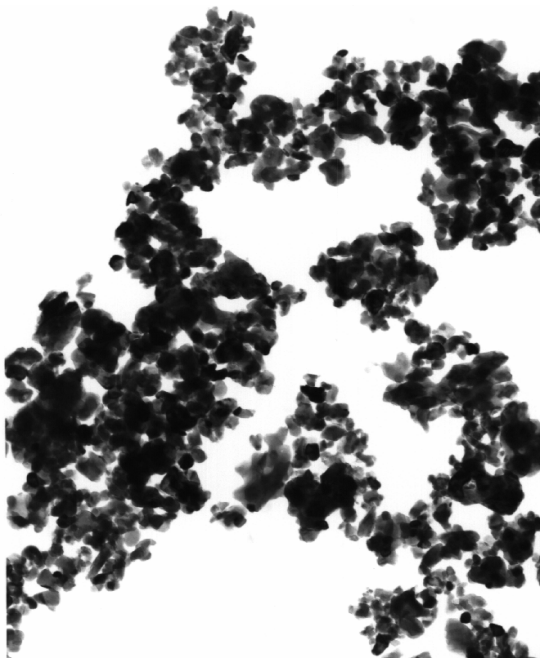

800 °C 4 h

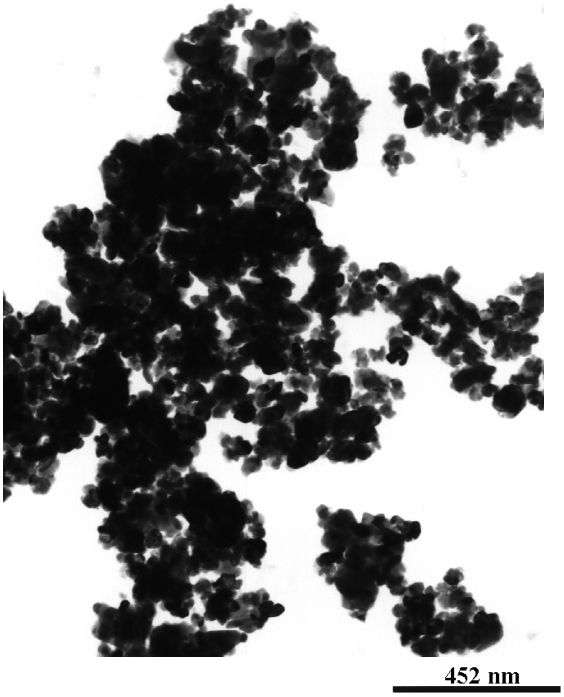

800 °C 16 h

Figure 4.8

Effects of Annealing Time (TEM)

Sample I.D.: w = 7.5, $[Y^{3+}]$ = 1.0 M, $[NH_3]$ = 5 M, [AOT] = 0.1 M

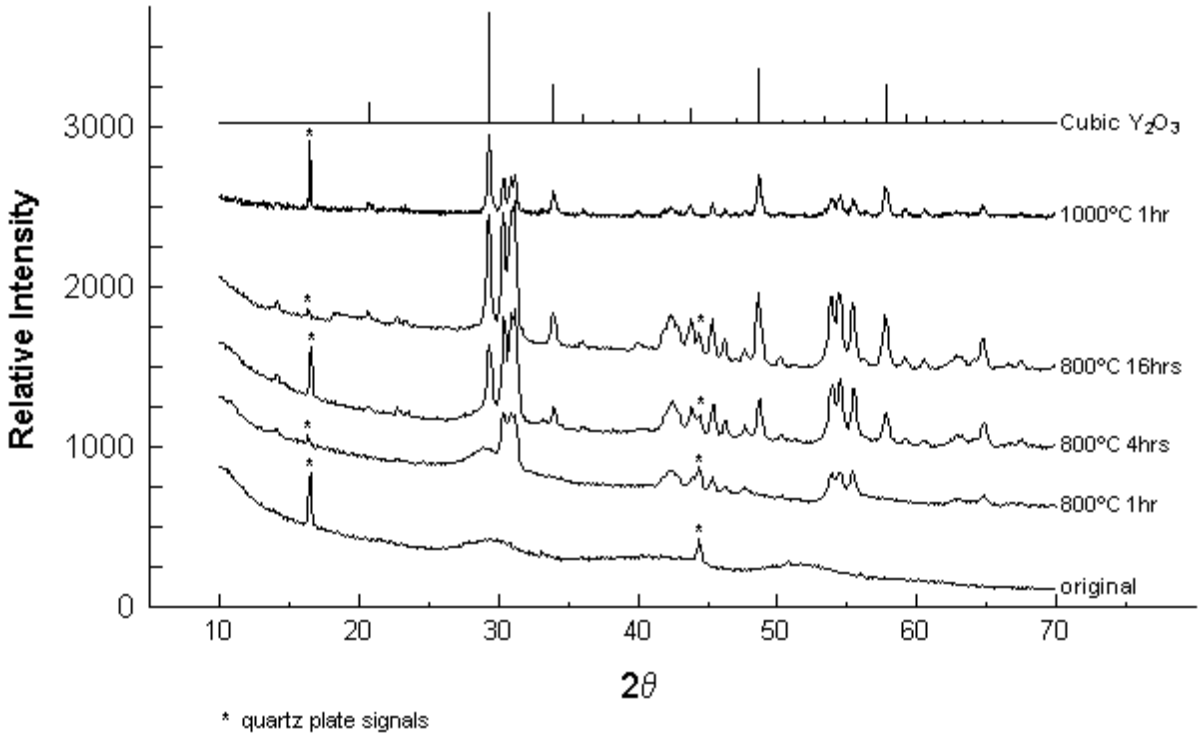

Figure 4.9

Effects of Annealing Time (XRD)

Sample I.D.: [AOT] = 0.1 M, [NH_3] = 5 M, [Y] = 1 M, H_2O/AOT=7.5

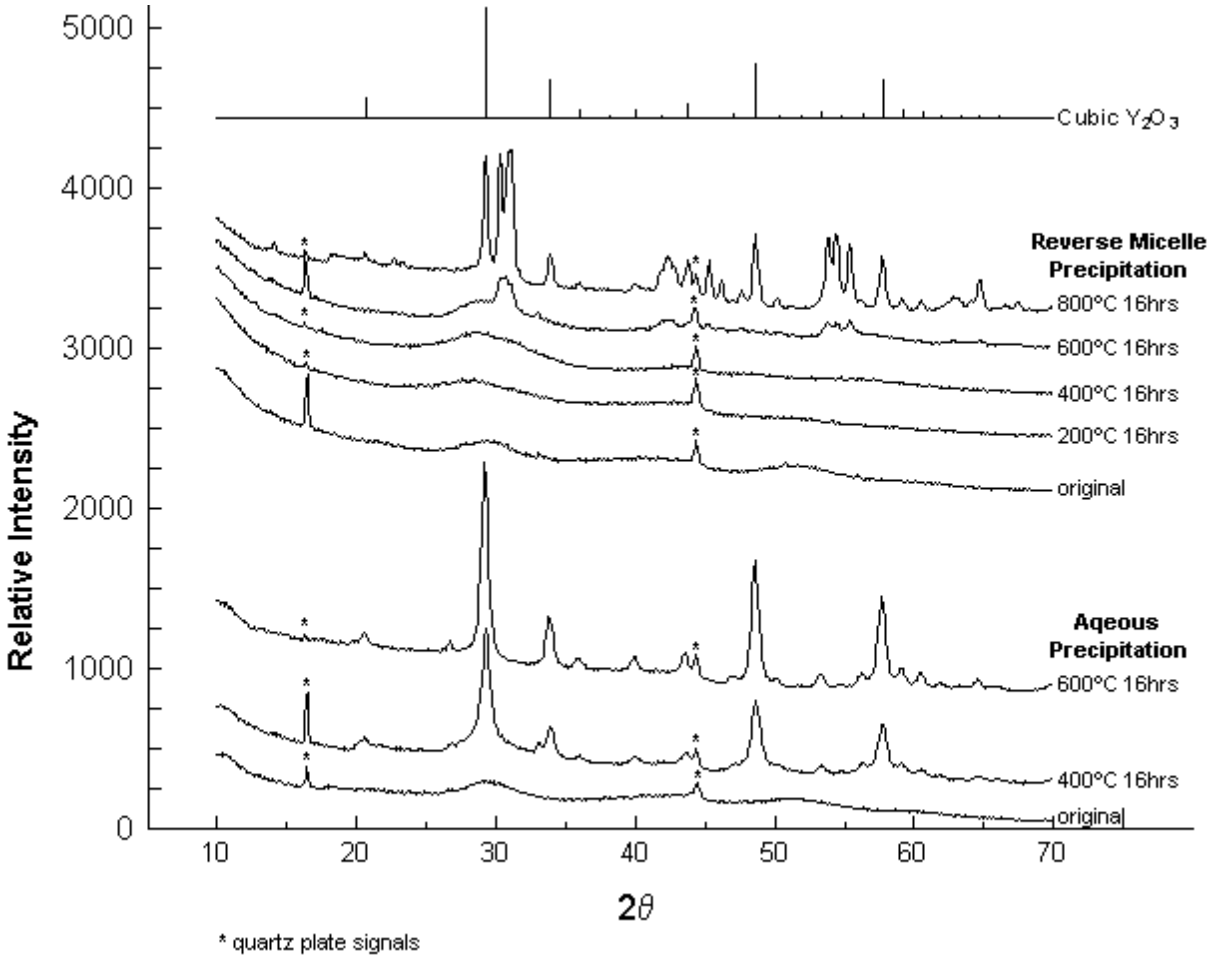

Figure 4.10

Effects of AOT (XRD)

Sample I.D.: [AOT] = 0.1 M, [NH_3] = 5 M, [Y] = 1 M, H_2O/AOT=7.5

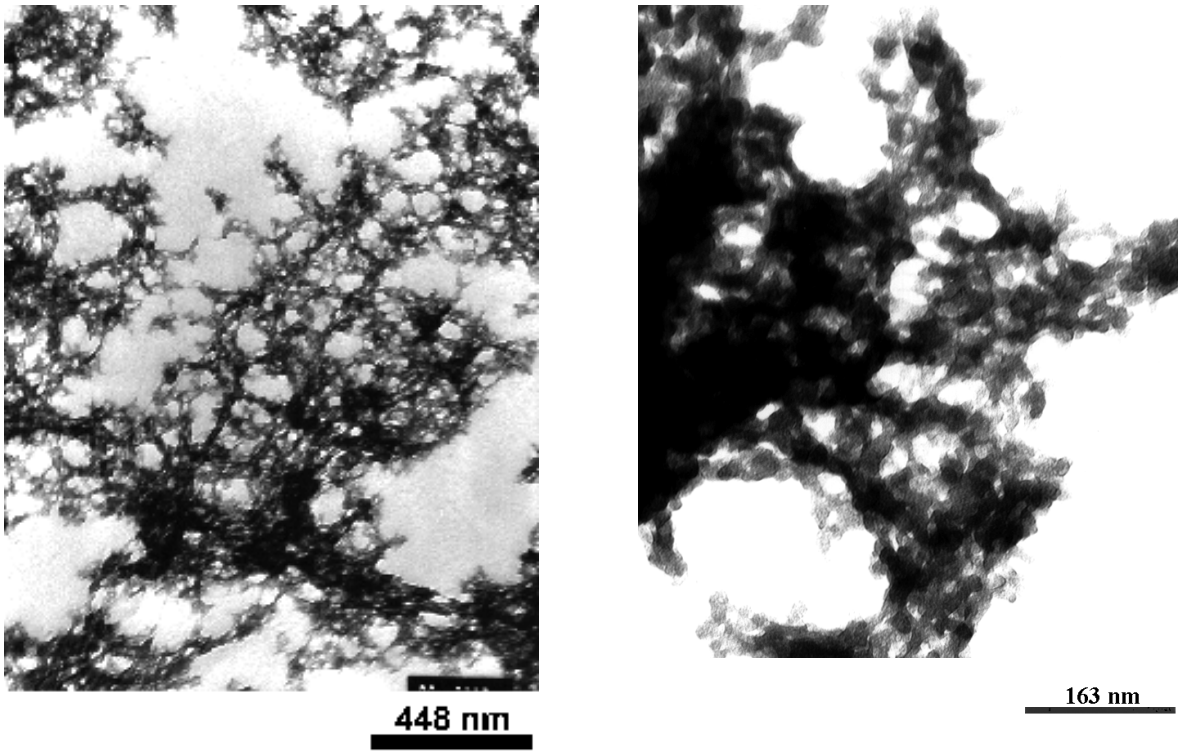

No Eu-doping **5% Eu-doped**

Figure 4.11

Effects of Eu-Doping (TEM)

Sample I.D.: w = 7.5, $[Y^{3+}+Eu^{3+}]$ = 0.5 M, $[NH_3]$ = 5 M, [AOT] = 0.1 M

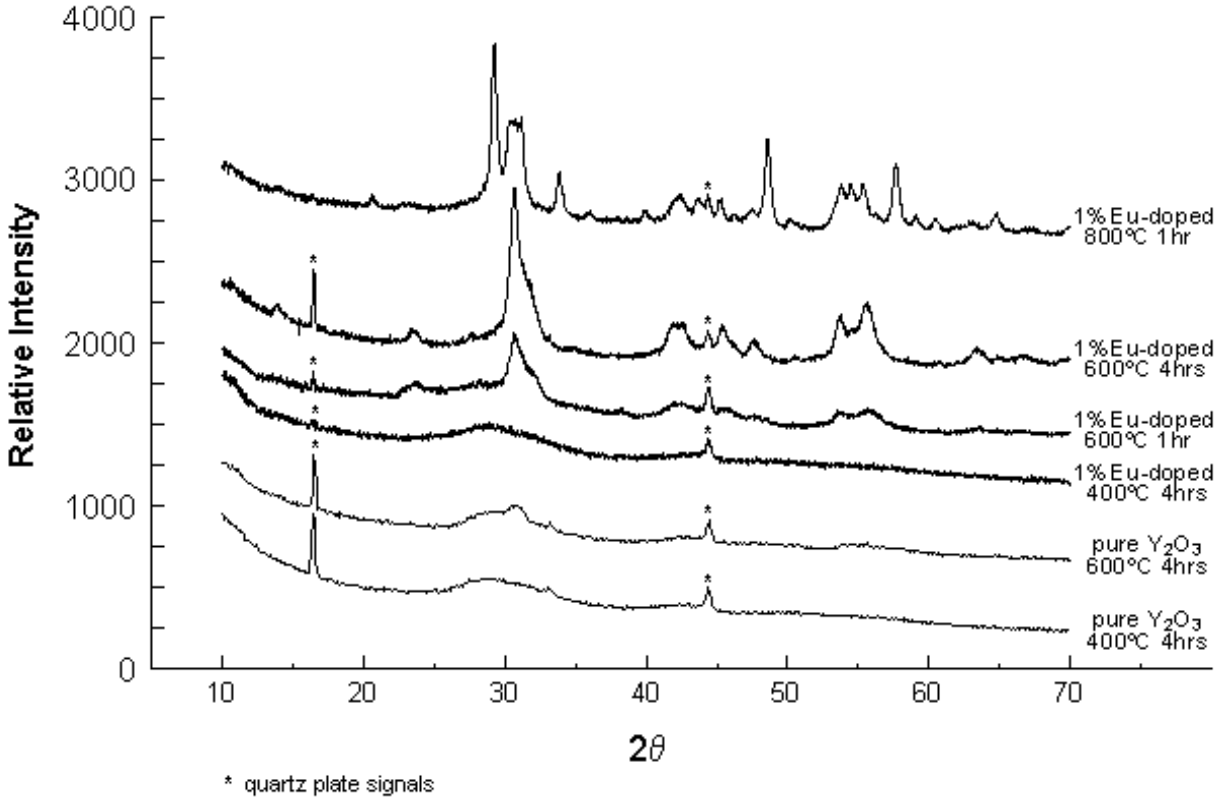

Figure 4.12

Effects of Eu-Doping (XRD)

Sample I.D.: w = 7.5, $[Y^{3+}+Eu^{3+}]$ = 0.5 M, $[NH_3]$ = 2 M, [AOT] = 0.1 M

Table 4.1

Weight Loss of Samples Annealed for 16 hrs

Annealing Temperature	Unannealed	200 °C	400 °C	600 °C	800 °C	1000 °C
Color	white	light yellow	dark brown	white	white	white
Weight Loss	0%	17%	42%	45%	51%	51%

Table 4.2

Sizes of Crystalline Regions in Samples Annealed at Different Temperatures

Sample I.D.: [AOT] = 0.1 M, [NH_3] = 5 M, [Y] = 1 M, H_2O/AOT=7.5

Annealing Temperature	Annealing Time	Particle Size from TEM	Cubic Phase		Unknown Phase			
			2θ	Size	2θ	Size	2θ	Size
original	-	10~40 nm	-	-	-	-	-	-
200°C	16 hrs	16~65 nm	-	-	-	-	-	-
400°C	16 hrs	16~65 nm	-	-	-	-	-	-
600°C	16 hrs	10~100 nm	28.51	3.7 nm	45.28	29.7 nm	55.43	17.4 nm
800°C	16 hrs	20~100 nm	29.24	67.2 nm	45.28	120.9 nm	55.39	61.9 nm
1000°C	16 hrs	20~130 nm	29.30	141.6 (48.68)	-	-	-	-

Table 4.3

Sizes of Crystalline Regions in Samples Annealed for Different Periods of Time

Sample I.D.: [AOT] = 0.1 M, [NH_3] = 5 M, [Y] = 1 M, H_2O/AOT=7.5

Annealing Temperature	Annealing Time	Particle Size from TEM	Cubic Phase		Unknown Phase			
			2θ	Size	2θ	Size	2θ	Size
800°C	1 hr	20~80 nm	28.95	3.3 nm	45.29	64.7 nm	55.39	38.7 nm
800°C	4 hrs	20~100 nm	29.27	49.3 nm	45.31	104.0 nm	55.42	63.1 nm
800°C	16 hrs	20~100 nm	29.24	67.2 nm	45.28	120.9 nm	55.39	61.9 nm
1000°C	1 hr	20~100 nm	29.28	139.6 nm	45.30	895.9 nm	55.41	119.5 nm

Chapter Five:
Conclusion and Outlook

Yttrium oxide nanoparticles could be synthesized from AOT/isooctane reverse micelle solution using both yttrium-nitrate hydrolysis and yttrium-isopropoxide hydrolysis reactions. Products of good morphology from both methods contained network-like nanoparticle aggregates. Their morphologies had no significant differences. The particle-size range of the products from the nitrate-hydrolysis method (10 nm ~ 40 nm) was comparable to that of the products from the isopropoxide-hydrolysis method (10 nm ~ 20 nm). Products of good morphology were obtained through the isopropoxide-hydrolysis method at all experimental conditions investigated, but products of good morphology were obtained through the nitrate-hydrolysis method in a relatively narrow range of experimental conditions. Therefore, the isopropoxide-hydrolysis method was more flexible than the nitrate-hydrolysis method.

The as-prepared nanoparticle products were in highly distorted structure related to the cubic Y_2O_3 phase. High temperature annealing caused evolution of the nanoparticle products from the distorted structure to the cubic Y_2O_3 structure. The evolution processes of the products from both methods were very similar. An unknown phase appeared in the annealed products at medium temperatures, which disappeared at high annealing temperatures (1000 ºC 4 h). High annealing temperatures caused growth and aggregation of nanoparticles. Eu-doping accelerated the annealing process. Residual AOT molecules delayed the annealing process.

This research suggests that further work should include the following thrusts. First, it is important to investigate the feasibility of other reverse micelle systems. Since sulfur in residual AOT molecules might be a problem for some applications, it can be replaced by other surfactants without sulfur or other harmful elements. Non-ionic surfactants such as NP-5 and OP-10 may also be used. Because they are expected to have only weak interactions with nanoparticles, they might be removed from nanoparticle products more easily. Second, investigation of the feasibility of other reaction systems and the effects of supporting anions and chelating ligands are also important. A comparison of different methods could clarify the mechanisms. Better controls over nanoparticle morphology, size, size distribution, and crystallinity may be achieved. Third, as the destination of this research is to prepare Y_2O_3:Eu nanoparticles in reverse micelles, investigation of the fluorescent properties of Y_2O_3:Eu nanoparticles prepared from the nitrate-

hydrolysis method and the isopropoxide-hydrolysis method is an obvious next-step. Fourth, because the as-prepared nanoparticles were in network-like aggregates, to minimize this aggregation will produce better dispersed nanoparticle products. As discussed in Section 2.6, residual AOT molecules covered surfaces of nanoparticles and prevented them from coalescence. However, These AOT molecules also caused loose aggregation of the protected nanoparticles by attractive interactions among AOT aliphatic chains. According to the modified DLVO theory,[102] the interaction between two colloid particles at certain distance h, V_h, is given as:

$$V_h = V_{dispersion} + V_{electrostatic} + V_{steric}$$

where $V_{dispersion}$ is the attractive interaction between two particles, $V_{electrostatic}$ is the repulsive electrostatic interaction between two charged particles, V_{steric} is the steric repulsive interaction between protecting long-chain molecule layers on the particles. To prevent aggregation of nanoparticles, one way is to increase $V_{electrostatic}$, and the other is to increase V_{steric}. More adsorbed ions of the same charge on nanoparticles increases $V_{electrostatic}$. Y^{3+} and OH^- are two ions that can be preferentially adsorbed on the yttrium oxide nanoparticles. Therefore, it is worth trying to wash the as-prepared products with $Y(NO_3)_3$ or NaOH aqueous solution. Molecules of longer alkyl chain can increase V_{steric}.[103] However, this repulsive steric interaction is partially compensated by the attractive interaction between the long-chain molecules. The attractive interaction is probably dominant among AOT molecules, whose alkyl chains are short, so that the protected nanoparticles form the network-like loose aggregates, which are hard to disperse. Molecules of longer alkyl chains, such as polymer molecules, can cause the repulsive steric interaction to dominate. In fact, polymer molecules have long been used to disperse colloid particles in solvents.[104] Therefore, future work should include using polymer or oligmer surfactant molecules, such as OP-10 and NP-5, instead of AOT, to minimize aggregation of the as-prepared nanoparticles.

Besides the possible directions for future work discussed above, some other interesting observations also suggest further investigation. The composition and structure of the unknown phase need to be illuminated. The observation of no precipitation from the reaction between $Y(NO_3)_3$ and NaOH in reverse micelles needs an explanation (Section 2.5). In addition, some

[102] Hiemenz, P. C.; Rajagopalan, R.: In *Principles of Colloid and Surface Chemistry 3rd ed.*, Marcel Dekker, New York, 575 (1997).
[103] Russell, W. B.; Saville, D. A.; Schowalter, W. R.: In *Colloid Dispersions*, Cambridge University Press, Cambridge (1989).

reason needs to be found for the observation that aqueous solution of 0.5 M $Y(NO_3)_3$ could not dissolve to form w = 1 reverse micelle solution with 0.1 M AOT/isooctane (Section 2.1).

[104] Fleer, G. et al.: In *Polymer at Interfaces 1st ed.*, Chapman & Hall, New York (1993).

Vita

Name: Cheng, Xu

Current Position, 1996-1998

M. S. Candidate in Chemistry

Department of Chemistry

Virginia Polytechnic Institute and State University, Blacksburg, VA 24060, U. S. A.

Thesis Title: Synthesis of Nanometer-sized Yttrium Oxide Particles in Diisooctyl Sodium Sulphosuccinate/Isooctane Reverse Micelle Solution

Advisor: Brian M. Tissue

Graduate Education, 1993-1996

Department of Materials Science

Fudan University, Shanghai 200433, P. R. China

Degree: M. S. in Materials Science, June 1996

Thesis Title: Synthesis of $InBO_3$:Eu and YBO_3:Eu Phosphors

Advisor: Jingeng Huang

Undergraduate Education, 1989-1993

Department of Chemistry

Nanjing University, Nanjing, Jiangsu 210090, P. R. China

Degree: B. S. in Chemistry, July 1993

Thesis Title: Modification of Clay Catalyst for p-Alkylation of Phenol with C_6 - C_8 Alkenes

Advisors: Yichun Yan and Wenxia Shen